ABSTRACT

Title of Document:	INVESTIGATION OF RHENIUM'S BIOGEOCHEMISTRY.
	Marvourneen Kimranee Dolor, Doctor of Philosophy, 2009
Directed By:	Professor *Emeritus* George R. Helz, Department of Chemistry and Biochemistry

The form of the paleoredox indicator, rhenium, that is sequestered in reducing sediments is not known. To probe this question, I used Laser Ablation ICP-MS to look for correlations between Re signals and those of other elements. My results point to the possibility that Re is incorporated into multiple host phases: sulfides and organic material.

Laser Ablation ICP-MS also provided a new way to analyze a large suite of elements in Chesapeake Bay sediments simultaneously. A number of rarely determined elements (Ag, Sn, Sb, Te and Bi) were discovered to exhibit profiles similar to known industrial pollutants such as Cu, Zn, Cd and Pb. This is one of the first demonstrations of LA-ICP-MS as a tool to perform a survey of anthropogenic impacts on modern sediments and suggests that the suite of elements monitored by environmental agencies should be broadened.

Rhenium is scavenged between iron and sulfate reduction, in the sequence of microbial terminal electron accepting processes, so I investigated whether Re could be reduced directly or indirectly by iron and/or sulfate reducing bacteria. This hypothesis was also based on the fact that Tc (also Group VIIB), is directly and indirectly reduced by the iron and sulfate reducers used in my experiments: *Geobacter metallireducens* GS-15, *Shewanella oneidensis* MR-1, *Desulfovibrio desulfuricans* subsp. *desulfuricans* and *Desulfovibrio desulfuricans* ND132. I concluded that neither direct nor short-term indirect microbial processes are likely to explain Re fixation in sediments.

In order to test the hypothesis that thioperrhenates play a role in Re fixation, experimentally determined stability constants, ($K_{(4-x)(5-x)}$) for the following types of reactions are needed.

$$ReO_xS_{4-x}^- + H_2S \leftrightarrow ReO_{x-1}S_{5-x}^- + H_2O \text{ where } 1 \leq x \leq 4$$

These compounds are analogous to thiomolybdates, which are the particle reactive form of Mo fixed under reducing conditions. The di- and tri- thioperrhenates were never observed, by UV-Vis spectrophotometry. The stability constant for mono-thioperrhenate, $K_{01}=10^4$, while the stability constant for tetra-thioperrhenate, $K_{04} = 10^{19}$.

Below pH 8, the formation of a rhenium-sulfur nano-phase competed with the formation of thioperrhenates. The formation of this nano-phase is most likely an important step in rhenium fixation. Future work should involve exploring the sorption characteristics of this material.

INVESTIGATION OF RHENIUM'S BIOGEOCHEMISTRY.

By

Marvourneen Kimranee Dolor.

Dissertation submitted to the Faculty of the Graduate School of the
University of Maryland, College Park, in partial fulfillment
of the requirements for the degree of
Doctor of Philosophy
2009

Advisory Committee:
Professor George R. Helz, Chair
Professor William F. McDonough
Dr. Cynthia C. Gilmour
Professor Neil V. Blough
Professor John A. Tossell

Dedication

To you Mummy, for always supporting me along my journey and for helping me to embrace the Here and Now.

Acknowledgements

My deepest thanks to Dr. Helz: You are an inspiring mentor and a generous person. Thank you always believing in me and seeing potential where I did not.

Special gratitude to my family, and in particular my sister Tamilia and brother Francois for always being so entertaining and encouraging: “a ja ja fighting!!!!!!” I am proud to be your big sister, co-conspirator and hopefully future co-worker. Mummy, thank you for all your support and most importantly your enthusiasm. To my cousin, Carlene, thank you for the stress-relieving conversations.

Thank you to my DC families: the Corls and the Magic Noquis Circle, for opening your homes to me and not letting me waste away to skin and bones.

Thank you to all of the members of NOBCChE-UMD, Department of Chemistry and Biochemistry, Department of Geology – Geochemistry Laboratories, BLSG, MCC DC, and Sister Mentors.

To the all people who have cooked me a meal, shared a night on the town or offered a sympathetic ear: thank you for keeping me somewhat sane over the last few years. It means more to me than I can express here.

Thank you to my committee members as well as the individuals who were willing to supply me with samples or assist me with different aspects of this work: Dr. Richard Ash, Dr. Rich Walker, Dr. H. J. Brumsack, Tyler Bell, Nise Butera, Georgia Riedel, Dr. Fritz Riedel, Dr. Elizabeth Canuel and Beth Lerberg.

This work has been funded by the National Science Foundation Grant No. EAR0229387 and a Smithsonian Pre-doctoral fellowship.

Table of Contents

List of Tables

List of Figures

Chapter 1: Introduction

1.1 Background and Significance

The goal of this research has been to build on the existing knowledge of rhenium's behavior under reducing conditions. The term reducing is used to refer to both suboxic (no O_2 or H_2S present) and anoxic (H_2S present but no O_2) conditions (Colodner et al., 1995). Rhenium enrichment in reducing sediments is the result of physical, chemical and/or biological processes occurring in the sediments (Brumsack, 2006), however we do not know which of these processes drive authigenic enrichment of Re.

This research will improve the use of Re as a paleoredox indicator. Paleoredox indicators are redox sensitive elements used to trace the evolution of the Earth's atmosphere, as well as the oceans. Paleoredox indicators are not limited to use for geological time-scales, but can also be used to evaluate the effect of anthropogenic activities on modern aquatic and marine ecosystems.

Rhenium's seawater concentration is on the order of 10^{-11} M (Anbar et al., 1992; Koide et al., 1987), this means that whatever Re species is trapped in reducing sediments must have an extremely low solubility (less than 10^{-11} M). Rhenium is present in very low concentrations in sediments where the overlying water is oxic. A typical Re concentration in oxic sediments is 0.1 ng/g (Koide et al., 1986), which is less than the average crustal value of 0.5 ng/g (Colodner et al., 1993a). This is consistent with the non-reactivity and low concentration of the perrhenate ion (ReO_4^-) in oxic waters (Anbar et al., 1992; Koide et al., 1987). However, Re is enriched up to 300 times in sediments deposited under reducing conditions compared to those

deposited under oxic conditions (Colodner et al., 1993a). This is a remarkable enrichment factor compared to other redox sensitive elements such as uranium and molybdenum that are enriched 10-50 times under reducing conditions (Colodner et al., 1993a).

In aquatic ecosystems, microbes make use of the most efficient oxidizing agents available to harvest energy from organic matter. These oxidizing agents are themselves reduced and these reductions are termed terminal-electron-accepting processes or TEAPs. The sequence of these TEAPs is illustrated in Figure 1, which also shows the change from oxic to anoxic conditions.

			ΔG (kJ/mole CH_2O)
OXIC	Respiration	$CH_2O + O_2 \Leftrightarrow CO_2 + H_2O$	-475
SUBOXIC	Denitrification	$5CH_2O + 4NO_3^- \Leftrightarrow 2N_2 + 4HCO_3^- + CO_2 + 3H_2O$	-448
	Mn reduction	$CH_2O + 3CO_2 + H_2O + 2MnO_2 \Leftrightarrow 2Mn^{2+} + 4HCO_3^-$	-349
	Fe reduction	$CH_2O + 7CO_2 + 4Fe(OH)_3 \Leftrightarrow 4Fe^{2+} + 8HCO_3^- + 3H_2O$	-114
ANOXIC	Sulfate reduction	$2CH_2O + SO_4^{2-} \Leftrightarrow H_2S + 2HCO_3^-$	-77
	Methanogenesis	$CH_2O \Leftrightarrow CH_4 + CO_2$	-58

Figure 1 Terminal electron acceptor processes coupled to organic matter oxidation in order of decreasing energy yield (Madigan and Martinko, 2005).

To date, environmental sampling has been used to argue that Re is enriched in suboxic sediments where the bottom waters are oxic but the oxygen is consumed within the first centimeter of pore waters (Crusius et al., 1996; Morford and Emerson, 1999). This means that Re is enriched, possibly via reduction, between iron and sulfate reductions (Crusius et al., 1996; Nameroff et al., 2002). It is possible that the initial steps of Re enrichment do not involve reduction. Nevertheless, lack of Re enrichment can be used to establish that conditions were not sufficiently reducing to form Fe, Cd or Mo sulfides at the time of sediment deposition (Calvert and Pedersen, 1993; Crusius et al., 1996; Morford and Emerson, 1999; Schaller et al., 2000).

The presence of Re enrichment could mean that either the bottom waters or the pore waters were reducing at the time of sediment deposition (Crusius et al., 1996). Since Mo is enriched in more reducing sediments than Re, the Re/Mo ratio of a particular sediment, as well as depth of enrichment can be used to determine whether the water column or the sediments were oxic, suboxic or anoxic (Crusius et al., 1996).

Morford and Emerson (1999) also analyzed a suite of redox sensitive elements, molybdenum, rhenium, vanadium, uranium, and cadmium to evaluate enrichment (or lack thereof) in sediments from the Northwest African margin, the U.S. Northwest margin and the Arabian Sea. They confirmed the findings of Colodner et al. (1993,1995) and Calvert and Pedersen (1993) and concluded that, while all of the metals tested are reduced under anoxic conditions, Re is the superior tracer of reducing conditions. This is because Re shows the highest degree of enrichment due to its low particulate concentrations (Morford and Emerson, 1999).

Unlike Mo, Re is not associated with manganese oxides under oxic conditions (Colodner et al. 1993a; Morford et al. 1999; 2005; 2007). Thus, Re enrichment is due only to reducing conditions.

There is consensus on the fact that Re is enriched in reducing sediments but not on the conditions required for this enrichment. Morford et al., (2005 and 2007) argue that Re is depleted from pore waters before sulfide accumulates to measurable levels (μM concentrations), while Chappaz et al. (2008) propose that the sequestered form of rhenium is rhenite (ReS_2). These disparate views point to the need for the answers to three key questions that this work seeks to answer:

1) What is the form of rhenium sequestered under reducing conditions?
2) What are the thermodynamic properties of the known rhenium-sulfur compounds?
3) What is the mechanism of rhenium sequestration?

1.2 Dissertation Outline

In Chapter 2, I present results of Laser Ablation Inductively Coupled Plasma Mass Spectrometry analysis of Chesapeake Bay sediments along with figures of merit for this analytical method. In this work, I demonstrate that fine grain sediment samples can be pelletized without a binder and analyzed for a large suite of elements simultaneously. At the time of this writing the Chesapeake Bay portion of this chapter is under review for publication in Marine Pollution Bulletin.

Most of the previous literature on Re in sediments focuses on the contrast between permanently oxic and permanently sulfidic environments (Calvert and Pedersen, 1993; Colodner et al., 1995; Ravizza et al., 1991). Chesapeake Bay is a seasonally anoxic basin and the bottom waters of the main channel transition between oxic and sulfidic states every summer (Adelson et al., 2001; Newcombe and Horne, 1938; Officer et al., 1984a). My goal was to investigate rhenium's sediment profile along with other chalcophile elements. The effort to determine Re's sediment profile had limited success because of analytical uncertainty. However, I generated a large amount of new information about rarely determined elements in this anthropogenically contaminated environment. Thus, this unplanned portion of my research became a major part of my dissertation.

In Chapter 3, I investigate the hypothesis that Laser Ablation ICP-MS can be used to determine what elements Re is associated with in sediments, in order to constrain whether Re is an oxide or sulfide in sediments. The fact that rhenium is enriched in suboxic sediments where there is no measurable sulfide (Colodner et al., 1993a) points to the possibility that the scavenged Re species may not be a sulfide.

In Chapter 4, I investigate and reject the hypothesis that the first step in Re deposition is a biologically mediated reduction. The kinetics of this multi-step mechanism would depend on organic carbon (C_{org}) (Crusius and Thomson, 2000) since the microbial degradation of C_{org} could be coupled to the direct or indirect reduction of ReO_4^-. Rhenium concentrations have been found to correlate well with C_{org} in black shales (Jaffe et al., 2002); this supports the hypothesis that Re enrichment is dependent on C_{org}. Chapter 4 has been submitted for publication in the Geomicrobiology Journal.

In chapter 5 I explore methods for determining the stability constants of rhenium sulfide species in order to test the hypothesis that Re is accumulated as a sulfide. Crusius et al., (1996) found that Re is highly enriched in pyrite-rich anoxic mud. More supporting evidence for this hypothesis is that rhenium sulfide species, once formed, are very stable, insoluble species (Dolor, 2005).

Chapter 2: Sediment Profiles of Less Commonly Determined Elements Measured by Laser Ablation ICP-MS

2.1 Introduction

2.1.1 Evaluating Laser Ablation ICP-MS

Trace element profiles in sediment cores can yield important information about coastal water quality before the modern era of environmental monitoring began. Profiles of such elements as Mo, Re and U have already been used extensively. (Adelson et al., 2001; Brown et al., 2000; Chaillou et al., 2002; Elbaz-Poulichet et al., 2005; Itoh et al., 2003; Schaller et al., 1997) Very likely, much more detailed histories can be deciphered from sediments if the number of elements determined simultaneously is greatly expanded. Of particular interest are chalcophile elements (Goldschmidt, 1958), which are sulfide-reactive to varying degrees and thus potentially affected by past redox conditions in the depositional environment.

With this application in mind, I have investigated laser ablation, inductively coupled plasma source mass spectrometry (LA-ICP-MS) (Durrant, 1999; Durrant and Ward, 1993; Durrant and Ward, 2005; Mokgalaka and Gardea-Torresdey, 2006; Russo et al., 2004; Winefordner et al., 2000), as a potentially efficient way of rapidly determining a large suite of chalcophile and other elements in large numbers of sediment samples.

Although first developed more than two decades ago (Gray, 1985), LA-ICP-MS is not yet being used for routine, high sample-throughput work. Among its great

advantages are diminished sample preparation time and lowered likelihood of sample contamination by reagents or analyte loss during sample preparation. Additionally, spatial distributions of elements can be determined (Arrowsmith, 1987; Olesik, 2000; Smith, 2007). On the other hand, calibration remains a challenge (Cromwell and Arrowsmith, 1995; Eggins, 2003). Ablation yields vary with physical properties of analytes (melting and boiling points) and of samples (reflectivity and thermal conductivity) (Hoffmann et al., 2002).

2.1.2 Harnessing the power of Laser Ablation ICP-MS

After determining that calibration challenges could be overcome, I used LA-ICP-MS to explore the behavior of a large suite of trace elements in Chesapeake Bay sediment cores. The cores cover the 20th century and can provide useful historic information about anthropogenic effects and redox conditions in the Bay.

Chesapeake Bay is the largest estuary in the United States and one of the largest in the world. It was the first estuary in the United States to be occupied permanently by Europeans. Chesapeake Bay has been adversely affected by over-fishing and pollution from a variety of sources such as manufacturing plants, agricultural run-off and atmospheric deposition of contaminants from sources such as inland coal-fired power-plants. The extensive efforts to restore the Bay such as the “Save the Bay” initiative have had limited success.

Numerous other authors have explored concentrations of trace elements in Chesapeake Bay. Those concerned with pollution and remediation have focused on a rather narrow list of elements: e.g. Cr, Ni, Cu, Zn, As, Cd, Hg and Pb, (Beyer et al., 1998; Helz, 1976; Helz et al., 1975; Lawson and Mason, 2001; Lawson et al., 2001;

Mason et al., 2004; Riedel and Sanders, 1998; Riedel et al., 1997; Riedel et al., 1999; Sinex and Helz, 1981; Sinex and Helz, 1982; Zheng et al., 2003). Those concerned with redox conditions (Adelson, 1997; Adelson et al., 2001; Colodner et al., 1993a; Miller, 1992; Shaw et al., 1994) have focused on Mo, Re and U.

The power of LA-ICP-MS affords an opportunity to greatly expand these lists of trace elements. In LA-ICP-MS, a laser beam is focused onto a sample and material is removed through a series of photochemical, photothermal and physiochemical processes, which results in the formation of a nanosecond plasma jet above the sample followed by condensation of submicron-sized particles and transport of these particles to the plasma torch of the mass spectrometer. These particles are introduced into the torch where they are disassociated into atoms and turned into ions, which are then introduced into the orifice of the mass spectrometer; there positive ions are separated from electrons and then mass-separated and counted.

From its inception, LA-ICP-MS has been used to characterize geological materials such as rocks, minerals and mineral inclusions (Gray, 1985; Darke et al.,1989; Balaram et al., 1990), soils and sediments (Baker et al., 1999; Crain et al., 1992; Durrant and Ward, 1993; Lee et al., 2003; Rauch et al., 2006) and ice cores (Reinhardt et al., 2003; Reinhardt et al., 2001). LA-ICP-MS has been used to determine mercury in sediments from Minamata Bay, Japan, with a precision of about 5% (Tao et al., 2002). Lake sediment cores have been analyzed using the spatial resolution capabilities of LA-ICP-MS (Rauch et al., 2006). In that work, two core sections were analyzed to produce concentration profiles for Al, Si, Fe, S, As, Cu and

Zn at a resolution of 0.25 mm. Such detailed resolution was possible because the layering of the accumulated sediments was preserved by freeze-coring.

2.2 Experimental Section

2.2.1 Samples and Sampling Sites

Three standard reference materials (SRM) were employed in this work. NIST 610 consists of 61 certified trace elements in a plug of polished glass and is widely used during analysis of geological materials. Details about this SRM can be obtained from the NIST website (Reed, 1992). SCo-1 is a Cody Shale powder from Natrona County, Wyoming and MAG-1 is a marine mud powder from the Wilkinson Basin of the Gulf of Maine (Schultz et al., 1976). Both of these materials were prepared by the U.S. Geological Survey in a similar fashion which involved mechanical crushing until 80% of the material could pass through a 200-mesh screen (Flanagan, 1967). The reference values used for all three SRMs were obtained from the online database GeoReM (Jochum, 2008; Jochum et al., 2005; Jochum and Willbold, 2006). NIST610 and SCo-1 were used solely to evaluate accuracy and precision while MAG-1 was used to calculate final concentrations as described below.

All Chesapeake Bay materials studied were archived samples. Sample localities are depicted in Figure 2. Core 55 (38º 48.5'N; 76º 23.5"W), is a gravity core collected in July 1979 by the Maryland Geological Survey in a water depth of 25 m (Adelson, 1997; Adelson et al., 2001; Helz et al., 1985b; Helz et al., 1985a). A mass accumulation rate of 0.41 g cm^{-2} y^{-1} was determined by Helz et al. (1985b) using excess ^{210}Pb and $^{239,240}Pu$ (after excluding a homogeneous layer deposited during Hurricane Agnes). An x-ray radiograph of the core as well as mathematical

modeling of the ^{210}Pb and ^{239,240}Pu profiles (Officer et al., 1984b) reveals no evidence of turbation. The sediment consists predominantly (>70%) of clay-sized particles (<4 μm) with the rest being silt-sized material (<63 μm).

Core RD (38º 53.2'N; 76º 23.5"W), is a piston core collected in November 1998 by the U.S. Geological Survey. It was collected in a water depth of 26.5 m and was located 9.2 kilometers north of core 55. Both core sites lie in the Bay's deep central trough which contains fine-grained mud. Owing to seasonal anoxia in this trough, the sediments are minimally disturbed by burrowing organisms. Based on excess ^{210}Pb, as confirmed by ^{137}Cs, ^{14}C, total Pb and ragweed pollen, the mass accumulation rate in core RD declines from 1.21 g cm^{-2} y^{-1} in the top 75 cm to 0.78 g cm^{-2} y^{-1} at the deepest level for which I have analyses (Zimmerman and Canuel, 2002).

In order to evaluate external influences on compositions of sediments at these sites, a number of samples from sites around the Bay were also analyzed. Three samples (Susq 8-10 cm, 28-30 cm and 44-46 cm with ^{210}Pb ages of 1977, 1972 and 1968.5 respectively) from a core in the Conowingo reservoir (39º 57.0'N; 76º 23"W) in the Susquehanna River were analyzed to characterize material entering the Bay from the watershed (Cantillo, 1982; Helz et al., 1985a).

Baltimore Harbor samples (B'more Harbor H, M and N; Sinex and Helz, 1982) were collected May/June 1981. Baltimore harbor has been intensely contaminated by industrial activities, and these cores in particular contain extremely high Cr and Zn concentrations.

Sediments obtained with a clamshell sampler on a traverse from shallow to deep water near cores 55 and RD (Water depths 3.4m, 6.7m and 26.2m) were analyzed to see if there is an effect of water-depth on sediment composition. These samples were collected on June 2, 1977 (Helz et al., 1985a; Sinex, 1981; Sinex and Helz, 1981).

Core PC-6 (38º 32.66'N; 76º 23.14"W) was collected about 30 km south of core 55 in 20 m water depth (Adelson et al., 2001; Helz et al., 2000). These samples were from horizons deposited before the 18th century (as determined from pollen evidence). They were analyzed to obtain further information on the background levels of the elements of interest before eutrophication and industrial pollution.

A Miocene shore deposit was also analyzed (Fairhaven unit of the Calvert Formation). One of the major sources of sediment to northern Chesapeake Bay is erosion of unconsolidated sediments of the Atlantic Coastal Plain (Biggs, 1970; Schubel, 1968). This sample is rich in redox-sensitive elements, probably due to a period of high productivity along the Atlantic Coast approximately 15 million years ago (Ferri, 1977; Helz et al., 2000).

All samples except those from core RD were dried (110^{o} C) and then crushed with a mullite mortar and pestle to eliminate clumps formed during drying. Subsequently, samples were stored in glass bottles at room temperature. Core RD samples were stored frozen until needed and then dried, crushed and packaged in polyethylene bags.

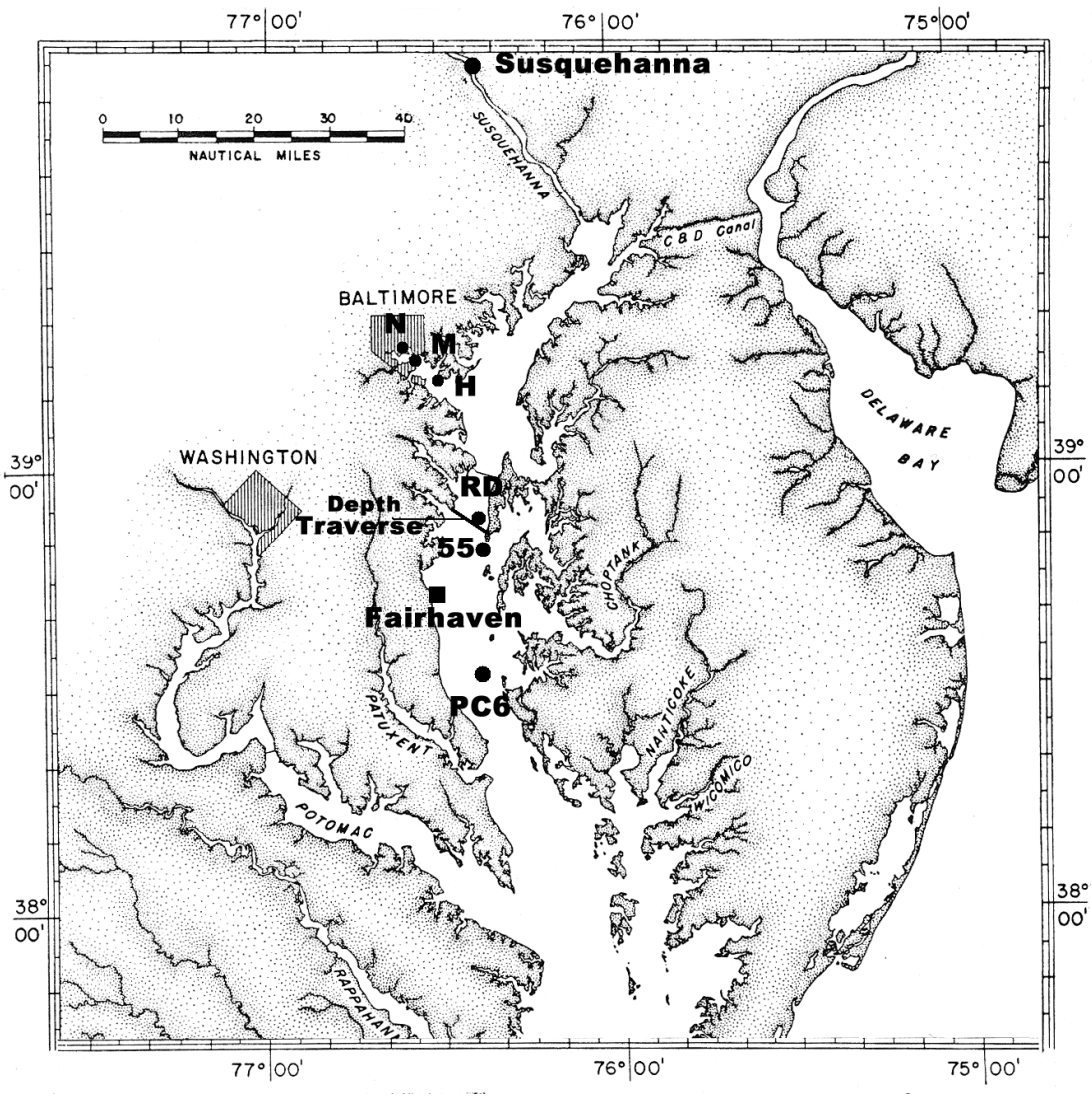

Figure 2 Map showing location of samples.

2.2.2 Procedures

Most previous authors have incorporated binding agents into powdered samples prior to pressing them into pellets for laser ablation (Crain et al., 1992; Denoyer, 1992; Lee et al., 2003; Morrison et al., 1995; Rauch et al., 2006; Williams and Jarvis, 1993). Binding agents can create high blanks. Additionally, using a binding agent dilutes the sample (Denoyer, 1992; Rauch et al., 2006). In this work I avoided binding agents and their associated analytical issues, relying on the ~3% organic matter inherent in the samples to provide sufficient binding during pelletization. Other authors have done this and reported precise and accurate results (Durrant and Ward, 1993; Tao et al., 2002).

To make 9 mm circular pellets, approximately 50 mg of a sample was inserted into a die (316 stainless steel) that is commonly used to make KBr pellets for infrared spectroscopy. The die was placed into a workbench clamp and tightened with a wrench. This formed pellets robust enough to remain whole during ablation. Between samples the die was cleaned with deionized water followed by acetone to accelerate drying.

The LA-ICP-MS instrument included a New Wave Nd-YAG (Neodymium doped: Yttrium aluminum garnet; Nd:$Y_3Al_5O_{12}$) laser and a Thermo ELEMENT2 double focusing magnetic sector field ICP-MS (Brenan et al., 2005). An ultraviolet laser was used since it produced less elemental fractionation than infrared lasers (Cromwell and Arrowsmith, 1995). The output of the Nd:YAG laser (1064nm) was frequency quintupled (to 213nm) using nonlinear crystals. Typical laser settings are outlined in Table 1.

Table 1 LA-ICP-MS Operating Conditions.

ELEMENT2 ICP-MS	
Rf power	1200 W
Cooling gas (Ar) flow rate	16 L/min
Auxiliary gas (Ar) flow rate	0.8 – 1.2 L/min
Sample gas (Ar) flow rate	0.6 – 1.0 L/min
Additional 1 (He) flow rate	1.06 – 1.10 L/min
Monitoring Ions	Refer to Table 2
Acquisition Type	Peak Hopping
Samples per peak	1
Sample Time for most elements*	10 milliseconds
*Sample Time for Re and Te	40 milliseconds
Laser Ablation	
LA System	New Wave Nd-YAG
Wavelength	213 nm
Scan Method	Translational line
Ablation frequency	20 Hz
Power density	1.5 – 2.5 J cm $^{-2}$
Measurement delay	25 seconds
Spot size	15 and 100 μm
Stage translation speed	10 μm/s

The ablation cell of the laser system was flushed with helium, which has been found to enhance sensitivity compared to argon (Bleiner and Gunther, 2001; Brenan et al., 2005; Eggins et al., 1998; Gunther and Heinrich, 1999). Laser power output was evaluated daily during tuning and was not changed throughout the course of the day. This value was usually 45% (equivalent to ~2 J cm^{-2}). Tuning to optimize instrument output was performed by monitoring ^{43}Ca, ^{238}U, ^{232}Th and ^{232}Th^{16}O while ablating NIST 610. Desired values were Ca ≥ 50000 counts per second (cps), U ≥ 150000 cps, and ThO/Th ≤ 0.03. Table 1 also summarizes typical instrument parameters.

Spot size, ablation frequency and power output of the laser system was adjusted to ensure that the power density remained at optimal values of between 1.5

and 2.5 J cm^{-2}. This photon fluence produces sufficient energy to ensure effective photon-material coupling during ablation. Laser line widths of 100 µm were used for MAG-1, SCo-1 and samples, while widths of 15 µm were used for NIST 610. In the first two cases, larger line widths were used because of weak signals from low concentrations of Re, Te, and Ag. In preliminary experiments an ablation frequency of 8 Hz was used, but this required 40 µm line widths for NIST 610 in order to obtain sufficient signal for all elements, and I expected to need at least 250 µm spot sizes for MAG-1, SCo-1 and sediment samples. Increasing the ablation frequency from 8 Hz to 20 Hz produced satisfactory results, and further experiments with different line widths and frequencies were not undertaken.

The particular isotopes analyzed (Table 2) were chosen on the basis of prior knowledge of isobaric interferences, as well as a desire to reduce differences in signal size between major and minor elements of interest. For major components (Ti and Fe) one of the less abundant isotopes was selected. For elements where more than one isotope was analyzed (Mo, Sb and Re), the abundance corrected concentrations were averaged. This was possible because there was good agreement between the abundance corrected concentrations for these elements.

Table 2 Isotopes analyzed via LA-ICP-MS

Isotope	Isotopic Mass	Isotopic Abundance	Isotope	Isotopic Mass	Isotopic Abundance
S	33	0.75	Mo	95	15.90
Ca	43	0.14	Mo	97	9.60
Ti	49	5.50	Ag	107	51.80
V	51	100.00	Cd	111	12.80
Mn	55	100.00	In	115	95.70
Fe	57	2.14	Sn	118	24.10
Co	59	100.00	Sb	121	57.21
Ni	60	26.10	Sb	123	42.79
Cu	63	69.20	Te	125	7.00
Zn	66	27.90	W	184	30.70
Ga	69	60.10	Re	185	37.40
Ge	72	27.40	Re	187	62.60
As	75	100.00	Tl	205	70.50
Se	77	7.60	Pb	208	52.40
Nb	93	100.00	Bi	209	100.00
			U	238	99.30

Each analysis consisted of 20-40 seconds with the laser on with the shutter closed to obtain a background signal, followed by 70-90 seconds with the shutter open to collect the ablation signal (Figure 2). Horizontal translation of the sample stage (at a rate of 10 $\mu m\ s^{-1}$) during sampling resulted in a track that was approximately 1.5 mm long. A 50-70 second steady plateau of counts was extracted from the ablation signal to determine element concentrations (Lundstrom et al., 2006).

The method of data analysis used in this work requires prior knowledge of the concentration of one element in both the samples and the calibration materials (SRM's). This internal standard is used to correct for variations in ablation efficiency. A common practice has been to create an internal standard by adding a

swamping concentration of one element to each sample. I wished to avoid such sample amendments and therefore used natural Mn concentrations, which were measured in the fine-grained sediments and SRMs via ICP-MS analyses as described below. Manganese occurs in sediments largely as Mn-oxyhydroxide grain coatings and thus tends to be evenly dispersed in sediments. Figure 2 demonstrates that the Mn signal, although subject to fluctuations, displays no irregularities suggestive of spatial heterogeneities that are large at the scale of a 100 μm laser beam.

For solution analyses a Finnigan Element 2 ICP-MS instrument, interfaced with a cyclonic spray chamber was used to determine the internal standard, Mn, in bulk sediment samples. Approximately 0.2 g of each sediment sample was digested via the open-vessel digestion method (Langmyhr, 1967; Van-Loon, 1985) using trace metal grade or better purity acids. A seven-point external calibration curve was used and both samples and standards were spiked with a 3 ppb yttrium internal standard to monitor analytical-drift (Dolor, 2005).

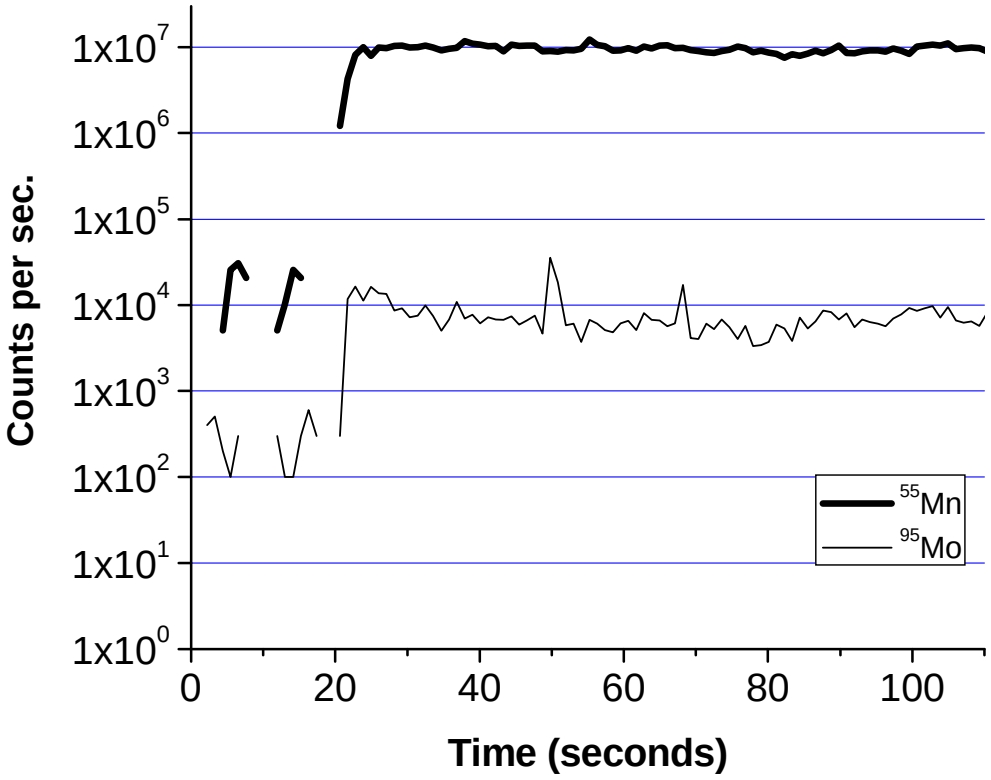

Figure 3 LA-ICP-MS results illustrating background vs. signal levels and uniformity of counts of the internal standard, Mn, in a Chesapeake Bay sample. Each analysis consisted of 20-40 seconds with the laser on and the shutter closed to obtain a background signal, followed by 70-90 seconds with the shutter open to collect the ablation signal. While the shutter was opened, the laser traversed 1.0mm x 0.1mm = 0.1 mm^2 of area on the sample surface.

2.2.3 Data Analysis

Raw counts per second data from the LA-ICP-MS instrument were imported into the LAMTRACE program (Brenan et al., 2003; Coedo et al., 2004; Wheeler et al., 2006). This program calculates the concentration of element, X, in the sample ($C_{X,SAM}$) relative to the literature value of the concentration of X in the standard reference material ($C_{X,SRM(LIT)}$) (Longerich et al., 1996). It requires using an internal standard that has a known value in both the sample and the SRM. In my work, Mn was the internal standard.

Equations 1, 2 and 3 outline the calculations performed by LAMTRACE. The background corrected signal from element X in the sample ($I_{X,SAM}$) was calculated by subtracting the mean signal obtained before the laser impinged on the sample from the mean signal obtained while the sample was being ablated (see Figure 3). The background corrected signal of Mn in the sample ($I_{Mn,SAM}$) was calculated in the same manner. Because the concentration of Mn in the sample ($C_{Mn,SAM}$) is known, a provisional value for the concentration of X in the sample ($C^*_{X,SAM}$) can be obtained:

$$C^*_{X,SAM} \Big/ C_{Mn,SAM} = I_{X,SAM} \Big/ I_{Mn,SAM} \qquad (2.1)$$

$C^*_{X,SAM}$ would be a correct determination of the concentration of X in the sample only if the instrumental efficiency for both X and Mn were identical, which need not be true.

An instrumental efficiency correction is applied by making use of an SRM. First, a provisional value of the concentration of X in the SRM is determined just as the equivalent quantity was determined in the sample:

$$C^*_{X,SRM} / C_{Mn,SRM} = I_{X,SRM} / I_{Mn,SRM} \quad (2.2)$$

Then the true concentration of X in the sample ($C_{X,SAM}$) is calculated by assuming that the ratio of true to provisional concentrations is the same in the sample and the SRM. The true concentration of X in the SRM is taken to be the certified or recommended value obtained from the literature:

$$C_{X,SAM} / C^*_{X,SAM} = C_{X,SRM(LIT)} / C^*_{X,SRM} \quad (2.3)$$

Inherent in this approach is an assumption that relative instrumental efficiencies for X and Mn in the sample and the SRM are the same. Therefore, the sample and SRM should be similar.

2.3 Results: Evaluation of LA-ICP-MS

2.3.1 Precision: Relative Standard Deviations

For each SRM, the relative standard deviation (RSD) was calculated from σ, the population standard deviation and μ, the population mean where RSD = (σ/μ)*100% (Skoog and J.J., 1992). The results in Figure 4 show the pooled RSDs for 30 components determined in NIST 610, MAG-1 and SCo-1. The analytes have been divided into 3 classes based on their RSDs: CLASS A elements have RSDs < 15%, CLASS B elements have 15%<RSDs<20% and CLASS C elements have RSDs >20%. These classes were established based on the typical cut-off points used to evaluate precision in the literature (Cromwell and Arrowsmith, 1995; Denoyer, 1992; Gunther et al., 1999; Winefordner et al., 2000). Figure 4 illustrates the fact that pellets made from powdered sediment and shale standard reference materials (i.e.

MAG-1 and SCo-1) generally yield precisions comparable to those from the synthetic glass standard reference material, NIST 610.

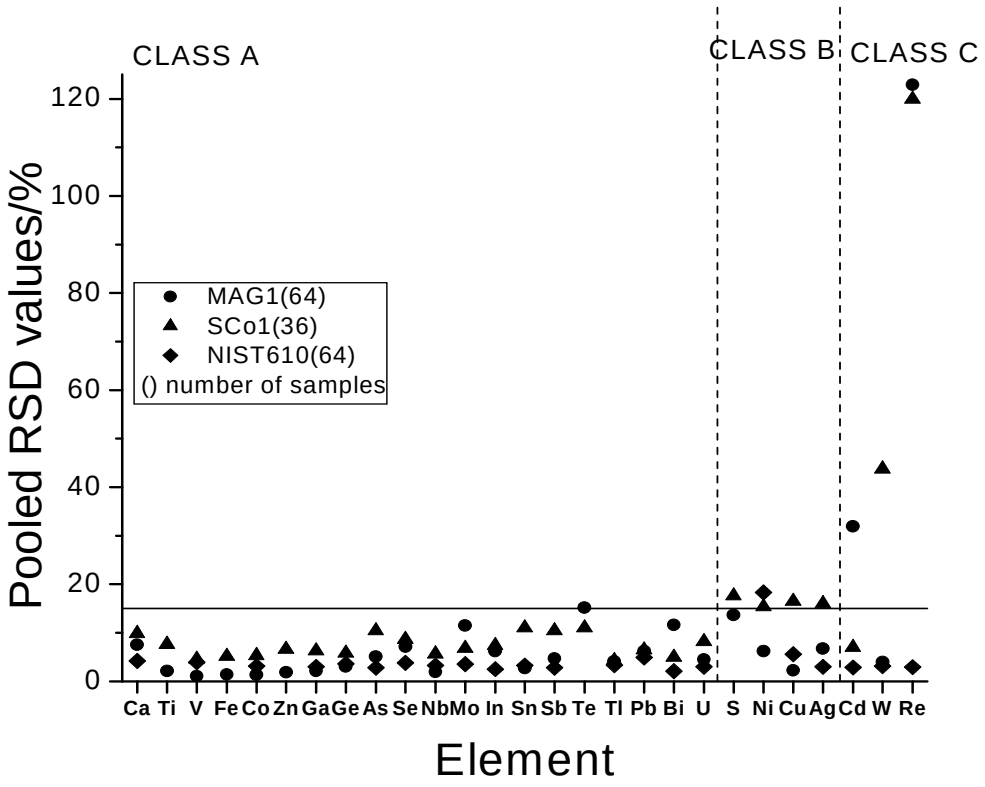

Figure 4 Pooled RSD values for repeated analyses of MAG-1, SCo-1 and NIST 610. CLASS A elements have RSDs < 15%, CLASS B elements have RSDs<20% and CLASS C elements have RSDs >20%

2.3.3 Accuracy

To assess accuracy of this LA-ICP-MS method, I have treated the sediment, MAG-1, and the shale, SCo-1, as "unknowns" and analyzed each of them using the other two SRM's as standards. Analytical errors are then calculated as the deviation of the values I determine from literature values reported for these "unknowns." Figure 5 shows the results when SCo-1 is treated as an unknown sample, and Figure 6 gives comparable values when MAG-1 is the unknown.

These figures show that the best analytical results are obtained when the shale is used as the standard to analyze the sediment, or *vice versa*; worse results are obtained if the glass (NIST610) is used as the standard. This is true for a large group of elements (Ca, Co, Ga, Ge, As, Nb, In, Sn, Sb, Ni, Ti, Zn, and Re) in both figures. For these elements, it appears that matrix-matched standards are important. These elements include both lithophiles (Ca and Ti) and chalcophiles (Zn, Ge, Sn and Sb) so host phase differences are not likely to be the cause of their differing behavior. They also include elements that have a large range in boiling points (Table 3).

For a few elements, determinations using any SRM are inaccurate: Ni, Ga, Mo, In, and Re. In some cases the literature values for SCo-1 and MAG-1may be incorrect. This is likely to be the case for Mo and Re, two trace-metals whose analytical determinations have only recently been made routine. Additionally these two elements are not very volatile (Table 3).

Table 3 Melting and Boiling points of inaccurately determined elements.

ELEMENT	MELTING POINT/ºC	BOILING POINT/ºC
Ca	839	1484
Ti	1660	3287
Zn	420	907
Ge	937	2830
Sn	232	2270
Sb	630	1750
Ni	1453	2732
Ga	30	2430
Cd	321	765
Mo	2617	4612
In	157	2000
W	3410	5660
Re	3180	5627

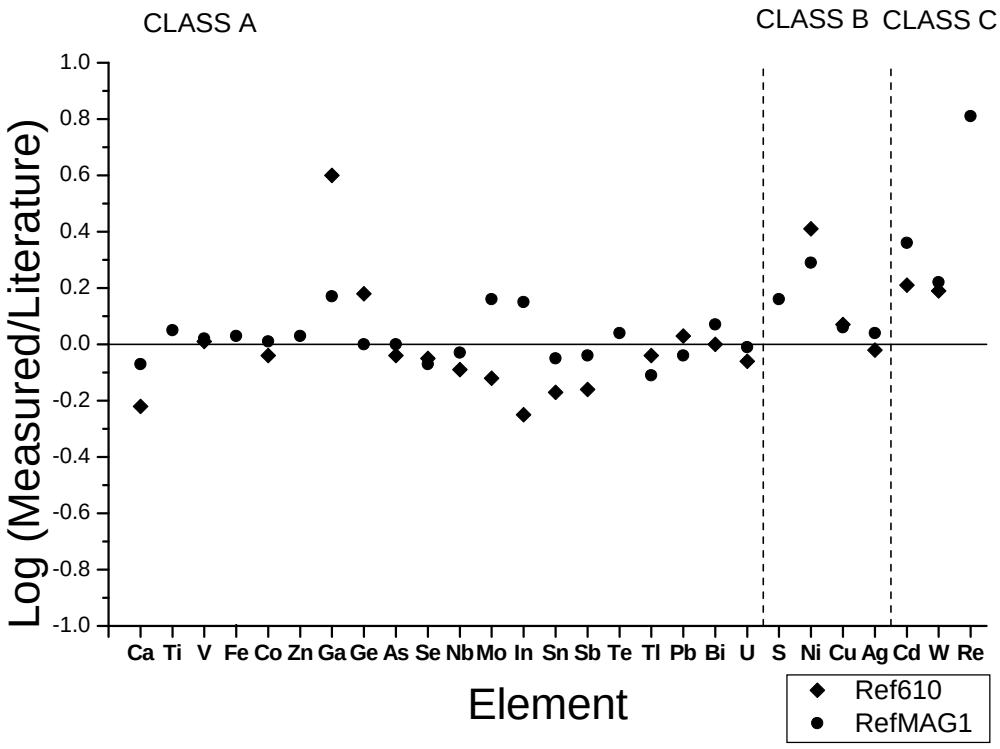

Figure 5 Log of Ratio of SCo-1 LA-ICP-MS determinations to literature values. Diamonds represent SCo-1 measurements when NIST610 was used as the standard while circles represent when MAG-1 was used. Note Re Ref610 value is off-scale.

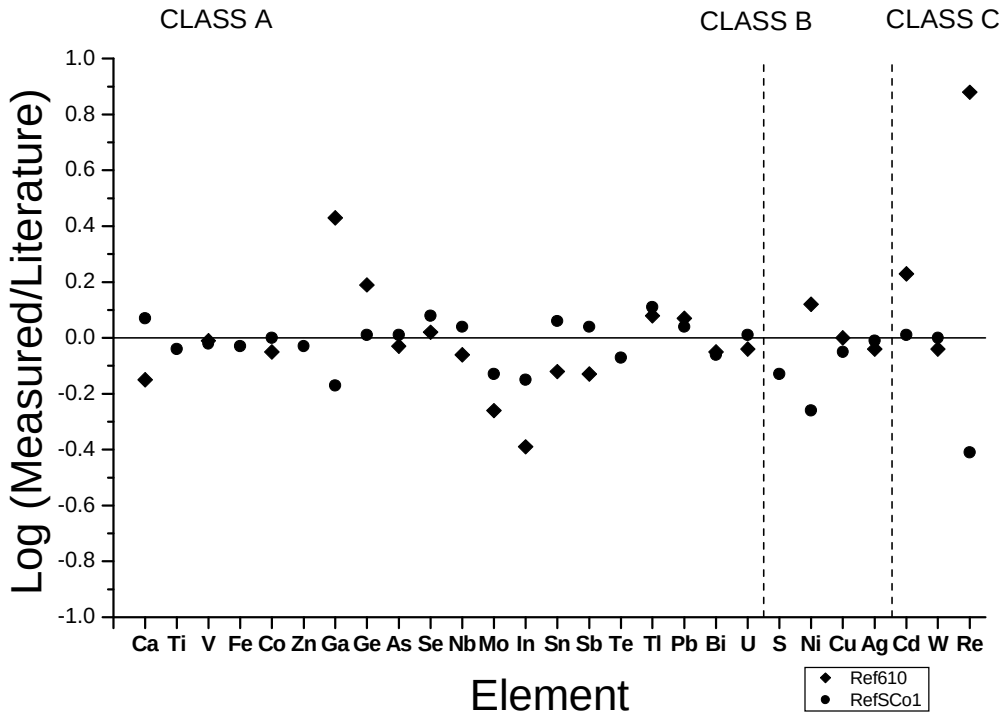

Figure 6 Log of Ratio of MAG-1 LA-ICP-MS determinations to literature values. Diamonds represent MAG-1-1 measurements when NIST610 was used as the standard while circles represent when SCo-1 was used.

2.4 Results and Discussion Chesapeake Bay Samples

I present the concentrations of the elements in Table 4. The uncertainties shown are standard deviations of 4 replicate analyses obtained from different laser tracks over the same sample pellet.

In Figure 7, I present some method comparisons based on previously published independent analyses of the same samples analyzed in this work. The vertical axis indicates results obtained by different operators at different times using several single-element methods; the horizontal axis indicates the results obtained simultaneously by laser ablation. The alternate methods were: Mn and Zn, Direct Current Plasma Emission Spectroscopy (Cantillo, 1982; Cantillo et al., 1984); Pb, Atomic Absorption Spectroscopy (Marcantonio et al., 2002; Zimmerman, 2000); Cu, Flame Atomic Absorption Spectroscopy; and Mo, Isotope Dilution ICP-MS (Adelson, 1997; Adelson et al., 2001).

Figure 7 illustrates the impressive dynamic range of LA-ICP-MS. Concentrations spanning 3 orders of magnitude were determined simultaneously and agreed reasonably with results from diverse single element methods. Except for Mo, deviations of points from the 1:1 line appear to be non-systematic, suggesting that they arise simply from random error in one or both methods being compared. The Mo points appear to lie along a line with a slope of 1.12, implying that the isotope dilution method is determining on average 12% more Mo than the LA-ICP-MS method. This kind of deviation could be caused by a systematic error in determining the Mo concentration by one of these methods.

An important implication of Figure 3 is that my use of Mn as an internal standard is not generating systematic errors in the LA-ICP-MS data. Such errors would affect the LA-ICP-MS results for all elements in the figure. It would be improbable that such errors could be compensated by offsetting systematic errors in the various independent methods against which LA-ICP-MS results are compared in Figure 7.

Table 4 Concentrations of elements ± standard deviations from four replicate LA-ICP-MS analyses on the same sample pellet. Mn values were determined by solution ICP-MS on a digested sub-sample of the sediment.

Depth (cm)	Year	Ti (%)	*Mn (µg/g)*	Fe (%)	Co (µg/g)	Cu (µg/g)	Zn (µg/g)	Ga (µg/g)	Ge (µg/g)	Nb (µg/g)	Mo (µg/g)	Ag (µg/g)	Cd (µg/g)
CORE 55													
-1	**1978.6**	0.43 ± 0.08	*540 ± 40*	3.8 ± 0.6	21 ± 4	44 ± 9	180 ± 40	15 ± 3	1.9 ± 0.6	11 ± 3	4.3 ± 1.4	0.37 ± 0.05	0.68 ± 0.22
-9	**1970**	0.42 ± 0.04	*720 ± 50*	3.9 ± 0.4	20 ± 2	47 ± 7	220 ± 40	15 ± 1	1.8 ± 0.2	11 ± 2	2.7 ± 0.3	0.46 ± 0.06	1.09 ± 0.30
-11	**1967.8**	0.44 ± 0.02	*940 ± 70*	4.3 ± 0.1	26 ± 1	48 ± 2	240 ± 10	17 ± 1	2.0 ± 0.1	13 ± 3	2.3 ± 0.3	0.64 ± 0.01	0.79 ± 0.21
-13	**1965.6**	0.42 ± 0.02	*820 ± 60*	4.2 ± 0.4	25 ± 3	49 ± 2	240 ± 10	14 ± 1	1.9 ± 0.1	11 ± 1	4.4 ± 0.9	0.66 ± 0.06	1.09 ± 0.04
-17	**1964**	0.47 ± 0.06	*790 ± 60*	4.8 ± 0.1	26 ± 1	57 ± 2	265 ± 10	15 ± 1	1.9 ± 0.1	11 ± 2	1.5 ± 0.1	0.72 ± 0.06	1.02 ± 0.22
-21	**1963.1**	0.43 ± 0.02	*870 ± 60*	4.7 ± 0.2	31 ± 2	60 ± 3	280 ± 10	20 ± 1	2.2 ± 0.1	11 ± 1	1.7 ± 0.2	0.85 ± 0.09	0.91 ± 0.05
-27	**1956.8**	0.43 ± 0.01	*840 ± 60*	3.9 ± 0.2	19 ± 1	45 ± 2	220 ± 10	16 ± 1	2.0 ± 0.3	10 ± 1	1.8 ± 0.1	0.38 ± 0.01	1.74 ± 0.16
-33	**1950.8**	0.47 ± 0.05	*810 ± 60*	3.8 ± 0.2	21 ± 1	49 ± 4	230 ± 10	16 ± 1	2.0 ± 0.1	11 ± 1	2.1 ± 0.6	0.48 ± 0.09	1.41 ± 0.26
-45	**1940.1**	0.41 ± 0.01	*980 ± 70*	4.1 ± 0.2	21 ± 1	49 ± 1	210 ± 10	16 ± 1	2.0 ± 0.1	10 ± 1	2.4 ± 0.1	0.16 ± 0.02	1.10 ± 0.12
-51	**1935.1**	0.45 ± 0.02	*730 ± 50*	4.2 ± 0.2	22 ± 1	49 ± 1	200 ± 10	19 ± 1	1.9 ± 0.1	11 ± 1	1.4 ± 0.2	0.17 ± 0.01	0.75 ± 0.06
-55	**1931.8**	0.46 ± 0.06	*650 ± 50*	3.7 ± 0.2	17 ± 1	35 ± 1	180 ± 10	15 ± 1	1.6 ± 0.2	12 ± 1	1.5 ± 0.2	0.13 ± 0.01	0.42 ± 0.07
-59	**1928.7**	0.47 ± 0.05	*710 ± 50*	4.1 ± 0.3	20 ± 2	45 ± 5	190 ± 20	17 ± 1	2.0 ± 0.1	12 ± 1	2.2 ± 0.2	0.15 ± 0.02	0.66 ± 0.17
-69	**1921**	0.51 ± 0.14	*700 ± 50*	3.9 ± 0.2	14 ± 1	29 ± 1	110 ± 10	17 ± 1	2.0 ± 0.2	12 ± 3	1.3 ± 0.1	0.09 ± 0.01	0.39 ± 0.12
-77	**1916.9**	0.48 ± 0.09	*720 ± 50*	4.4 ± 0.1	15 ± 1	29 ± 1	120 ± 10	17 ± 1	1.9 ± 0.1	12 ± 2	1.3 ± 0.1	0.08 ± 0.01	0.28 ± 0.02
-95	**1906.7**	0.40 ± 0.02	*430 ± 30*	3.9 ± 0.2	14 ± 1	26 ± 2	100 ± 10	16 ± 1	2.3 ± 1.2	10 ± 1	1.1 ± 0.3	0.07 ± 0.04	0.25 ± 0.03
-97	**1905.8**	0.43 ± 0.04	*550 ± 40*	4.1 ± 0.2	13 ± 1	26 ± 2	100 ± 10	15 ± 1	1.7 ± 0.1	9 ± 1	1.7 ± 0.1	0.10 ± 0.05	0.24 ± 0.02
-101	**1904**	0.45 ± 0.09	*530 ± 40*	4.0 ± 0.1	15 ± 4	26 ± 3	100 ± 20	15 ± 1	1.8 ± 0.2	10 ± 2	1.4 ± 0.4	0.08 ± 0.02	0.40 ± 0.19
CORE RD													
Depth (cm)	**Year**	**Ti (%)**	***Mn (µg/g)***	**Fe (%)**	**Co (µg/g)**	**Cu (µg/g)**	**Zn (µg/g)**	**Ga (µg/g)**	**Ge (µg/g)**	**Nb (µg/g)**	**Mo (µg/g)**	**Ag (µg/g)**	**Cd (µg/g)**
-5	**1997.8**	0.40 ± 0.05	*600 ± 40*	3.6 ± 0.2	18 ±1	35 ± 2	153 ± 6	10 ± 1	1.7 ± 0.1	10 ± 1	2.3 ± 0.4	0.22 ± 0.04	0.59 ± 0.18
-7	**1997.3**	0.39 ± 0.04	*590 ± 40*	3.7 ± 0.2	18 ± 1	35 ± 1	157 ± 6	10 ± 1	1.8 ± 0.1	9 ± 1	2.2 ± 0.4	0.24 ± 0.03	0.64 ± 0.05
-19	**1994.6**	0.44 ± 0.05	*980 ± 70*	4.2 ± 0.3	18 ± 1	39 ± 2	180 ± 8	11 ± 1	1.8 ± 0.1	11 ± 3	1.9 ± 0.1	0.32 ± 0.10	0.63 ± 0.16
-29	**1992.3**	0.51 ± 0.16	*840 ± 60*	4.8 ± 0.6	22 ± 1	52 ± 5	200 ± 20	10 ± 1	2.1 ± 0.2	12 ± 2	7.0 ± 1.9	0.33 ± 0.08	0.79 ± 0.20
-35	**1990.9**	0.42 ± 0.05	*830 ± 60*	4.0 ± 0.3	23 ± 1	42 ± 2	230 ± 10	15 ± 1	1.7 ± 0.1	10 ± 1	2.4 ± 0.3	0.51 ± 0.11	1.31 ± 0.48
-39	**1989.8**	0.46 ± 0.14	*940 ± 70*	4.1 ± 0.3	21 ± 2	42 ± 3	210 ± 10	16 ± 2	1.9 ± 0.1	11 ± 2	2.0 ± 0.2	0.45 ± 0.08	0.94 ± 0.34
-47	**1987.8**	0.42 ± 0.03	*990 ± 70*	4.2 ± 0.2	23 ± 1	46 ± 3	240 ± 20	9 ± 1	1.6 ± 0.1	11 ± 1	2.3 ± 0.1	0.65 ± 0.31	0.83 ± 0.09
-53	**1986.2**	0.45 ± 0.02	*1220 ± 90*	4.8 ± 0.2	38 ± 3	56 ± 2	370 ± 30	10 ± 1	2.0 ± 0.2	11 ± 1	1.6 ± 0.1	0.74 ± 0.06	1.39 ± 0.76
-59	**1984.7**	0.47 ± 0.03	*1210 ± 90*	4.7 ± 0.2	30 ± 2	51 ± 4	320 ± 30	12 ± 1	2.2 ± 0.1	11 ± 1	1.5 ± 0.1	0.88 ± 0.05	1.04 ± 0.13
-82.5	**1972**	0.37 ± 0.07	*690 ± 50*	3.4 ± 0.2	19 ± 2	39 ± 3	230 ± 20	9 ± 1	1.6 ± 0.1	8 ± 2	1.8 ± 0.2	0.52 ± 0.17	1.09 ± 0.23
-122.5	**1944.5**	0.44 ± 0.08	*750 ± 50*	4.0 ± 0.1	23 ± 1	50 ± 5	250 ± 10	10 ± 1	1.9 ± 0.1	10 ± 1	2.1 ± 0.3	0.33 ± 0.12	1.00 ± 0.19
Chesapeake Bay Sites													
Susq. 8-10cm		0.94 ± 0.17	*2700 ± 200*	7.5 ± 0.3	69 ± 2	101 ± 3	470 ± 40	33 ± 1	3.2 ± 0.2	24 ± 3	2.0 ± 0.2	1.9 ± 0.4	1.9 ± 0.3
Susq 28-30cm		0.37 ± 0.07	*1800 ± 130*	3.4 ± 0.2	42 ± 3	53 ± 8	270 ± 40	15 ± 1	1.6 ± 0.2	9 ± 2	1.5 ± 0.3	1.2 ± 0.3	1.07 ± 0.01
Susq. 44-46cm		0.56 ± 0.07	*1800 ± 130*	5.7 ± 0.2	55 ± 6	102 ± 8	470 ± 60	24 ± 1	2.5 ± 0.1	14 ± 2	2.8 ± 1.3	2.1 ± 0.1	1.2 ± 0.2
Fairhaven		0.36 ± 0.08	*110 ± 10*	2.4 ± 0.3	4 ± 1	17 ± 4	140 ± 10	9 ± 2	1.5 ± 0.1	9 ± 2	13 ± 2	0.44 ± 0.05	10 ± 1.5
B'More Harbor H		0.58 ± 0.04	*650 ± 50*	10 ± 1	36 ± 14	500 ± 100	1800 ± 400	17 ± 1	4.2 ± 0.4	18 ± 1	8.5 ± 1.4	2.5 ± 1	9 ± 7
B'More Harbor M		0.48 ± 0.03	*4800 ± 400*	7.4 ± 0.3	21 ± 2	1800 ± 200	900 ± 150	20 ± 1	2.5 ± 0.2	9 ± 1	5.9 ± 1	7.2 ± 4	7.7 ± 2
B'More Harbor N		0.54 ± 0.07	*860 ± 60*	6.8 ± 0.6	30 ± 4	730 ± 80	1000 ± 100	21 ± 2	2.9 ± 0.2	14 ± 2	3.2 ± 0.2	4.1 ± 0.2	6.8 ± 0.8
PC6 369 cm		0.43 ± 0.08	*520 ± 40*	3.9 ± 0.1	13 ± 1	18 ± 3	75 ± 10	15 ± 1	1.6 ± 0.2	9 ± 1	1.8 ± 0.3	0.07 ± 0.01	0.17 ± 0.05
PC6 424 cm		0.59 ± 0.15	*510 ± 40*	4.1 ± 0.2	15 ± 1	18 ± 1	84 ± 7	16 ± 2	1.7 ± 0.2	14 ± 3	4.1 ± 0.7	0.07 ± 0.03	0.19 ± 0.04
PC6 482 cm		0.44 ± 0.12	*510 ± 40*	3.7 ± 0.1	13 ± 1	14 ± 1	77 ± 2	15 ± 1	1.5 ± 0.1	10 ± 2	1.8 ± 0.2	0.11 ± 0.09	0.11 ± 0.05
Water-depth 3.4		0.46 ± 0.05	*3000 ± 200*	6.3 ± 0.4	39 ± 1	62 ± 2	490 ± 20	19 ± 1	2.6 ± 0.1	13 ± 1	1.9 ± 0.1	0.88 ± 0.02	1.37 ± 0.13
Water-depth 6.7		0.48 ± 0.15	*2200 ± 200*	5.7 ± 1	48 ± 8	80 ±20	500 ± 100	19 ± 4	2.5 ± 0.6	14 ± 4	2.4 ± 0.5	1.7 ± 0.4	0.94 ± 0.32
Water-depth 26.2		0.42 ± 0.09	*1000 ± 70*	4.1 ± 0.9	28 ± 4	50 ± 10	290 ± 40	15 ± 4	2.2 ± 0.6	11 ± 2	2.2 ± 0.8	0.89 ± 0.18	0.77 ± 0.18

Table 4 cont.

CORE 55

Depth (cm)	Year	In (µg/g)	Sn (µg/g)	Sb (µg/g)	Te (µg/g)	W (µg/g)	Re (ng/g)*	Tl (µg/g)	Pb (µg/g)	Bi (µg/g)	U (µg/g)
-1	1978.6	0.18 ± 0.03	4.6 ± 0.8	0.93 ± 0.19	0.08 ± 0.02	1.45 ± 0.34	8 ± 3	0.87 ± 0.17	45 ± 7	0.37 ± 0.08	5.9 ± 2.2
-9	1970	0.19 ± 0.01	4.8 ± 0.7	1.02 ± 0.10	0.10 ± 0.01	1.62 ± 0.10	6 ± 3	0.90 ± 0.10	50 ± 5	0.35 ± 0.04	4.7 ± 0.5
-11	1967.8	0.23 ± 0.02	5.9 ± 0.2	1.17 ± 0.04	0.13 ± 0.01	1.82 ± 0.29	20 ± 9	0.88 ± 0.08	56 ± 3	0.42 ± 0.02	4.2 ± 0.8
-13	1965.6	0.24 ± 0.04	5.7 ± 0.3	1.09 ± 0.09	0.12 ± 0.04	1.67 ± 0.21	4 ± 3	1.02 ± 0.08	63 ± 5	0.45 ± 0.03	4.9 ± 0.6
-17	1964	0.24 ± 0.04	6.2 ± 1.2	1.18 ± 0.13	0.13 ± 0.01	1.65 ± 0.07	11 ± 2	0.97 ± 0.04	67 ± 3	0.46 ± 0.01	5.1 ± 0.2
-21	1963.1	0.22 ± 0.01	6.6 ± 0.5	1.13 ± 0.10	0.10 ± 0.01	1.84 ± 0.14	12 ± 34	0.86 ± 0.07	59 ± 2	0.41 ± 0.02	3.4 ± 0.4
-27	1956.8	0.17 ± 0.01	4.1 ± 0.3	0.84 ± 0.06	0.12 ± 0.01	1.27 ± 0.16	2.0 ± 0.2	0.96 ± 0.06	44 ± 2	0.31 ± 0.02	3.2 ± 0.2
-33	1950.8	0.18 ± 0.01	4.4 ± 0.2	0.86 ± 0.11	0.13 ± 0.02	1.23 ± 0.06	4 ± 3	0.85 ± 0.08	46 ± 4	0.33 ± 0.03	3.1 ± 0.6
-45	1940.1	0.22 ± 0.03	6.3 ± 0.2	1.4 ± 1	0.11 ± 0.01	1.23 ± 0.02	22 ± 13	0.93 ± 0.04	55 ± 1	0.38 ± 0.01	4.8 ± 0.7
-51	1935.1	0.21 ± 0.01	5.8 ± 0.4	0.81 ± 0.06	0.15 ± 0.01	1.27 ± 0.07	0.8 ± 0.4	0.73 ± 0.03	42 ± 2	0.37 ± 0.01	2.7 ± 0.1
-55	1931.8	0.18 ± 0.01	4.4 ± 0.1	0.82 ± 0.05	0.10 ± 0.02	1.13 ± 0.10	1.1 ± 0.2	0.55 ± 0.01	32 ± 1	0.30 ± 0.01	2.6 ± 0.2
-59	1928.7	0.21 ± 0.01	5.6 ± 0.3	0.82 ± 0.03	0.12 ± 0.02	1.16 ± 0.11	3 ± 02	0.67 ± 0.05	42 ± 5	0.39 ± 0.03	3.3 ± 0.5
-69	1921	0.16 ± 0.01	2.9 ± 0.2	0.46 ± 0.03	0.04 ± 0.02	1.25 ± 0.24	4 ± 5	0.59 ± 0.03	25 ± 2	0.27 ± 0.03	3.0 ± 0.8
-77	1916.9	0.17 ± 0.01	3.2 ± 0.1	0.65 ± 0.15	0.04 ± 0.01	1.41 ± 0.16	2.7 ± 0.5	0.64 ± 0.03	24 ± 2	0.28 ± 0.01	2.7 ± 0.2
-95	1906.7	0.17 ± 0.05	2.7 ± 0.3	0.44 ± 0.03	0.03 ± 0.02	1.11 ± 0.07	3 ± 3	0.54 ± 0.03	21 ± 1	0.28 ± 0.03	2.8 ± 0.4
-97	1905.8	0.15 ± 0.06	2.7 ± 0.4	0.44 ± 0.05	0.03 ± 0.01	1.14 ± 0.15	5 ± 3	0.58 ± 0.04	20 ± 2	0.24 ± 0.02	2.6 ± 0.3
-101	1904	0.13 ± 0.02	2.6 ± 0.2	0.52 ± 0.22	0.04 ± 0.01	1.20 ± 0.27	5 ± 4	0.65 ± 0.21	20 ± 2	0.23 ± 0.02	2.3 ± 0.2

CORE RD

Depth (cm)	Year	In (µg/g)	Sn (µg/g)	Sb (µg/g)	Te (µg/g)	W (µg/g)	Re (ng/g)*	Tl (µg/g)	Pb (µg/g)	Bi (µg/g)	U (µg/g)
-5	1997.8	0.15 ± 0.01	4.0 ± 0.5	0.82 ± 0.35	0.07 ± 0.01	1.54 ± 0.39	6 ± 3	0.86 ± 0.03	40 ± 2	0.31 ± 0.02	2.8 ± 0.3
-7	1997.3	0.21 ± 0.05	7 ± 5	0.74 ± 0.10	0.05 ± 0.01	1.41 ± 0.15	30 ± 20	0.80 ± 0.03	39 ± 3	0.29 ± 0.02	2.6 ± 0.1
-19	1994.6	0.20 ± 0.04	6 ± 2	0.84 ± 0.09	0.09 ± 0.01	1.89 ± 0.89	20 ± 10	0.82 ± 0.04	45 ± 3	0.32 ± 0.02	2.5 ± 0.2
-29	1992.3	0.23 ± 0.05	5.2 ± 0.5	1.0 ± 0.1	0.08 ± 0.01	1.53 ± 0.20	6 ± 2	1.01 ± 0.10	64 ± 4	0.39 ± 0.03	5.6 ± 1.1
-35	1990.9	0.17 ± 0.01	4.7 ± 0.3	0.87 ± 0.09	0.09 ± 0.01	1.31 ± 0.09	5 ± 1	0.79 ± 0.04	67 ± 10	0.37 ± 0.02	3.2 ± 0.9
-39	1989.8	0.17 ± 0.02	4.8 ± 0.5	0.88 ± 0.09	0.10 ± 0.01	1.39 ± 0.23	8 ± 2	0.78 ± 0.07	58 ± 8	0.36 ± 0.02	2.8 ± 0.5
-47	1987.8	0.19 ± 0.01	5.1 ± 0.3	1.15 ± 0.06	0.12 ± 0.01	1.36 ± 0.13	5.6 ± 0.3	0.81 ± 0.04	60 ± 7	0.38 ± 0.02	2.9 ± 0.2
-53	1986.2	0.21 ± 0.01	6.2 ± 0.6	1.49 ± 0.35	0.13 ± 0.01	1.53 ± 0.06	20 ± 10	0.92 ± 0.07	63 ± 4	0.48 ± 0.03	3.0 ± 0.1
-59	1984.7	0.24 ± 0.02	6.6 ± 0.5	1.32 ± 0.05	0.17 ± 0.01	1.62 ± 0.10	7 ± 1	0.82 ± 0.05	65 ± 6	0.43 ± 0.02	2.8 ± 0.2
-82.5	1972	0.16 ± 0.01	4.2 ± 0.4	0.78 ± 0.06	0.12 ± 0.01	1.11 ± 0.10	16. ± 3	0.66 ± 0.05	50 ± 2	0.31 ± 0.02	2.7 ± 0.2
-122.5	1944.5	0.23 ± 0.01	5.5 ± 0.3	1.03 ± 0.05	0.15 ± 0.01	1.19 ± 0.05	17 ± 7	0.76 ± 0.02	57 ± 5	0.37 ± 0.01	2.5 ± 0.1

Chesapeake Bay Sites

Susq. 8-10cm	0.34 ± 0.05	9.3 ± 0.3	1.81 ± 0.10	0.11 ± 0.01	5.02 ± 0.39	4 ± 1	1.04 ± 0.04	76 ± 1	0.63 ± 0.06	4.8 ± 0.4
Susq 28-30cm	0.18 ± 0.02	5.0 ± 0.5	0.98 ± 0.12	0.04 ± 0.01	3.29 ± 0.74	2 ± 1	0.53 ± 0.05	44 ± 7	0.41 ± 0.08	3.2 ± 0.7
Susq. 44-46cm	0.34 ± 0.03	9.6 ± 1.3	2.09 ± 0.34	0.07 ± 0.01	4.00 ± 0.72	3 ± 1	0.88 ± 0.09	65 ± 5	0.77 ± 0.34	4.7 ± 0.3
Fairhaven	0.11 ± 0.02	1.9 ± 0.2	1.08 ± 0.2	0.13 ± 0.04	0.74 ± 0.11	15 ± 2	0.66 ± 0.14	10 ± 2	0.14 ± 0.01	9.7 ± 3.4
B'More Harbor H	1.7 ± 0.2	105 ± 18	10 ± 4	9 ± 2	3.72 ± 0.31	4 ± 2	0.78 ± 0.11	320 ± 30	1.54 ± 0.13	8.0 ± 0.7
B'More Harbor M	0.70 ± 0.09	37 ± 4	17 ± 3	75 ± 22	1.73 ± 0.13	2 ± 1	1.04 ± 0.08	640 ± 80	5.1 ± 1.2	6.1 ± 0.8
B'More Harbor N	0.72 ± 0.12	37 ± 2	8 ± 2	14 ± 2	3.36 ± 0.41	4 ± 1	0.96 ± 0.04	370 ± 30	1.44 ± 0.10	6.0 ± 0.7
PC6 369 cm	0.13 ± 0.01	2.3 ± 0.3	0.44 ± 0.06	0.11 ± 0.07	0.95 ± 0.06	16 ± 7	0.48 ± 0.02	19 ± 2	0.26 ± 0.03	2.6 ± 0.4
PC6 424 cm	0.15 ± 0.04	2.8 ± 0.6	0.57 ± 0.07	0.05 ± 0.02	1.34 ± 0.32	11 ± 1	0.53 ± 0.06	16 ± 1	0.22 ± 0.09	3.9 ± 0.8
PC6 482 cm	0.16 ± 0.03	2.4 ± 0.3	0.43 ± 0.10	0.04 ± 0.01	0.92 ± 0.13	4 ± 2	0.46 ± 0.02	16 ± 2	0.21 ± 0.03	2.7 ± 0.4
Water-depth 3.4	0.29 ± 0.02	8.7 ± 1.8	2.1 ± 0.2	0.24 ± 0.01	2.67 ± 0.10	7 ± 2	0.73 ± 0.06	77 ± 2	0.55 ± 0.04	3.7 ± 0.2
Water-depth 6.7	0.33 ± 0.08	9.1 ± 2.1	2.0 ± 0.5	0.24 ± 0.06	2.38 ± 0.57	3 ± 1	0.81 ± 0.17	80 ± 20	0.59 ± 0.14	4.1 ± 1.0
Water-depth 26.2	0.22 ± 0.05	5.5 ± 1.3	1.2 ± 0.4	0.13 ± 0.04	1.51 ± 0.39	2 ± 1	0.68 ± 0.14	48 ± 6	0.35 ± 0.08	2.7 ± 0.5

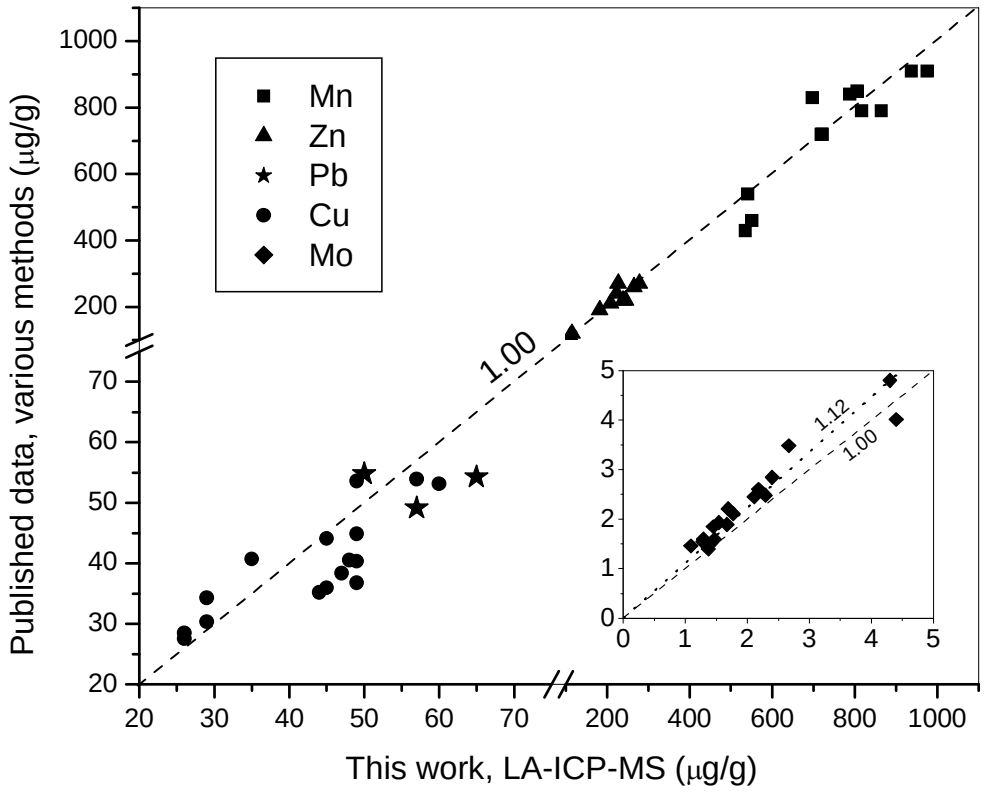

Figure 7 Good agreement between independent determinations of five elements. Alternate methods: Mn and Zn, direct current plasma emission spectroscopy; Pb, atomic absorption spectroscopy; Cu, flame atomic absorption spectroscopy; and Mo, isotope dilution ICP-MS. See text for sources of alternate method data.

To facilitate comparisons among the large number of element concentrations that have been determined in Chesapeake Bay sediments and related samples, I present analytical results graphically in terms of enrichment factors (EFs). Enrichment factors have the advantage of putting all elements on a common scale, representing the proportionate departure of each element in a sample from a reference composition.

Element concentrations are double-normalized when generating an EF. The first normalization is to a major component of the fine-grained fraction of the sediment. Iron or aluminum are common choices and have been shown to be equally suitable (Daskalakis and O'Connor, 1995). In this work, Fe is used for normalization; Al was not determined owing to analytical complications arising from its high abundance. The purpose of this first normalization is to compensate for variable dilution of samples by sand-sized particles. Such large particles, typically of quartz, tend to dilute both Fe and trace elements but have much less effect on X/Fe ratios.

The second normalization is to the X/Fe ratio in a reference material:

$$EF = \frac{\left(X/Fe\right)_{SAMPLE}}{\left(X/Fe\right)_{REF}} \qquad (2.4)$$

This second normalization is simply a scaling factor that makes EF = 1 for all elements if their X/Fe ratios are the same as in the reference material. As reference values, I will use average (X/Fe) ratios in the three oldest samples from Core 55 (94-96 cm, 96-98 cm and 100-102 cm). Sediments in these samples were deposited near the beginning of the 20th century. In Table 5, I give the reference concentrations for

each element and compare them to the corresponding median values in fine-grained sediments or average shale.

Table 5 Average element concentrations (μg/g) in the three deepest samples in core 55 and comparison to median values in shale. Median shale values are from (Hu and Gao, 2008) except those marked by an asterisk which are from (Turekian and Wedepohl, 1961). [1] The Re median shale value is from Li (2000).

Element	Deep core 55	Median shale	Element	Deep core 55	Median shale
Ti	4300	4375	Mo	1.4	0.48(2.6*)
V	117	110	Ag	0.082	0.07*
Mn	505	620	Cd	0.3	0.063(13*)
Fe	40100	42000	In	0.15	0.073
Co	14	14	Sn	2.7	3.3
Ni	73	36(68*)	Sb	0.47	0.75
Cu	26	27	Te	0.032	0.039
Zn	98	71	W	1.6	2.22
Ga	15	20	Re	0.004	0.0004[1]
Ge	1.9	1.9	Tl	0.59	0.84
As	13	4.4(13*)	Pb	20	19.3
Se	0.85	0.6*	Bi	0.25	0.37
Nb	9.5	15	U	2.6	2.88

For the most part, my reference composition, determined by the LA-ICP-MS method, resembles median values of fine-grained sediments. Exceptions include Mo and Cd, which are more abundant in my reference composition than in fine-grained sediments as determined by Hu and Gao (2008) but not relative to average shale as determined by Turekian and Wedepohl (1961; see parenthetical values in the Table).

In Figure 8, results are presented for Cu, Zn, Cd and Pb, the most commonly determined industrial pollutants. Four replicate analyses on different parts of each pressed sediment pellet are represented by small closed symbols; average values are represented by larger open symbols. The replicate determinations agree so well that

most of the closed points lie within the open symbols (Cd is an exception). The vertical line in each graph denotes an enrichment factor of 1. After 1920, all four elements are enriched relative the early 20th century reference composition, but a slight decrease in enrichment seems to occur after 1980. The four elements in Figure 4 are all enriched in Baltimore Harbor and the Susquehanna River, but not in the pre-European settlement samples of PC6. The considerable enrichment of these elements in the Harbor is most likely due to historical smelting operations in Baltimore (Mason et al., 2004). These elements have been found to be associated with smelting operations at other locations (Buchauer, 1973; Du et al., 2008; Hong et al., 1996). Additionally, Pb and Cd pigments would have been used in paint manufacturing, an important industry in Baltimore. Only Cd is strongly enriched in the Miocene Fairhaven sample. All the profiles shown in the graphs indicate that there is good agreement between cores 55 and RD.

Lead is a major indicator of anthropogenic influence in the Chesapeake Bay. The Pb profile presented here agrees with others from this region as well as others around the U.S. and indicates that Pb concentrations began to decrease very soon after the decrease in the use of leaded gasoline in the late 1970's (Alexander and Smith, 1988; Edgington and Robbins, 1976; Eisenreich et al., 1986; Graney et al., 1995; Heit et al., 1981; Lantzy and Mackenzie, 1979; Lima et al., 2005; Marcantonio et al., 2002).

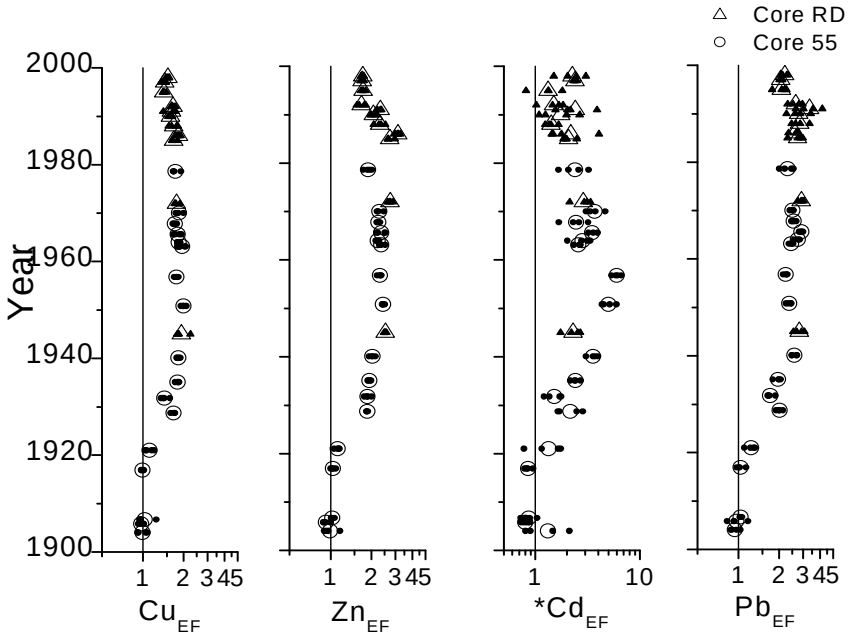

	Cu_{EF}	Zn_{EF}	Cd_{EF}	Pb_{EF}
Susq 8-10 cm	2.06	2.50	3.46	1.98
Susq 28-30 cm	2.40	3.24	4.40	2.55
Susq. 44-46 cm	2.77	3.34	2.88	2.25
Fairhaven	1.09	4.84	59.61	0.84
B'more Harbor H	6.89	6.84	12.45	5.78
B'more Harbor M	38.45	5.01	14.46	17.01
B'more Harbor N	16.52	6.28	14.00	10.71
PC6 369 cm	0.72	0.78	0.61	0.99
PC6 424 cm	0.66	0.82	0.64	0.77
PC6 482 cm	0.57	0.85	0.43	0.86
Water-depth 3.4 m	1.51	3.11	3.03	2.40
Water-depth 6.7 m	2.06	3.50	2.30	2.75
Water-depth 26.2 m	1.95	2.88	2.61	2.26

Figure 8 Enrichment factors (Equation 2.4) for four commonly determined industrial pollutants: Cu, Zn, Cd, Pb. The table gives corresponding EF values for samples from potential sediment sources: Susq, Susquehanna River sediments from Conowingo Reservoir; Fairhaven, unlithified Miocene seacliff material that is undergoing wave erosion; B'more Harbor, sediments from Baltimore Harbor; PC6, deep samples from below the oak/ragweed pollen horizon that marks the onset of European land clearance. The Water-depth samples are surface sediments taken from shallow to deep water near the site of cores RD and 55. Sample localities are given in Figure 2.

In Figure 9, results are presented for some rarely determined elements: In, Sn, Sb, Te and Bi. To my knowledge, these elements have never been determined previously in Chesapeake Bay sediments. Like the commonly determined pollutants, these elements all show enrichment after 1920 and a slight decrease after 1980. Commercial usages of all of these elements, except Te, have increased in recent decades as substitutes for Pb because they are less toxic (Hou et al., 2005). These elements are strongly enriched in the Harbor and only mildly enriched in the Susquehanna sediments. As discussed below, all of these elements are potentially hazardous in the environment. These results provide evidence that these elements are pollutants in Chesapeake Bay and their concentrations should be monitored along with the more commonly determined elements presented in Figure 8.

Indium is produced during zinc ore processing and is used in a wide range of electronic industries such as semi-conductor and opto-electronic manufacturing (USGS, 2005). Indium is frequently associated with mineral deposits of Zn, Cu, Mn, Sn and Pb which points to its geochemical similarities to these elements (Poledniok, 2007). Indium has been found to be toxic to embryos in animal experiments (Hou et al., 2005; Nakajima et al., 2000).

Tin is mainly mined from cassiterite (SnO_2) deposits and has many uses in alloys, electrical/electronic applications as well as in glass-making (USGS, 2005). One particularly relevant modern source of Sn in the Chesapeake Bay is marine paint since organotin compounds are used as anti-fouling agents (Antizar-Ladislao, 2008;

Beaumont and Budd, 1984). Historically, Sn was used in canning foods, a major industry in Baltimore after about 1860.

Antimony has been used for centuries as a medicine and cosmetic. It is used as a hardener in lead for storage batteries and in flame-retardant formulations (USGS, 2005). Antimony is one of the pollutants from coal-fired power plants (Klein et al., 1975) and despite its known toxicity, its geochemical behavior in sediments has not been extensively studied (Chen et al., 2003; Hou et al., 2005). One key finding is that it is associated with iron and manganese hydroxides and is thus released under reducing conditions in sediments (Chen et al., 2003). This is of particular importance in the Chesapeake Bay where seasonal anoxia occurs.

Tellurium is produced as a by-product of copper processing (USGS, 2005), a major industry in Baltimore from the early 19th to the middle 20th centuries. Tellurium is used in semiconductor materials, a wide range of electronics and metallurgy (D'Ulivo, 1997). Tellurium affects the nervous system and produces selenium-deficiency symptoms (Sadeh, 1987). Organisms transform inorganic Te to organotellurium compounds which are volatile and can be more easily released (D'Ulivo, 1997; Sadeh, 1987). Tellurium has not received as much attention as two of its periodic table neighbors As and Se, but my results show that it is among the most highly enriched elements in Chesapeake Bay sediments, so the origin of this contamination should be further investigated.

Bismuth is a by-product of lead-ore processing. It is used in solders, a variety of alloys, additives, medications and in atomic research (USGS, 2005). Like Sb, Bi is released during the combustion of fossil fuels (Karlsson et al., 2007). Very little

environmental monitoring of bismuth has been done because its inorganic form exhibits low toxicity, however organobismuth compounds such as triphenylbismuth are toxic (Arata et al., 2002; Dopp et al., 2004). Bismuth causes disorders of the kidneys, liver and nervous system (Dipalma, 1988; Hou et al., 2005; Winship, 1983).

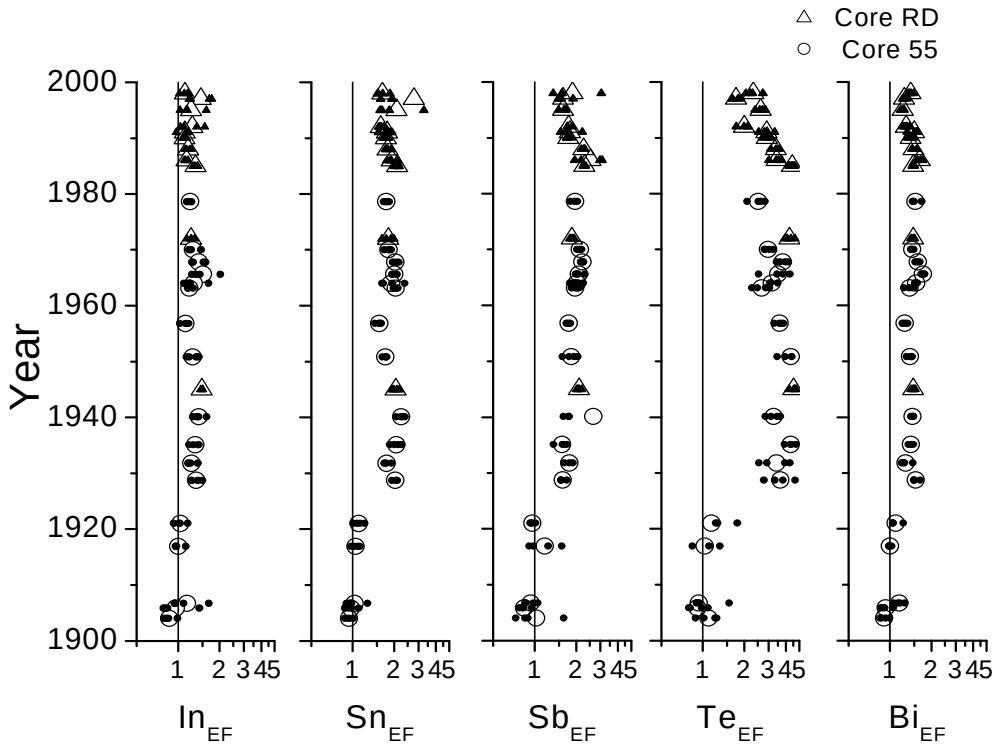

	In	Sn	Sb	Te	Bi
Susq 8-10cm	1.18	1.82	1.92	1.80	1.34
Susq 28-30cm	1.39	2.17	2.30	1.47	1.93
Susq 44-46cm	1.58	2.50	2.95	1.60	2.19
Fairhaven	1.26	1.17	3.67	6.98	0.96
B'more Harbor H	4.11	14.67	7.64	102.88	2.33
B'more Harbor M	2.47	7.38	18.29	1059.82	11.08
B'more Harbor N	2.81	8.19	9.21	266.54	3.41
PC6 369cm	0.87	0.87	0.92	3.65	1.07
PC6 424cm	0.98	1.01	1.10	1.60	0.84
PC6 482cm	1.12	0.96	0.95	1.19	0.90
Water-depth 3.4 m	1.22	2.05	2.60	4.65	1.40
Water-depth 6.7 m	1.53	2.34	2.82	5.18	1.65
Water-depth 26.2 m	1.37	1.96	2.35	4.01	1.36

Figure 9 Enrichment factors (Equation 2.4) for rarely determined industrial pollutants: In, Sn, Sb, Te, Bi. The table gives corresponding EF values for samples from potential sediment sources (see Figure 8 for details).

In Figure 10 results are presented for Mn, Co, Ag and Tl. Once more these elements follow the pattern of industrial pollutants and are enriched after 1920. It is somewhat surprising to find Mn included here. Profiles of Mn in sediments usually are controlled by diagenesis. However, in Chesapeake Bay, diagenetically active Mn tends to be refluxed out of the reduced, deep-channel sediments and deposited in shallower sediments that are exposed to oxic water throughout the year (Helz et al. 1985a). This effect can be seen in Figure 6 in the data taken at three water depths; at the shallowest site, Mn is 3-fold enriched relative to my deep water reference composition. As a consequence of refluxing, deep channel sites accumulate Mn in forms that are less active diagenetically. Possibly, the modest Mn enrichment after 1920 in Figure 6 reflects contamination of the Bay with diagenetically refractory Mn.

Silver is highly enriched in all the supplementary samples in Figure 6 except PC6. Silver has been found to cycle with lead and copper in coastal waters (Sanudo-Wilhelmy and Flegal, 1992). My results are consistent with these findings since Ag is enriched in the same samples and to a similar degree that Cu and Pb are. Notably, Tl is enriched only in the Fairhaven sample and seems to be depleted in Baltimore Harbor, so it is curious that Tl displays a profile that I associate with industrial contaminants, however faintly.

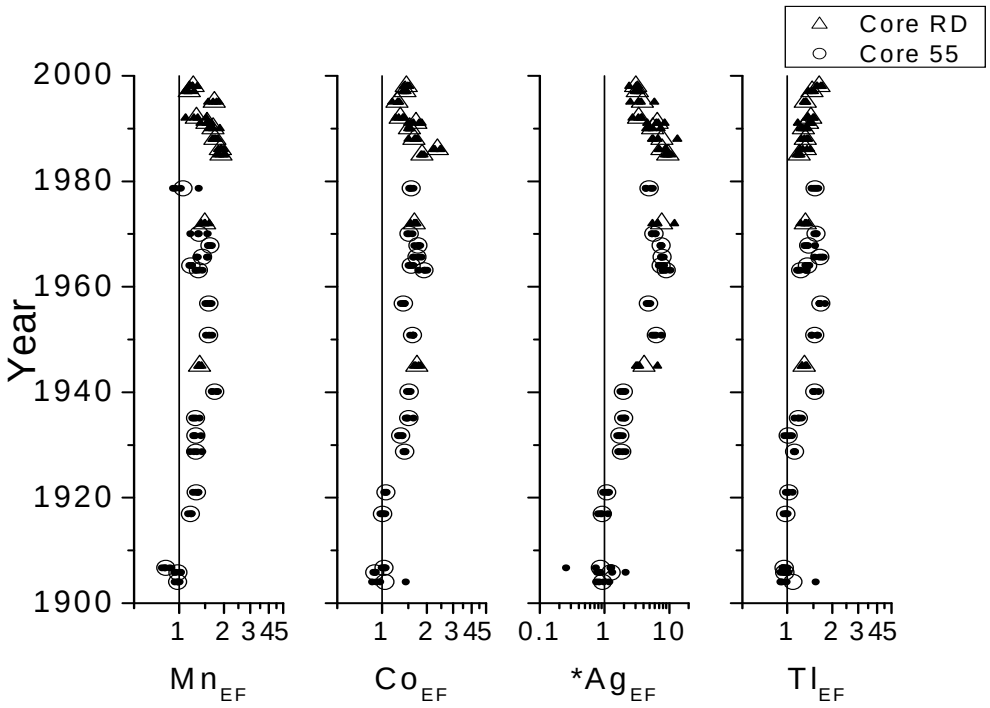

	Mn_{EF}	Co_{EF}	Ag_{EF}	Tl_{EF}
Susq 8-10cm	2.62	2.70	12.76	0.94
Susq 28-30cm	3.87	3.58	17.99	1.07
Susq. 44-46cm	2.35	2.83	18.15	1.06
Fairhaven	0.33	0.51	9.44	1.92
B'more Harbor H	0.45	1.00	11.81	0.50
B'more Harbor M	0.48	0.83	48.88	0.96
B'more Harbor N	0.96	1.32	30.34	0.96
PC6 369cm	1.00	0.97	0.89	0.85
PC6 424cm	0.92	1.03	0.85	0.88
PC6 482cm	1.01	1.04	1.45	0.85
Water-depth 3.4 m	3.50	1.82	6.70	0.79
Water-depth 6.7 m	2.87	2.48	15.42	0.96
Water-depth 26.2 m	1.81	2.00	10.22	1.13

Figure 10 Enrichment factors (Equation 2.4) for elements which appear to be industrially enhanced: Mn, Co, Ag, Tl. The table gives corresponding EF values for samples from potential sediment sources (see Figure 8 for details).

In Figure 11, results are presented for the redox-sensitive elements Mo, Re and U and the possible redox-sensitive element W. These elements are only modestly enriched, if at all, in the Susquehanna and Harbor sediments. In this respect, their distributions contrast with distributions of most of the other elements discussed up to this point. Mo, Re and U are all strongly enriched in the Miocene Fairhaven unit, which resembles black shales in composition. Erosion of the unlithified Fairhaven formation may have supplied enriched sediments to the PC-6 site prior to European settlement, accounting for the modest enrichment of those samples (Adelson et al. 2001).

Tungsten is directly below molybdenum in Group VIB and these two elements form analogous thio-compounds i.e. thiomolybdates and thiotungstates. Since Mo has been established as a redox-sensitive element due to the formation of particle-reactive thiomolybdates (Helz et al., 1996), I hypothesized that W would exhibit similar behavior. However, the profile presented here illustrates that W does not follow Mo. In fact, in the Susquehanna and depth-traverse sediments, W closely mirrors Mn (Bednar et al., 2008).

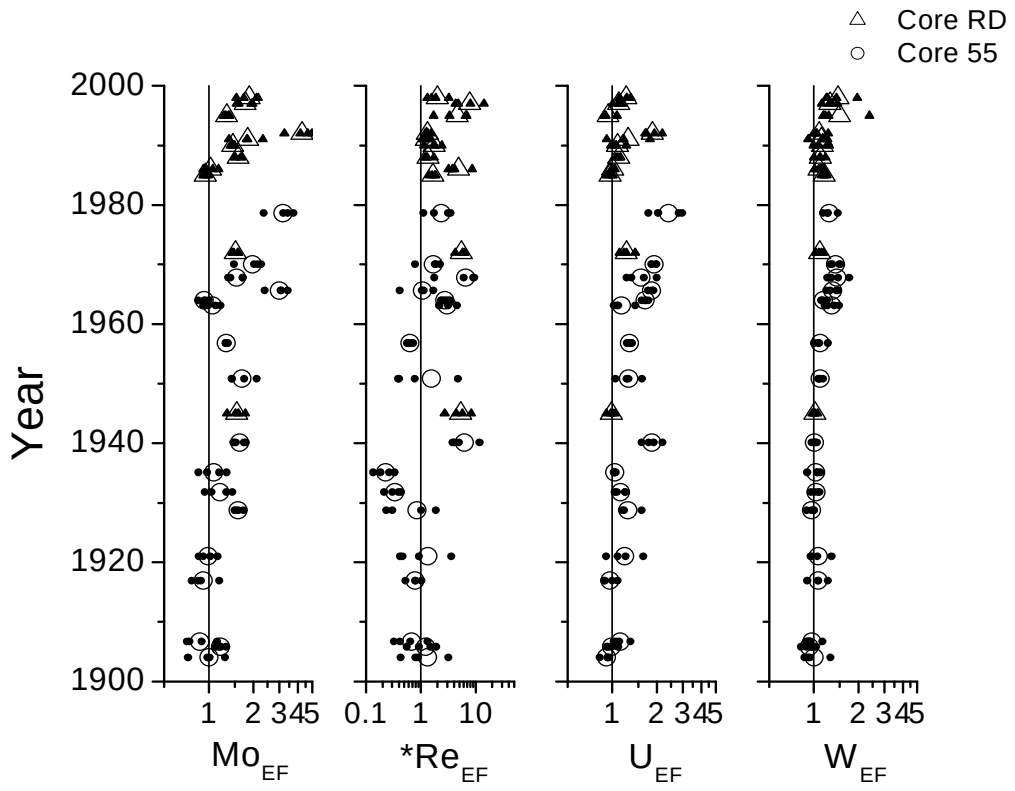

	Mo_{EF}	Re_{EF}	U_{EF}	W_{EF}
Susq 8-10cm	0.82	0.51	1.02	2.26
Susq 28-30cm	1.38	0.61	1.47	3.27
Susq. 44-46cm	1.50	0.48	1.33	2.39
Fairhaven	16.88	6.83	6.57	1.06
B'more Harbor H	2.43	0.41	1.20	1.18
B'more Harbor M	2.42	0.26	1.31	0.79
B'more Harbor N	1.46	0.65	1.41	1.69
PC6 369cm	1.40	4.43	1.09	0.83
PC6 424cm	3.04	2.86	1.49	1.10
PC6 482cm	1.48	1.21	1.19	0.85
Water-depth 3.4 m	0.92	1.20	0.94	1.43
Water-depth 6.7 m	1.27	0.53	1.15	1.41
Water-depth 26.2 m	1.66	0.61	1.05	1.25

Figure 11 Enrichment factors (Equation 2.4) for redox sensitive elements: Mo, Re, U, (W). The table gives corresponding EF values for samples from potential sediment sources (see Figure 8 for details).

The Mo mean values also appear to be greatly scattered, but in contrast to Re, I believe that the Mo scatter reflects actual fluctuations in the Mo deposition rate, not analytical uncertainty. To illustrate this, in Figure 12 I plot three independent determinations of Mo and corresponding determinations of Cu. I have connected the mean values of these independent determinations with line segments. It is apparent that the highly variable vertical Mo profile is affirmed by all three sets of data. This excludes analytical error as a source of the variation. Furthermore there is a marked contrast between the profiles of Mo and Cu. Whereas Cu, representative of industrial pollutants, rises to a steady level of enrichment between 1920 and 1980, Mo fluctuates between high and low enrichment in the same period. Adelson et al. (2001) have attributed this to fluctuations in redox conditions in Chesapeake Bay related to year-to-year variations in river flow. The pronounced minimum in the Mo profile in the 1960's occurred during a period of multi-year drought. Drought deters seasonal anoxia and consequent Mo enrichment (Adelson et al. 2001).

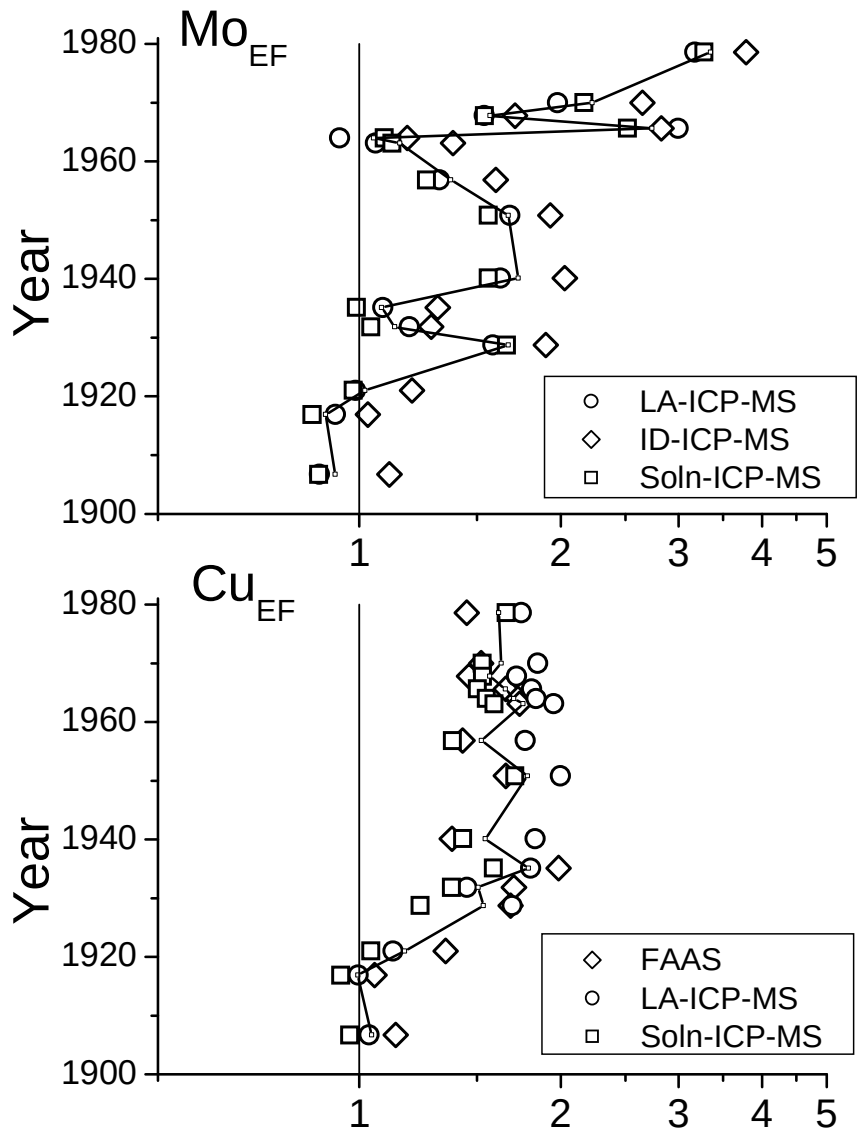

Figure 12 Method comparison illustrating agreement between 3 independent determinations of Mo and Cu in the same samples. LA-ICP-MS (this work), ID-ICP-MS (Isotope Dilution ICP-MS, Adelson et al. 2001), Soln-ICP-MS (Solution ICP-MS analyses, this work), FAAS (Flame Atomic Absorption Spectroscopy, Adelson et al. 2001).

Figure 13 contains results for Ti, Ga, Ge and Nb. Except for Ti, these data are also believed to represent the first determinations of these elements in Chesapeake Bay. These elements display negligible temporal trends in their deposition history and are neither substantially enriched nor depleted relative to my reference composition. Geochemically, Nb tends to occur as a minor constituent in Ti minerals, so the similar behavior of these two elements is not surprising. Ga and Ge tend to associate with their more abundant cohorts in the periodic table, Al and Si, respectively.

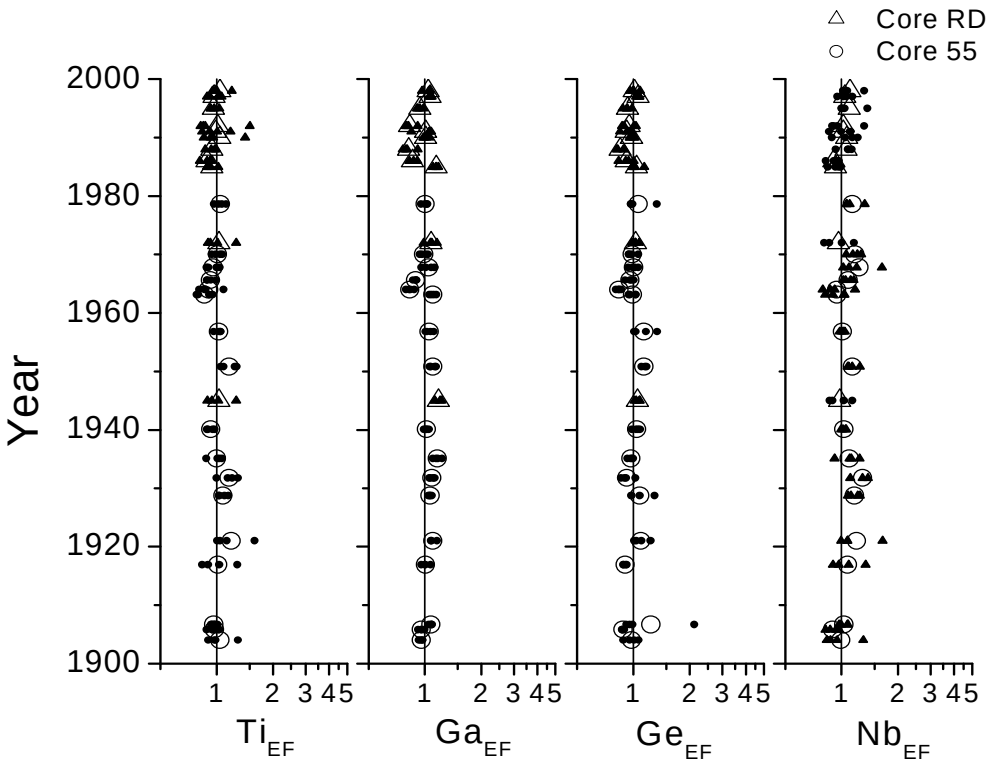

	Ti	Ga	Ge	Nb
Susq 8-10cm	1.17	1.15	0.92	1.32
Susq 28-30cm	1.00	1.14	1.02	1.10
Susq. 44-46cm	0.92	1.11	0.97	1.00
Fairhaven	1.42	0.99	1.36	1.53
B'more Harbor H	0.50	0.42	0.84	0.67
B'more Harbor M	0.60	0.69	0.73	0.51
B'more Harbor N	0.75	0.80	0.92	0.86
PC6 369cm	1.05	0.99	0.89	0.93
PC6 424cm	1.33	1.03	0.90	1.34
PC6 482cm	1.13	1.06	0.91	1.11
Water-depth 3.4 m	0.68	0.78	0.90	0.82
Water-depth 6.7 m	0.79	0.85	0.97	1.02
Water-depth 26.2 m	0.95	0.95	1.15	1.07

Figure 13 Enrichment factors (Equation 2.4) for unperturbed elements: Ti, Ga, Ge, Nb. The table gives corresponding EF values for samples from potential sediment sources (see Figure 8 for details).

Excluding the redox sensitive elements in Figure 11, all the elements generally have EFs near one in the pre-European samples from PC-6. However, in the case of Figure 8 (Cu, Zn, Cd and Pb), EFs are consistently less than one for the pre-European samples. My early 20th century reference sediments (Table 5) may have been already somewhat enriched in these four elements relative to the pre-European sediments. This result would be consistent with derivation of these elements from smelting. The Baltimore Copper Smelting Company was formed around 1850, and for several decades, it and its allied companies operated within Baltimore the largest copper smelter in the United States.

It is already clear that Laser Ablation ICP-MS is going to be a very valuable tool in the effort to evaluate trace element contaminants in Chesapeake Bay. For many of the elements discussed here, no previous determinations have been made in Chesapeake Bay sediments and few determinations have been made in estuaries anywhere.

Rhenium is the least abundant of the elements determined in this survey (Table 4), and owing to analytical uncertainty its individual determinations (small, closed symbols, Figure 11) are the most scattered relative to mean values (open symbols). It is questionable whether useful historical information about Re deposition can be inferred from the data.

Despite this uncertainty, however, these results show that Re behaves similarly to Mo and U and unlike the majority of other elements discussed. Rhenium is depleted in the Susquehanna and Harbor sediments while it is enriched in both the

Miocence Fairhaven sample and the PC-6 sediments. These results reaffirm the identity of Re as a paleoredox-indicator and not an industrial pollutant. These results cannot be used to determine what accounts for Re enrichment in anoxic sediments, however. In the next chapter I present results for experiments where I used LA-ICP-MS to investigate the elements associated with Re in sediments deposited under reducing conditions. The goal of these experiments was to narrow-down the chemical form of Re and thereby account for its enrichment in reducing sediments.

Chapter 3: Investigating the Host-phases of trace elements using Laser Ablation ICP-MS

3.1 Introduction

Little is known about the host phases of Re in sediments e.g. whether they are sulfides, oxides, organic matter or something else. Dellwig et al., (2002) undertook sequential leaching experiments on Holocene coastal peats and found evidence that Re is accumulated in sulfide host phases. In the first step of these leaching experiments, 1 M HCl was used to extract amorphous and crystalline iron and manganese oxyhydroxides, carbonates and hydrous aluminosilicates. In the second step, 10 M HF was used to extract clay minerals. In the third and final step 15.8 M HNO_3 was used to extract pyrite and associated trace metals (Dellwig et al., 2002; Huertadiaz and Morse, 1990). Re was present mainly in the final pyrite fraction of the peats.

Alternatively, the fact that rhenium is enriched in suboxic sediments where there is no measurable sulfide in pore waters (Colodner et al., 1993a) points to the possibility that the scavenged Re species may not be a sulfide. The species may be ReO_2 according to Crusius et al.(1996).

In this chapter, I attack the question Re's host phase with a novel approach using Laser Ablation ICP-MS. I hypothesize that the correlation of Re counts with counts from other elements as the ablating laser beam moves across the sample, can provide information about the host phase. In Figure 3, Chapter 2, the Mo peak near 70 sec. has no counterpart in the Mn trace, suggesting that the laser impinged on a Mo-rich phase that was not a Mn-oxyhydroxide, at the point in the track. I am

proposing that correlation coefficients between counts for different elements can be used to determine whether certain elements rise and fall together as the laser moves across the pellet. These correlations would be evidence that these elements are co-located in the sample pellet and thus possibly incorporated in the same host phase.

The precision of Re analysis in Chesapeake Bay samples was poor (Figure 11) so in this chapter, I test this approach on samples containing exceptionally high Re, with the hope that stronger Re signals will result in better precision. These samples were graciously provided by H. J. Brumsack of Carl von Ossietzky University, Oldenburg, Germany. Brumsack and his associates have done extensive studies of trace elements in sediments and shales from reducing environments.

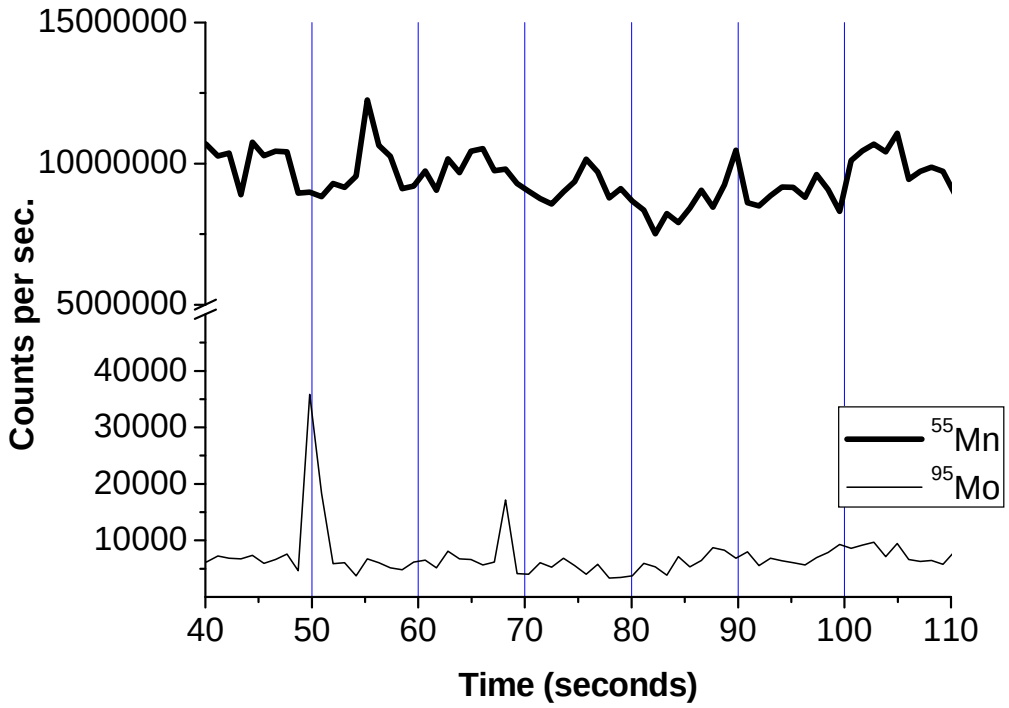

Figure 14 Reproduction of Figure 3, Chapter 2 illustrating that LA-ICP-MS can be used to find evidence that certain elements rise and fall together as the laser moves across the pellet. Note the Mo peak at 50 sec. that has no counterpart in the Mn trace.

3.2 Methods

3.2.1 Samples

ODP Leg 160 samples are Eastern Mediterranean sapropels of Pliocene to Pleistocene age with high organic carbon and sulfur content (Warning and Brumsack, 2000). The Re concentration in *ODP Leg 160* is 1180 ppb (Brumsack, personal communication). The samples *7430 54, 17* and *7430 54, 55* are black shale samples of Jurassic to Cretaceous age from the Norwegian Shelf Drilling Program (Lipinski et al., 2003). The Re concentration in *7430 54, 17* is 1220 ppb and in *7430 54, 55* is 1060 ppb (Brumsack, personal communication). Rhenium's average crustal abundance is 0.4 ppb (Li, 2000), four orders of magnitude smaller than in these samples.

In Table 6, my measured concentrations for the samples studied are presented and compared to those reported by Brumsack and associates. The RSD values presented are my relative standard deviations of the four laser track analyses performed on each sample. The agreement between the measured and previously reported values is poorer for many elements than would be expected based on the RSD values of my method. It is not clear which data set is at fault. My experiments were performed before my assessment of the precision and accuracy presented in Chapter 2 so I did not yet fully appreciate the importance of matrix-matched standards. NIST 610 was used as the SRM for all the elements, except Fe, where JB sulfide was used. JB Sulfide, an in-house standard, is a cut and polished portion of a Ni-Fe-S bead which contains PGEs and Re (Brenan et al., 2005; Brenan et al., 2003).

Table 6 Measured and literature concentrations for the samples presented in this work. Mn was used as the internal standard. Published values are from Warning and Brumsack (2000), Lipinski et al. (2003) and Brumsack (personal communication).

	ODP Leg160				*7430_10 54_17*				*7430_10 54_55*		
Element	Average/ ppm	RSD/ %	Published Value/ ppm		Average/ ppm	RSD/ %	Published Value/ ppm		Average/ ppm	RSD/ %	Published Value/ ppm
Ca	47684	4.4	67967		1453	14.2	1358		7522	23.7	8076
Ti	1839	8	2598		1153	41	1301		1509	12	1858
Mn	**480**	**0**	**480**		**163**	**0**	**163.0**		**163**	**0**	**163.0**
Fe	73661	3.9	69733		192337	6	235357		150432	6.5	179962
Co	402	6.3	401		92	1.8	67		72.4	8.1	63
Ni	681	7.9	491		1277	12.4	817		951.6	6.3	806
Cu	298	8.8	264		112	5.5	75		119	8.5	83
Zn	348	6.5	353		1690	10.0	1891		1699	8.6	1583
As	233	6.5	198		931	4.2	1126		760	6.7	986
Se	41	4.9			66	1.0			72	11.8	
Mo	95	12	58		866	1.5	1233		568	6.6	833
Sb	47	5.1	47		62	2.4	58.9		51	9.9	44.7
Re	3.2	4.0	1.18		4.3	7.7	1.2		3.8	14.3	1.1
Tl	5.0	3.7	4.1		18	8.4	17.3		15	11.8	15.2
Pb	43	6.6	37		22	5.9	16.8		28	22.9	21.4

3.2.2 Instrumentation

Details of the instrument and set-up were presented in section 2.2.2 Procedures in the previous chapter and any differences are outlined as follows. In correlation experiments an ablation frequency of 8 Hz and line width of 40 µm were used for ODP Leg 160 and Core *7430* samples. For total concentration work an ablation frequency of 20 Hz was used for all standards and samples. Laser line widths of 40 µm were used for standards and widths of 100 µm were used for samples, because of weak signals from Re.

3.2.3 Data Analysis

Total concentration values were calculated using the equations presented in Chapter 2 (Equations 2.1 – 2.3). The internal standard used for calculating these concentrations was Mn.

Along each laser track at least 100 measurements of each element were taken. Each element was measured sequentially in mass order. The total time required for each of the 100 measurements for one laser track was 0.6 seconds so that 100 measurements took 60 seconds. In Table 7, I present details of the ICP-MS method used. Each change in magnet mass required a larger settling time than 0.001s. For example, between ^{33}S and ^{43}Ca when the magnet mass changed from 32.971 to 42.958 the settling time was 0.120 s. Sample time was 0.040 s for Re isotopes because of their low abundance, while the sample time for all other isotopes was 0.010 s. Detection mode was "Analog" for elements with high abundance while the detection mode was "Both" for the less abundant elements. In "Analog" mode the ion beam strikes the detector directly. The designation "Both" allows the Element 2 software to choose the appropriate measurement method based on the strength of the signal detected. In the "Counting" mode the ion beam is channeled through a secondary electron-multiplier before hitting the detector. This means that the signal for less abundant elements is amplified before hitting the detector.

Table 7 Method details for the ICP-MS measurements.

Isotope	Accurate Mass	Mass Window	Magnet Mass	Settling Time/ s	Sample Time/s	Samples per Peak	Detection Mode
S33	32.9709	1	32.971	0.120	0.010	1	Both
Ca43	42.9582	1	42.958	0.025	0.010	1	Both
Ti49	48.9473	1	42.958	0.001	0.010	1	Analog
V51	50.9434	1	42.958	0.001	0.010	1	Analog
Mn55	54.9375	1	42.958	0.001	0.010	1	Analog
Fe57	56.9349	1	56.935	0.030	0.010	1	Analog
Co59	58.9327	1	56.935	0.001	0.010	1	Both
Ni60	59.9302	1	56.935	0.001	0.010	1	Analog
Cu63	62.9291	1	56.935	0.001	0.010	1	Analog
Zn66	65.9255	1	56.935	0.001	0.010	1	Analog
As75	74.9211	1	74.921	0.033	0.010	1	Both
Se77	76.9194	1	74.921	0.001	0.010	1	Both
Mo95	94.9053	1	74.921	0.001	0.010	1	Both
Mo97	96.9055	1	74.921	0.001	0.010	1	Both
Sb121	120.9033	1	120.903	0.070	0.010	1	Both
Sb123	122.9037	1	120.903	0.001	0.010	1	Both
Re185	184.9524	1	184.952	0.070	0.040	1	Both
Re187	186.9552	1	184.952	0.001	0.040	1	Both
Os189	188.9576	1	184.952	0.001	0.010	1	Both
Tl205	204.9739	1	184.952	0.001	0.010	1	Both
Pb208	207.9761	1	184.952	0.001	0.010	1	Analog

3.3 Results

Most of the results presented are for 5 laser track analyses. Results for V are the main exception: there are no laser tracks on Core *7430 54, 55*, two laser tracks on Core *7430 54, 17* and four on *ODP Leg 160*. In Figure 15 selected results from one laser track are shown: the third laser track of Core *7430 54, 17*. Titanium is a high boiling point element that tends to be concentrated in illmenite mineral grains, manganese is the internal standard, sulfur is expected to correlate with chalcophile elements and molybdenum and rhenium are redox sensitive elements. Note the spikes in Ti between 60 and 70 seconds that are not mirrored by any of the other elements. This implies that the Ti-rich grains ablated in this portion of the track did not contain measurable enrichments in any of the other elements shown.

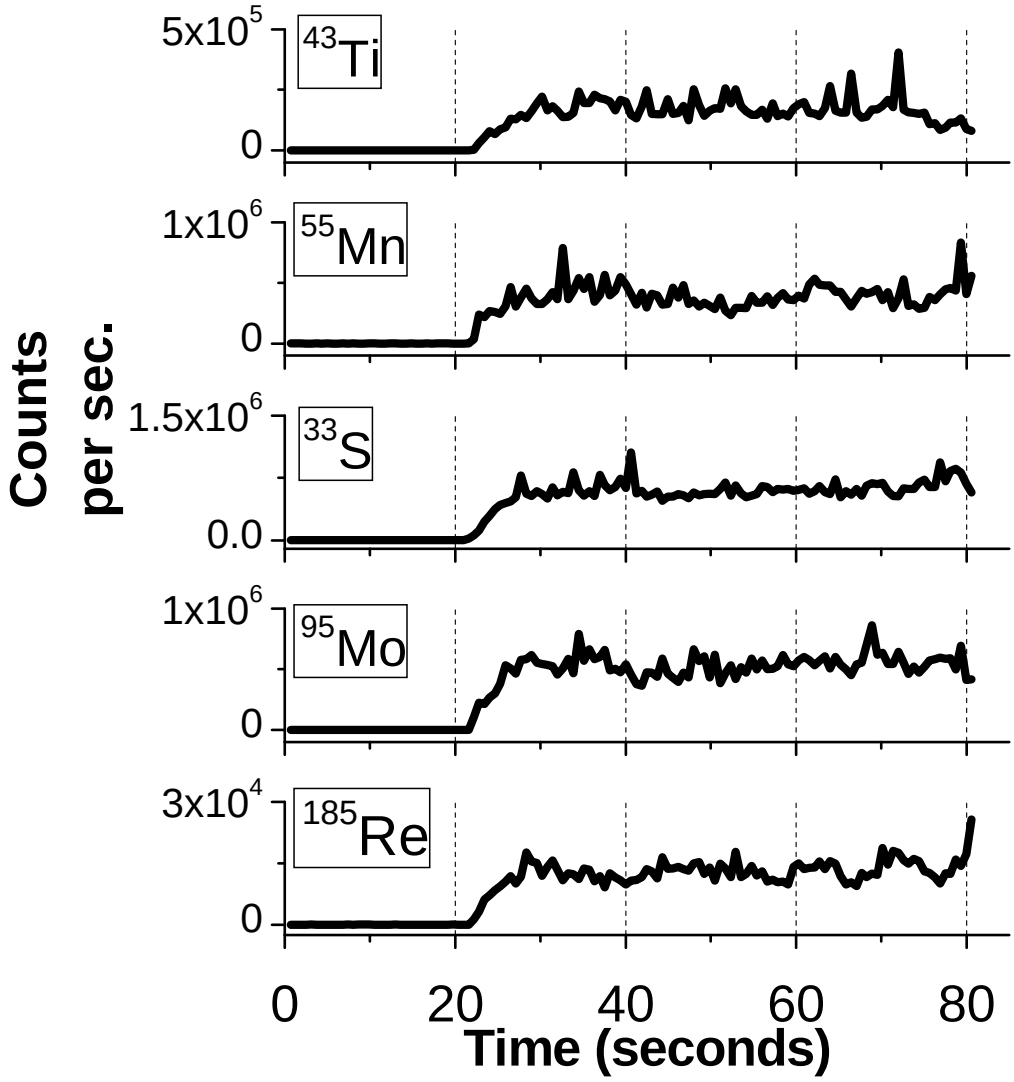

Figure 15 LA-ICP-MS results illustrating background vs. signal for Core *7430 54,17* laser track 3. Each analysis consisted of 20-30 seconds with the laser on and the shutter closed to obtain a background signal, followed by 50-70 seconds with the shutter open to collect the ablation signal. This corresponded to an area 1.2mm*0.1mm on the sample surface.

Pearson's Product Moment Correlation Coefficients (r's) were calculated from the raw counts per second data collected along a laser track using the Data Analysis Tool in Excel (see Appendices, Table A I to Table A XV). The correlation coefficients presented are based on correlations between counts taken for the various elements as the laser moved across the sample.

To facilitate further discussion, I am going to summarize the multiple tables in the Appendices in Figure 16. In order to do this I have arbitrarily divided the correlation coefficients in the appendices into three categories, and each is represented by a color: $r<0.3$ (blue), $0.3\leq r < 0.5$ (green) and $r \geq 0.5$ (red). Each panel in Figure 16 represents correlation coefficients for one of the three samples studied. Within each panel, correlation coefficients are represented in horizontal bars. Each bar typically consists of five individual boxes, with each box representing one of the five replicate laser tracks along which counts were taken. For example, in the upper left corner of Figure 16, it is shown that in one laser track across Core *7430 54, 55*, the correlation coefficient between Pb208 and S33 exceeded 0.5, whereas in the remaining four laser tracks, the correlation coefficients between these same isotopes was less than 0.3.

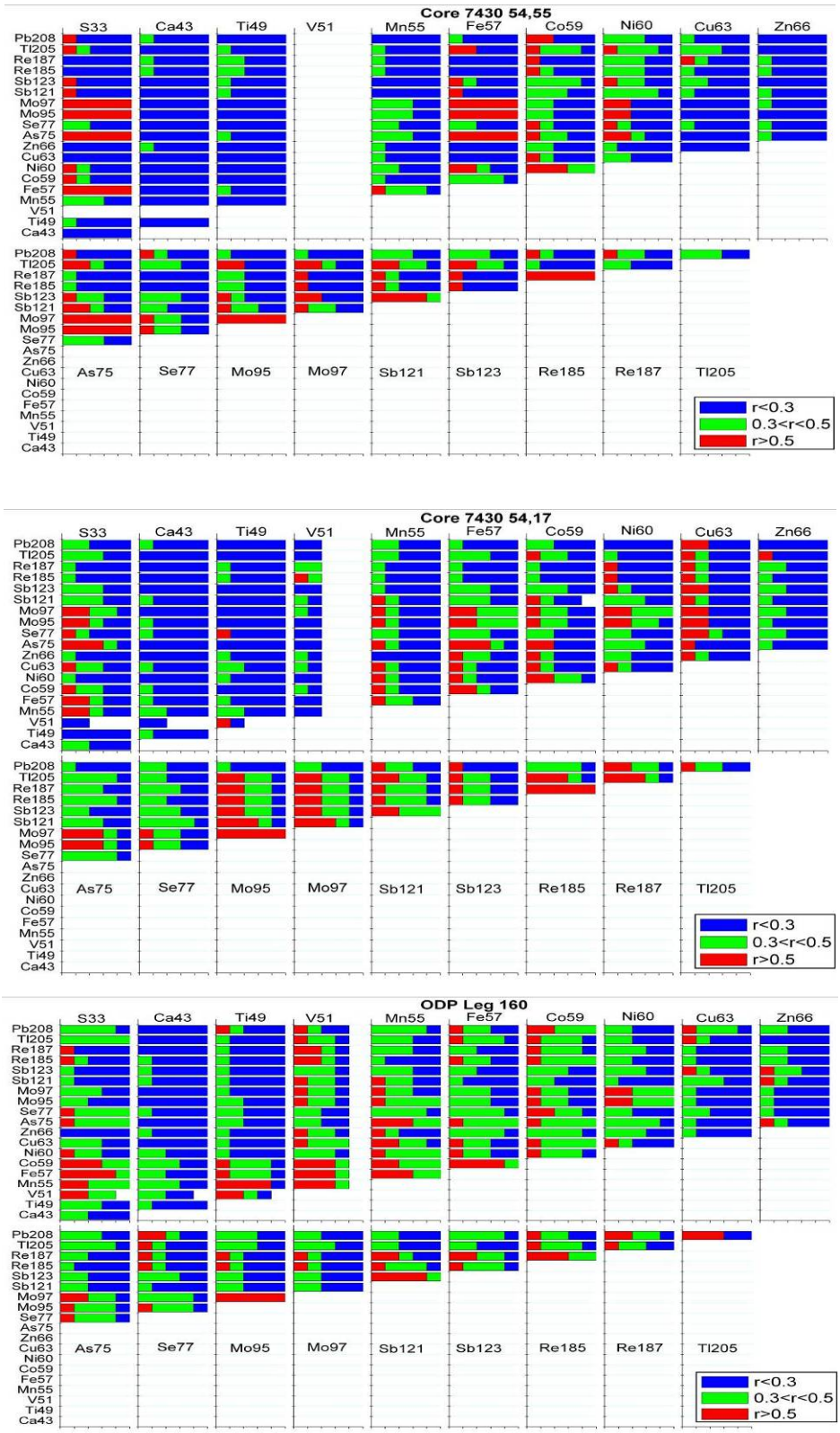

Figure 16 Correlation plots for Core *7430 54, 55*, Core *7430 54, 17* and *ODP leg 160* illustrating three degrees of correlation

In Core *7430 54, 55* (Figure 16), there are correlations with $r \geq 0.5$ along all five laser tracks between Mo, Fe, S and As. This could mean that during deposition, conditions were favorable for Mo and As to be incorporated into the pyrite being formed. Arsenic and molybdenum are known to co-precipitate with pyrite: FeS_2 (Huerta-Diaz and Morse 1992). This example is encouraging with regards to the use of LA-ICP-MS to get an idea of what elements are deposited in similar fractions of sediments.

In Core *7430 54, 17* (Figure 16), there are correlations with $r \geq 0.3$, between Mo, Fe, S and As in three laser tracks. In *ODP Leg 160* (Figure 16), there are correlations with $r \geq 0.3$, between Fe, S and As in five laser tracks and between Mo, Fe, S and As in 3 laser tracks. Correlations between As, Mo, Fe and S for Core *7430 54, 17* and *ODP Leg 160* are not as consistently strong as those for Core *7430 54, 55*. Reasons for this could include less pyrite in these samples, pyrite containing lower trace element concentrations or alternate phases that contain more of these elements so that the signal due to pyrite, if it is present, is less distinctive relative to background.

In Core *7430 54, 55*, the correlation coefficient between Re and Ni is moderately high in three of five tracks. In Core *7430 54, 17*, the correlation coefficient of Re with Mo, As, Sb and Tl is high in most tracks and in both V tracks measured. In *ODP Leg 160*, correlations of Re with V, Sb and Tl are again high, whereas a high correlation with Mo is apparent in only two of five tracks. Rhenium's correlation with V is intriguing. Vanadium is often associated with organic matter in

sediments and Anbar (2007) has found correlations of rhenium with organic carbon in late Archean shales.

3.4 Discussion

Laser Ablation ICP-MS can be used to demonstrate correlations between certain elements as the laser moves across the sample. Most notably, Mo was correlated with Fe and S in the majority of laser tracks for all three samples, consistent with knowledge that it is scavenged with pyrites (Bostick et al., 2003; Helz et al., 1996; Vorlicek et al., 2004). Also, As was correlated with Fe and S in the majority of laser tracks for all three samples. This makes sense geochemically since As is a chalcophile element i.e. it is associated with sulfides. Additional proof of the usefulness of this method for this purpose is the fact that only a few elements correlate significantly with Ca. The suite of metals analyzed is not expected to be associated with calcium carbonates.

Since the results for Re based on Figure 16 are inconclusive, I will assess the actual correlation coefficients from the Appendices. In general, the correlation between S and Fe is high along all tracks, consistent with the expectation that iron sulfides are major host phases of these elements in sediments from reducing environments.

When the element that correlates most highly with Re is identified in each track, this element is found to be Sb in 7 of the 15 tracks; it is Mo in 3 tracks and Co in 2 tracks. Antimony, molybdenum and cobalt are all regarded as chalcophile elements in the Earth's crust and thus rhenium's association with this group points toward the possibility of its association with sulfides. Sb, Mo and Co are also well

known to concentrate in Mn oxyhydroxides. This association is less likely since these samples are from reducing marine environments; two of the three samples are strongly depleted in Mn relative to average shale Table 5.

In more than one third of the laser tracks (see Tables AII, AVI, AX, AXI, AXII, AIII) the correlation coefficient between Re and S exceeds 0.2 which would occur less than 5% of the time in a set of 100 pairs of random numbers. In all but one of those tracks in which the Re/S correlation coefficient exceeds 0.2, Re/As and Re/Mo also correlate with $r > 0.2$. (The one exception is track XII.)

Since S, As and Mo all tend to be enriched in pyrite in the marine environment, these results are consistent with the possibility that Re is also enriched in pyrite. There is also evidence that Re is correlated with V, which indicates a possible association with organic matter. These findings indicate that Re could be enriched in multiple host phases, including both sulfides and organic matter.

Chapter 4: Experimental work on Re – Test of Microbial fixation hypothesis

4.1 Introduction

Immense enrichments of the trace element rhenium can occur in sediments deposited in suboxic or anoxic environments compared to sediments deposited in oxic environments (Boning et al., 2004; Calvert and Pedersen, 1993; Colodner et al., 1993a; Crusius et al., 1996; Koide et al., 1986; Morford and Emerson, 1999; Nameroff et al., 2002; Rinna et al., 2002). Consequently Re is potentially useful as an indicator of the environmental redox state during sediment deposition. This aspect of Re geochemistry is being exploited not only to investigate redox conditions during Earth's history (Anbar et al., 2007; Morford et al., 2001; Rinna et al., 2002), but also to investigate the redox status of modern environments (Chappaz et al., 2008).

The principal form of Re in oxygenated natural waters is perrhenate (ReO_4^-), which is present in seawater at only 40 pM and in fresh waters usually at much lower concentrations (Anbar et al., 1992; Chappaz et al., 2008; Colodner et al., 1993a; Dalai et al., 2002). As attested by its long mean residence time in the ocean (0.75 My), ReO_4^- is biogeochemically quite inert in oxic water. However in pore waters of suboxic and anoxic sediments, as well as in anoxic water columns of poorly ventilated basins like the Black Sea, dissolved Re decreases appreciably relative to overlying waters (Chappaz et al., 2008; Colodner et al., 1993a; Morford et al., 2003; 2005; 2007). The biological or chemical mechanism that depletes Re in suboxic and anoxic waters and enriches Re in sediments remains to be discovered.

Current constraints on the nature of this mechanism are inconclusive. In the laboratory, reductive precipitation of ReO_4^- as insoluble ReO_2 at near-neutral pH and room temperature is sluggish, even with strong reducing agents like $LiBH_4$ (Dolor, 2005) and $SnCl_2$ (Maset et al., 2006). Various evidence demonstrates negligible sorption of ReO_4^- by (hydr)oxides of Si, Mn and Fe or by clay minerals like kaolinite at near-neutral pH (Colodner et al., 1993a; Crusius et al., 1996; Morford et al., 2005). On the other hand, Re correlates well with organic carbon in black shales (Anbar et al., 2007; Jaffe et al., 2002), possibly pointing toward a biologically mediated scavenging or fixation mechanism. Supporting this idea, Yamashita et al. (2007) show that incubation of a glucose-amended, anoxic sediment slurry results in some uptake of ^{183}Re tracer, but that uptake is blocked if the sediment is dried, ashed or leached with H_2O_2 prior to forming the slurry. In related experiments, they show by x-ray spectroscopy that ReO_4^- is sorbed as mixed Re^{VII} and Re^{IV} species in sediments that reach biological sulfate reduction during two weeks' incubation.

Crusius et al. (1996) argue that Re removal from sediment pore waters occurs toward the end of biological Fe(III) reduction and precedes SO_4^{2-} reduction in the standard sequence of microbial terminal electron accepting processes Figure 1. However Maset et al. (2006) find that ReO_4^- is not removed during 40-day soil microcosm experiments that reach Fe(III) reducing conditions; they suggest that ReO_4^- removal requires SO_4^{2-} reducing conditions. One of the first products of biological sulfate reduction in natural environments is FeS, which can be observed to form under conditions where sulfide is immeasurable by conventional methods (i.e. < 1 μM; Burton et al., 2007). Abiotic precipitation of FeS scavenges some ReO_4^- as an

Fe-S-Re product (Wharton et al., 2000). However, selective leaching of peats shows that Re is predominantly extracted with the FeS_2 fraction rather than the FeS fraction (Dellwig et al., 2002). Chappaz et al. (2008) were able to model dissolved Re profiles in lake sediment pore waters by assuming chemical equilibrium with ReS_2. Unfortunately, their model relies upon the dubious postulate that H_2S/SO_4^{2-} equilibrium controls pore water redox states.

The close analogy between the chemistry of Re and Tc has long encouraged the idea that the behavior of one element serves as a model for qualitatively predicting the behavior of the other (Brookins, 1986). It is well-established that TcO_4^- can be removed from solution by reduction to insoluble $TcO_2 \cdot nH_2O$ (Burke et al., 2005; Livens et al., 2004; Peretyazhko et al., 2008; Wharton et al., 2000; Wildung et al., 2004). Microbes facilitate this process both directly (enzyme mediation) and indirectly (metabolite mediation). Iron(II) appears to be the most important metabolite in the indirect pathway. Additionally, sulfide reacts with TcO_4^- by an indirect pathway to form insoluble sulfides of uncertain composition (Henrot, 1989; Liu et al., 2007; Livens et al., 2004; Lloyd et al., 1998). Bacteria that have been shown to facilitate reactions that fix Tc include *Escherichia coli* (Lloyd et al., 1997), *Desulfovibrio desulfuricans* (Lloyd et al., 1998; Lloyd et al., 1999), *Geobacter sulfurreducens* (Lloyd et al., 2000), and *Shewanella* sp. (Burke et al., 2005).

Evidence for bacterially facilitated TcO_4^- fixation led me to hypothesize that analogous bacterial activity drives ReO_4^- fixation in reducing sedimentary environments. Here I examine the potential for Re fixation in pure culture by four Fe(III)- and SO_4^{2-}-reducing strains previously shown to reduce TcO_4^-. The

experiments are designed to detect direct or indirect removal of Re from solution on the time scale of culture growth to stationary phase. I do not test the possibility that very slow reactions involving metabolites, especially Fe(II) or sulfide, might cause Re fixation over long periods of time. This latter question demands different kinds of experiments, the results of which are presented in the next chapter.

4.2 Methods

4.2.1 Microbial Experiments

Desulfovibrio desulfuricans ND132 (Gilmour et al., 1985) was obtained from the laboratory culture collection of the Microbial Ecology lab at the Smithsonian Environmental Research Center, where this work was performed. *Desulfovibrio desulfuricans* subsp. *desulfuricans* (ATCC 29577), and *Shewanella oneidenis* MR-1 (ATCC 700550) (Venkateswaran et al., 1999) were purchased from ATCC (Manasas, VA). *Geobacter metallireducens* GS-15 (ATCC 53744) (Lovley et al., 1993) was provided by E. Roden. The cells were grown at standard incubation temperatures in media described below alongside both abiotic and inoculated control experiments, to observe whether sorption to cells or precipitation with medium components controlled rhenium solubility.

Desulfovibrio desulfuricans subsp. *desulfuricans* (ATCC 29577) and *Desulfovibrio desulfuricans* ND132 (Gilmour et al. 1985) were grown with lactate as the electron donor and sulfate as the electron acceptor. The sulfate-reduction medium contained lactate (24 mM), salts (9 mM Na_2SO_4, 1.7 mM NaH_2PO_4, 4.7 mM NH_4Cl, 6.7 mM KCl, 1.5mM $CaCl_2$ and 1.5mM $MgCl_2$), yeast extract (0.5 g/L), trace metals and vitamins (Laanbroek and Pfennig 1981), 24 nM selenate, 25 nM tungstate, 3.6

μM $FeCl_2$, and 10 mM MOPS buffer (final pH 7.0). Resazurin at 1 mg/L was used as a redox indicator.

Geobacter metallireducens GS-15 (Lovley et al. 1993) was grown with acetate as the electron donor and Fe(III) citrate as the electron acceptor (Lovley and Phillips, 1992). The iron-reduction medium contained sodium acetate (18 mM), Fe(III) citrate (55 mM) salts (1.7 mM NaH_2PO_4, 28 mM NH_4Cl, 1.4 mM KCl), yeast extract (0.5 g/L), trace metals and vitamins (Laanbroek and Pfennig, 1981), 24 nM selenate, 25 nM tungstate and 10 mM MOPS buffer (final pH 7.0). *Shewanella oneidenis* MR-1 (Venkateswaran et al. 1999) was also grown anaerobically in the same media with 2.0 g/L yeast extract and 1 g/L peptone and 48 mM lactate as the electron donor instead of acetate.

Aliquots of media for sulfate or iron reducing bacteria (10 ml) were dispensed into anaerobic pressure tubes (Fisher Scientific) inside an O_2-free glove bag. After these tubes were autoclaved, 1.5mM $CaCl_2$, 1.5mM $MgCl_2$ and 100 μM Ti(II)-nitrilotriacetic acid (NTA) as an oxidant scavenger (sulfate reducers only) were added by syringe, along with the desired amounts of $NaReO_4$ and 1mL of a log phase culture per 10 mL of media. Rhenium doses reported in this chapter were corrected for dilution by the inoculum.

After one week's incubation at either 4ºC or 30 ºC, culture tubes were opened and aliquots were filtered through 0.2 μm (Whatman) syringe filters. In the case of sulfate reducers, the unfiltered samples were analyzed for total sulfide and optical density (A_{660}) to assess extent of culture growth. Subsamples for sulfide analysis were preserved in fresh sulfide antioxidant buffer (2M NaOH, 0.2M ascorbic acid and

0.2M Na_2EDTA), and assayed within 4 hours using an ion-selective electrode. Growth of iron reducers was assessed visually by the loss of brown ferric iron color.

To prepare culture samples for Re analysis, they had to be digested to destroy cellular material that might otherwise clog the ICP-MS inlet. Both the unfiltered and the filtered aliquots were digested identically by an open vessel method (Van-Loon, 1985). All of the concentrated acids used in these digestions were Trace Metal Grade or better purity. One milliliter of each aliquot was warmed with 5 mL of 15.8 M HNO_3 for 30 minutes in Teflon vials. After the samples cooled, 5 mL of 15.8 M HNO_3 and 3 mL 11.65 M HCl were added. The mixtures were then heated at 220 ºC until most of the liquid was evaporated. After the samples cooled, 0.5 mL of 31 % H_2O_2 was added to the vials and the mixtures were once again heated to near dryness. At this time the samples were pale white gelatinous residues at the bottom of the vials. Residues were taken up in approximately 5 mL of 2% HNO_3.

4.2.2 Total Rhenium Analysis

A Finnigan Element 2 ICP-MS instrument, interfaced with a cyclonic spray-chamber, was used for total Re analyses. Table 8 describes the operating conditions. A seven-point calibration curve covering the range 0.1 to 10 nM was prepared by diluting a multi-element standard (Specpure) with HNO_3 (Ultra-pure). All unknowns were diluted into the nanomolar working range of the ICPMS with 2% v/v HNO_3 prior to analysis. The HNO_3 matrix was found to perform better, with lower background counts, than a deionized water matrix. The calibration curve served two purposes. It provided a means to convert counts per second supplied by the instrument into concentrations. It also served as an indicator that the instrument had

been correctly tuned. Tuning was performed prior to each day's run to establish the optimum sample gas and nitrogen flow rates.

Table 8 ICP-MS Operating Conditions

ICP rf power, W	1350
Detector	conversion dynode at ~8kV, discrete dynode Secondary Electron Multiplier
Run mode	reverse geometry: Magnetic Sector Field followed by Electric Sector Analyzer (ESA)
Mass window	10%
Scanning per peak	1
Run time per sample, s	75
Autosampler	ASX-100

Digestion blank corrections were on the order of 2-3 nanomoles, which was negligible in most samples. Analytical precision assessed by the scatter of standards along the calibration curve was quite good, on the order of ±2%. However precision assessed by differences between digestion duplicates was approximately ±15%.

4.3 Results

Little or no Re was removed from solution by any of the cultures tested, or in any of the parallel controls. Figure 17 compares filtered and unfiltered Re concentrations after one week in *Desulfovibrio desulfuricans* ND132 cultures and controls. Cultures reached stationary phase during this time. The three panels in the figure present data obtained at three of the five different ReO_4^- dosage levels tested (complete data are given in the Appendix). The tubes represented in the bottom panel received no $NaReO_4$ amendment and were exposed only to Re present as a contaminant in the medium. The Re concentration in samples with no added Re was roughly 4 orders of magnitude more than in seawater. Digestates of unfiltered and filtered pairs of sample aliquots are represented respectively by open and cross-hatched bars.

Starting from the left, the first four pairs of bars in Figure 17 are controls, intended to reveal sources of Re contamination or Re sorption behavior that is unrelated to bacterial growth. Moving from left to right, the pairs of bars depict Re concentrations in uninoculated culture medium; sterile medium plus 100 μM TiNTA, medium with a 10% vol/vol bacterial inoculum but no TiNTA, and inoculated medium with TiNTA. Each of these controls was incubated anaerobically for one week at 4ºC. As intended, bacterial growth was minimal in the inoculated controls at this temperature, as indicated by negligible development of turbidity and sulfide (see Appendix). Rhenium concentrations in active cultures are shown in the fifth pair of bars. These cultures were grown at 30ºC in medium containing TiNTA. Bacterial growth was vigorous at all ReO_4^- dosages, as shown both by the rise in optical density (turbidity) and by generation of up to 2.5 mM sulfide (Appendix). The optical density and sulfide concentrations did not vary significantly with ReO_4^- dose, indicating that doses in the 0.04 to 7 μM range neither stimulate nor suppress growth of this organism under our experimental conditions. Figure 18 presents results for analogous data for *Desulfovibrio desulfuricans* subsp. *desulfuricans*.

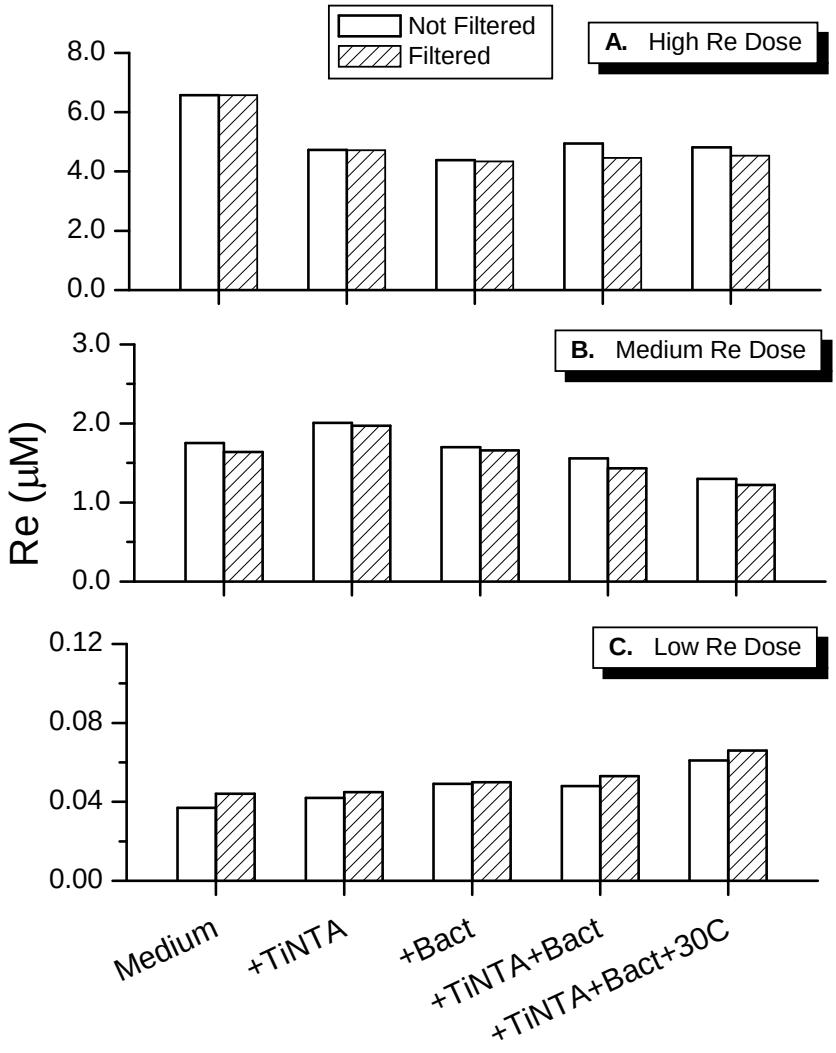

Figure 17 Unfiltered (open) and filtered (hatched) Re concentrations in *Desulfovibrio desulfuricans* ND132 cultures and controls, at three levels of total Re, after one week incubation. From left, pairs of bars represent uninoculated culture medium, uninoculated medium + TiNTA reductant; inoculated medium incubated at 4ºC, inoculated medium + TiNTA incubated at 4ºC, and inoculated medium +TiNTA incubated at 30ºC.

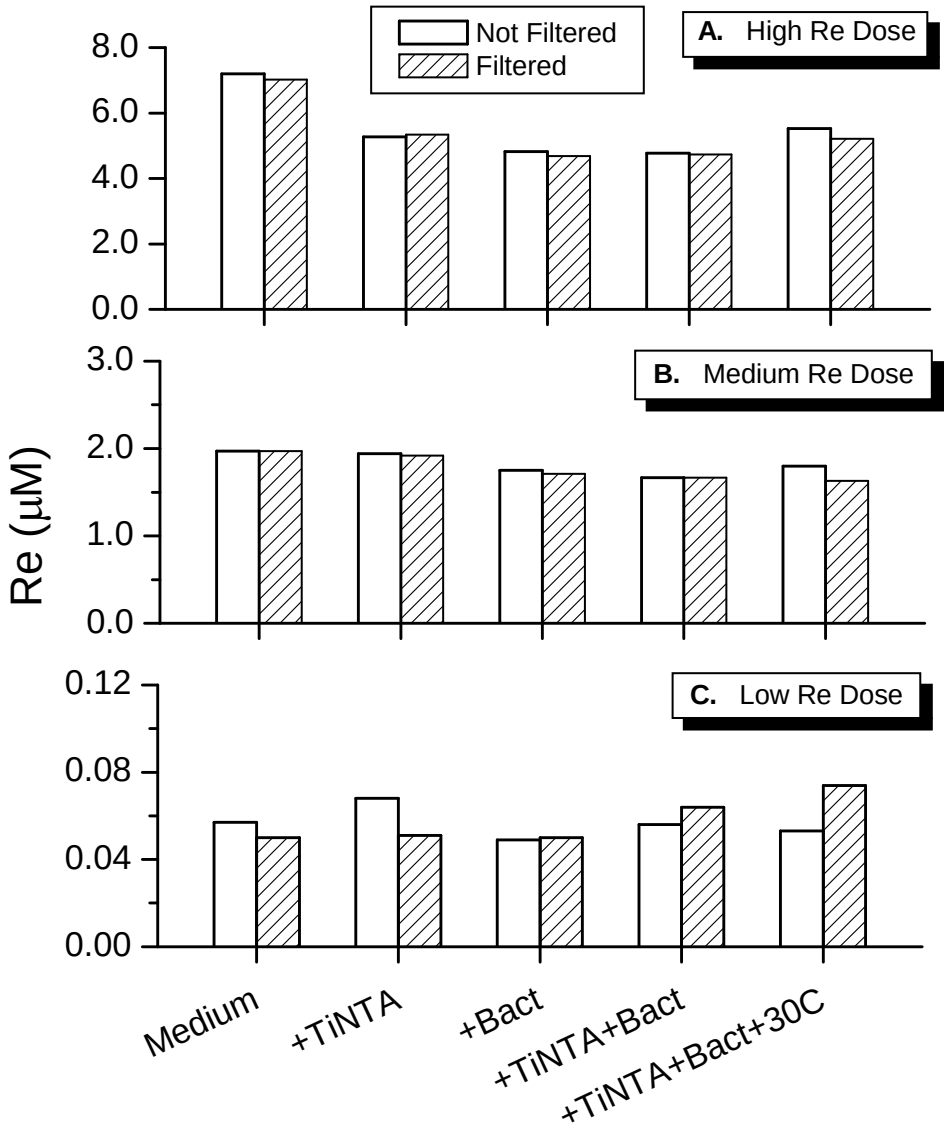

Figure 18 Summary of results for *Desulfovibrio desulfuricans* subsp. *desulfuricans* experiments. Experimental design as in Figure 17.

Figure 19 and Figure 20 present results for the two iron reducers, *Geobacter metallireducens* GS-15 *and Shewanella oneidensis* MR-1. As in the case of the sulfate reducers, incubation at 4ºC hindered bacterial growth, resulting in negligible Fe(III) reduction, whereas Fe(III) was completely reduced in active cultures (see Appendix).

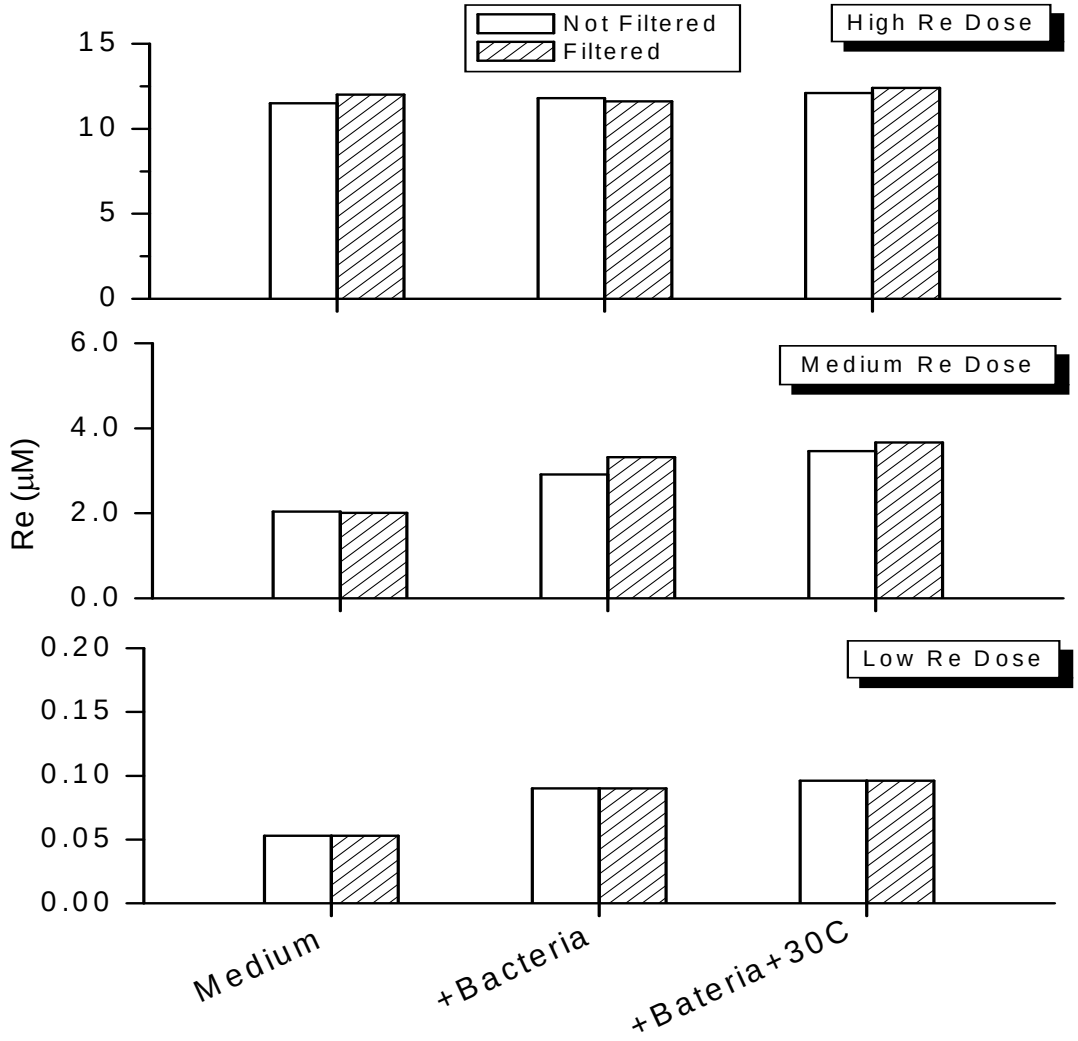

Figure 19 Unfiltered (open) and filtered (hatched) Re concentrations in *Geobacter metallireducens* GS-15 cultures and controls, at three levels of total Re, after one week incubation. From left, pairs of bars represent uninoculated culture medium, inoculated medium incubated at 4ºC, and inoculated medium incubated at 30ºC. Growth of iron reducers does not require a strong reductant so there are no TiNTA controls in these experiments.

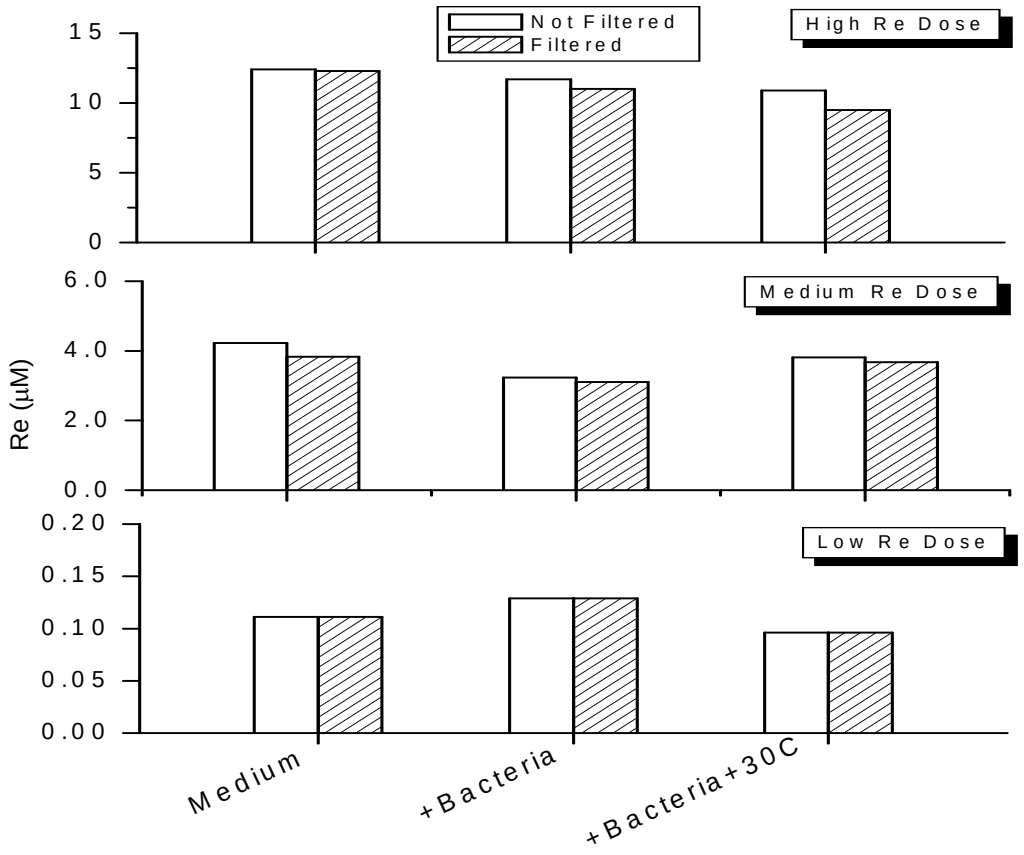

Figure 20 Summary of results for *Shewanella oneidensis* MR-1 experiments. Experimental design as in Figure 19.

4.4 Discussion

4.4.1 Sulfate Reducing Bacteria

Given the estimated analytical precision of ±15% in digested samples, none of the bacterial cultures removed Re significantly from solution. Particularly important is that filtration showed no systematic reduction in the amount of Re recovered in the aqueous phase (compare open and cross-hatched pairs of bars in Figure 17 and Figure 18) suggesting that any differences between filtered and unfiltered Re samples should be attributed to analytical error. Further, the assays were carried out at five levels of Re, to allow regression analysis of the data. In Figure 21, I plot filterable Re concentrations recovered from the various controls and the active cultures vs. filterable Re recovered from the uninoculated, unamended medium.

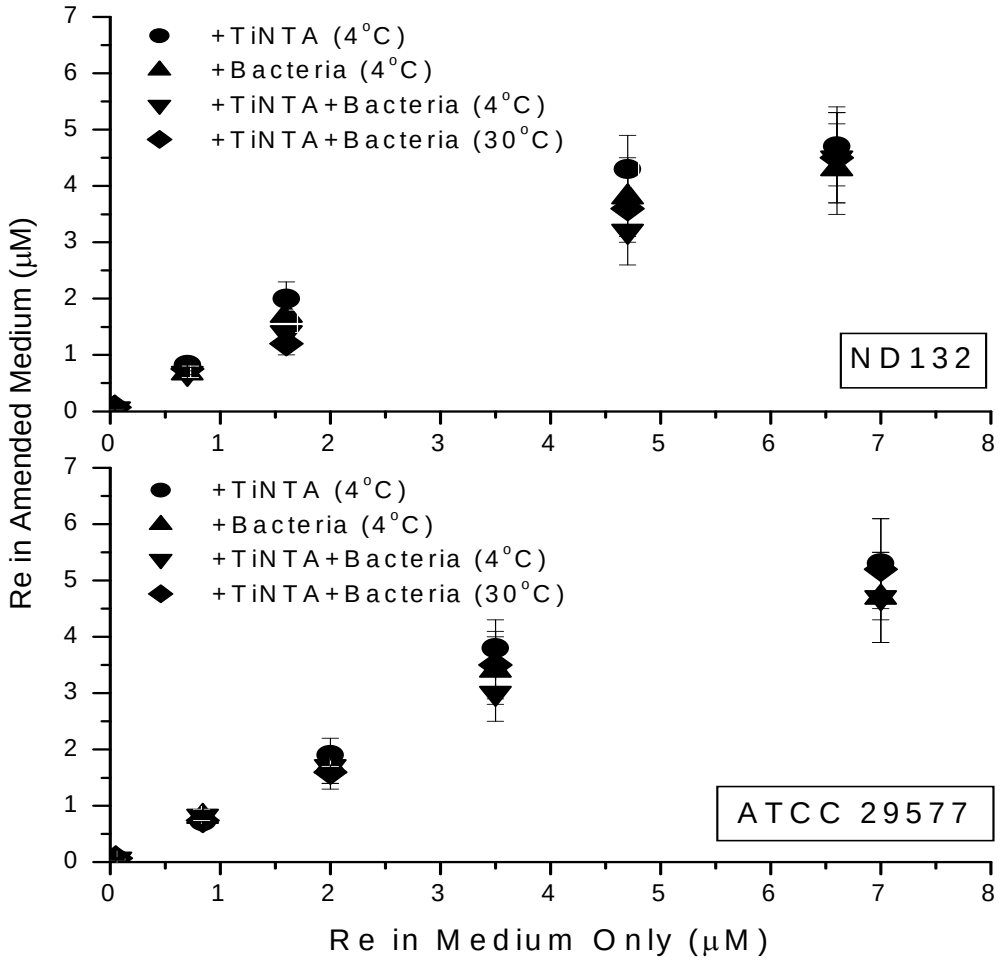

Figure 21 Cross plot showing Re recovered in filtered media that had been amended as shown in the key vs. Re in the unamended medium (also filtered) for all the experiments involving sulfate reducers.

Table 9 gives the linear regression slopes obtained from Figure 21. It is clear in this table that the slopes obtained for the actively growing cultures do not stand apart within standard error from the controls in which bacterial growth was negligible. Thus I must conclude that within uncertainty, neither actively growing SRB, inactive SRB cells, or Ti-NTA reductant converted ReO_4^- to a form that could be trapped on 0.2 μm filters. Because the bacteria themselves are trapped by filtration, I further conclude that Re had not become bioconcentrated within cells or sorbed to them to a significant extent.

Table 9 Regression slopes for data in Figure 21. For these regressions, data were weighted by analytical error and the regression was forced through zero. Uncertainties associated with the slopes are statistical standard errors.

Sample	ND132	ATCC 29577
Medium+TiNTA (4°C)	0.95 ± 0.06	0.90 ± 0.06
Medium+bacteria (4°C)	0.86 ± 0.07	0.86 ± 0.06
Medium+TiNTA+bacteria (4°C)	0.81 ± 0.07	0.87 ± 0.06
Medium+TiNTA+bacteria (30°C)	0.86 ± 0.06	0.90 ± 0.07

This outcome with Re contrasts with the Tc results of Lloyd et al. (1998) who exposed resting cells of *Desulfovibrio desulfuricans* to 250 μM TcO_4^- with H_2 as electron donor. After only 16 h, a black, cell-associated precipitate, probably a Tc oxide, had formed and > 85% of the Tc could be removed from solution with the biomass. When H_2S production was stimulated by adding lactate and sulfate (corresponding to conditions in our experiments), a different product, probably a Tc sulfide, was produced in high yield within 16 h. Henrot (1989) made similar observations with other sulfate reducing bacteria.

To my knowledge the only previous investigation of perrhenate reduction by a sulfate-reducing bacterium is a study by Xu et al. (2000). The paper suggested ReO_4^-

reduction by *Desulfovibrio desulfuricans* but provided few experimental details. These workers used H_2 as a electron donor in the presence of 5000 μM of ReO_4^- and within 60 min obtained a black, cell-associated precipitate which they postulated was an amorphous form of ReO_2 or $Re(OH)_4$. They did not determine Re in the aqueous phase, and it is not clear whether they confirmed that the black precipitate contained Re. When they grew the bacterium with lactate as the electron donor, they obtained only small amounts of black precipitate in five days. Both their results and mine suggest that growing *Desulfovibrio desulfuricans* on lactate under sulfate reducing conditions ineffectively removes ReO_4^- from solution, contrary to results for TcO_4^-.

An important difference between my experiments and those of Xu et al. (2000) is that they investigated a solution containing ~10^3-fold higher ReO_4^- concentration than our highest concentration. This is significant because the solubility of $ReO_2 \cdot nH_2O$ in the neutral pH range is estimated to be on the order of 0.4 μM (Kim and Boulegue, 2003). The total Re concentration in my experiments spanned this solubility limit. In principle, $ReO_2 \cdot nH_2O$ could have precipitated at my higher Re concentrations if the bacteria had accomplished Re^{VII} reduction to Re^{IV} even in moderate yield. Yet it would also be plausible that such reduction occurred without precipitation because the degree of supersaturation was too low to overcome a nucleation barrier. I recognize this as a possibility but regard it as unlikely because the stable form of dissolved Re^{IV} in the neutral pH range is believed to be $Re(OH)_4^o$ or $ReO(OH)_2^o$, and I would expect this uncharged species to be adsorbed to bacteria and to the filter, resulting in observable differences between the filtered and unfiltered aliquots. In any case, the solubility of Re^{IV} (hydr)oxide (Kim and Boulegue, 2003)

appears to be large compared to dissolved Re in natural waters, so precipitation of such phases cannot explain Re fixation in nature.

4.4.2 Iron Reducing Bacteria

To my knowledge this is the first investigation of the effect of iron-reducing bacteria on the behavior of Re in solution. I investigated two species with different iron-reducing pathways: *Geobacter metallireducens* GS-15 and *Shewanella oneidensis* MR-1. Just as with the sulfate reducing bacteria I found that rhenium was not removed significantly from solution by either of the iron-reducing bacteria. This result for perrhenate contrasts with pertechnetate, which is reduced both enzymatically and non-enzymatically by *Geobacter metallireducens* GS-15 (Lloyd and Macaskie, 1997).

4.4.3 Thermodynamic Feasibility of Re Removal from Solution

Although I observed no significant Re removal from solution in these experiments, removal was thermodynamically feasible. Based on the following reaction and equilibrium constant, ReS_2 (rhenite) would be expected to be very insoluble in our 30^o C-incubated, sulfate-reducing culture (thermodynamic data from (Pankratz et al., 1987; Wagman et al., 1982)):

$$H^+ + ReO_4^- + {}^7/_2\, H_2S_{(aq)} = ReS_{2(s)} + {}^3/_2\, S^0_{(s)} + 4\, H_2O_{(l)}, \qquad \log K = +56.7 \qquad (1$$

Under conditions in the culture after one week (pH 7, H_2S 1.2 mM), the equilibrium ReO_4^- concentration would be on the order of 10^{-40} M. Clearly precipitation of rhenite must have been kinetically inhibited or else Re would have precipitated quantitatively. In this regard, rhenite behaves like its structural isomorph, molybdenite (MoS_2). The latter mineral does not precipitate in the laboratory at room

temperature even from highly supersaturated solutions (Vorlicek et al., 2004). In fact, there is evidence that it does not form over geologic time periods unless host rocks are subject to elevated temperatures through metamorphism or hydrothermal activity (Helz et al., 1996).

Evidence presented thus far in this chapter, gives no indication of why precipitation of ReS_2 fails. A plausible thermodynamic hypothesis, however, is that Re becomes trapped as a filterable species in a metastable free energy minimum. Efforts to precipitate ReO_4^- in the laboratory with sulfide commonly produce a Re sulfide in a nanoparticulate form. This material approximates Re_2S_7. Although these nanoparticles are unstable against coagulation in water over a week's time (Tu and Denizot, 2007) it is possible that bacterial metabolites could stabilize them in a filterable form in culture. Proteins in the extracellular medium would be a particularly effective stabilizing agent for sulfide nanoparticles (Horzempa and Helz, 1979).

In the iron-reducing cultures, precipitation of Re as ReO_2 was probably feasible, although the free energy drive for this process is not as strong as for precipitation of ReS_2 in the sulfate reducing cultures. Ferrous iron, the principal metabolite of iron reducing bacteria, could reduce ReO_4^- to ReO_2, provided free $Fe^{2+}_{(aq)}$ were produced in high yield. From the data of Wagman et al. (1982):

$$7H_2O_{(l)} + ReO_4^- + 3Fe^{2+} \rightarrow ReO_{2\,(s)} + 3Fe(OH)_{3\,(s)} + 5H^+, \quad \log K = -23.4 \qquad (2$$

If all of the initial Fe(III) in my cultures (i.e. 0.055 M) became free $Fe^{2+}_{(aq)}$ during the incubation period, the equilibrium concentration of ReO_4^- at pH 7.0 would be 0.01 μM. However, this result is quite sensitive to the activity of free $Fe^{2+}_{(aq)}$. If one-tenth

as much free $Fe^{2+}_{(aq)}$ (0.005 M) was produced, owing to incomplete reduction or to complexing by citrate, acetate or organic metabolites, all of which are present in my cultures, then the equilibrium ReO_4^- concentration would be about 20 μM. Only in the first example would ReO_2 precipitation be thermodynamically feasible; in the second example, all of my cultures would remain undersaturated.

It should be noted that the concentration of ReO_4^- in equilibrium with ReO_2 is also extremely sensitive to pH (reaction 2). Consequently, in marine systems, where pH is as much as one unit higher than in my cultures, the $Fe^{2+}_{(aq)}$ requirements for supersaturation are more relaxed. Nonetheless, as already pointed out, the relatively high solubility of ReO_2, as aqueous Re^{IV} species, makes reaction (2) a dubious mechanism for fixing Re from marine waters, where the ReO_4^- concentration is only 40 pM (Anbar et al., 1992).

To summarize, my data show that in short term (one week) experiments, ReO_4^- is neither directly nor indirectly transformed to nonfilterable forms by the sulfate reducing and iron reducing bacteria tested. The specific culture conditions I investigated involved microbial growth with organic electron donors and either sulfate or iron as the electron acceptor, not H_2. Further, these results add to the evidence (Wharton et al., 2000) that despite being in the same group and forming similar compounds, the chemical analogy in the chemistry of Tc and Re is only qualitative; quantitatively, Re is more difficult to remove from solutions. I investigate the hypothesis that Re in reducing sediments is fixed abiotically by kinetically slow reactions involving biogenic sulfide in the following chapter.

Chapter 5: Experimental work on Re – Thioperrhenate Thermodynamics

5.1 Introduction

5.1.1 Thioperrhenate Thermodynamics

Rhenium was not discovered until 1925 and this is probably due to the fact that Re is one of the rarest elements (Colton, 1965). As a result, thermodynamic information about rhenium compounds lags behind its periodic table neighbors by decades. In particular, no data exists for the formation constants of thioperrhenates. These constants are the very first step in assessing the importance of sulfur in rhenium's geochemical behavior and improving its usefulness as a paleoredox indicator. In this chapter, I present the first experimentally determined values for thioperrhenate formation constants. The experiments performed approach thioperrhenate formation from two angles: 1) reactions of perrhenate and sulfide and 2) dissolution of Re-S solid species.

The main thrust of my M.S. thesis work (Dolor, 2005) was to measure the stability of tetra-thioperrhenate or tetra-sulfidorhenate (ReS_4^-). Exposing perrhenate (ReO_4^-) to sulfide leads to the formation of thioperrhenates. The mechanism of sulfidation is the successive replacement of oxygen atoms in ReO_4^- by sulfur atoms, but mono-thioperrhenate (ReO_3S^-) and tetra-thioperrhenate (ReS_4^-) were the only thioperrhenates observed by UV-Vis spectrophotometry. The di- and tri-thioperrhenates ($ReO_2S_2^-$ and $ReOS_3^-$) were absent due to their relative instability (Tossell, 2005). Ranade et al. (1970) propose that $ReO_2S_2^-$ absorbs at 313 nm and 400 nm. They were able to observe $ReOS_3^-$ and show that it absorbs at 310 nm, 392

nm and 505 nm (Ranade et al., 1970). The formation reactions of thioperrhenates are difficult to characterize thermodynamically, because thioperrhenates in aqueous solution polymerize and form an insoluble polymeric rhenium sulfide species before equilibrium is achieved (Peacock, 1966, Ranade et al., 1970, Dolor 2005). This insoluble Re-S species is probably structurally related to Re_2S_7 (Hibble et al., 1990; Schwarz et al., 2004).

5.1.2 Solubility of Re_2S_7 and ReS_2

The goal of these experiments was to test the hypothesis that rhenium sulfides (ReS_2 and Re_2S_7) have very low solubilities under typical deep-water conditions and as such, are potential sinks for rhenium. Currently, there are no experimentally determined solubility data for these compounds. McDonald and Cobble (1962) have measured ΔH_f values for ReS_2 and Re_2S_7 using bomb calorimetry and have calculated free energy of formation values.

5.2 Methods

5.2.1 Materials

Purchased Reagents

The following reagents were purchased and used as received: NaCl (J. T. Baker), NaOH (J. T. Baker), HCl (J. T. Baker), NaH_2PO_4 (J. T. Baker), Na_2HPO_4 (J. T. Baker), NH_4Cl (J. T. Baker), NH_3-H_2O (J. T. Baker), ReS_2 (Alfa Aesar, 99% purity, XRD analysis Figure 21) and $NaReO_4$ (Sigma-Aldrich, 99.99 % purity). All solutions were prepared from >18 MΩ· cm resistivity water (B-Pure, Barnstead). Glass ware was soaked in 5% HNO_3 and rinsed with deionized water before use.

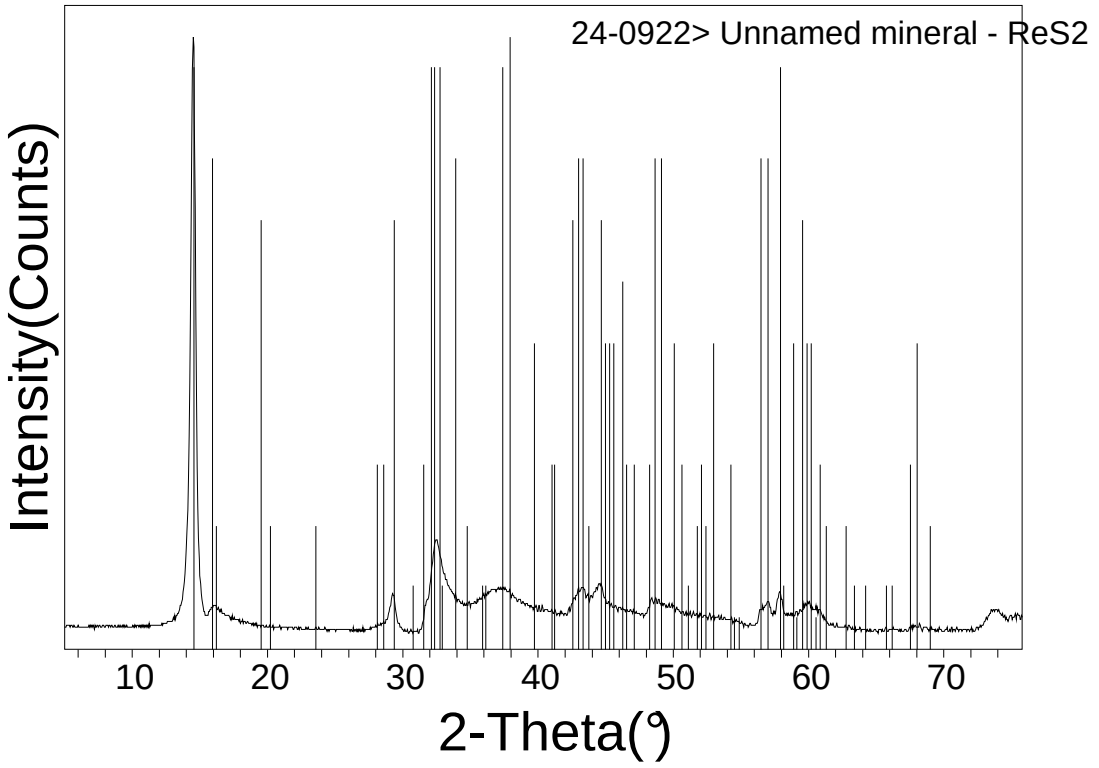

Figure 22 X-Ray Diffraction analysis of ReS_2 indicating the compound is crystalline. The curve is the intensity of X-Rays (of varying angles of incidence) diffracted as they are reflected from successive planes formed by the crystal lattice of the material. The vertical lines are the reference pattern of ReS2. Note the peak at 14.5º that coincides with a vertical line.

Sulfide Stock Solution

A one molar NaOH solution was prepared, placed in a three-neck round bottom flask, and deoxygenated with (High Purity) N_2 gas for 30 mins. High Purity H_2S gas (Air Gas East) was then bubbled through the solution for a minimum of 15 minutes. At this stage the solution contained approximately 1M NaHS and 0.1M $H_2S_{(aq)}$ Nitrogen gas was again passed through the solution for 15 minutes to remove most of the $H_2S_{(g)}$. A two-way valve was used to ensure that no oxygen could enter the flask when switching between the two gases. Stopcocks on both the inlet and outlet adapters were closed immediately after the N_2 gas was turned off to ensure no oxygen leaked into the flask while it was transferred to the N_2 filled glovebox.

Polysulfide Stock Solution

This method was obtained from Vorlicek (2002). A stock polysulfide solution (a_s=1) was prepared by adding 25 mL of 1M HS^- to 0.8 g orthorhombic sulfur; the suspension was capped and allowed to age for 150 days in an N_2 filled glove box.

Re_2S_7 Synthesis

This synthesis was adapted from McDonald and Cobble (1962) and Broadbent et al. (1954). Three grams of sodium perrhenate was dissolved in 100 mL 6M HCl and poured into a 500 ml three necked Schlenk flask. The mixture was heated to boiling and then bubbled with High Purity H_2S gas (Air Gas East) for one hour. The mixture was maintained at the boiling point during this time. After precipitation the mixture was allowed to stand overnight. The next day the suspension was filtered using a fine sintered glass funnel. A 100 mL 1:4 hydrochloric acid aliquot was added after the suspension had been allowed to drain. A second 100 ml 1:4 HCl aliquot was added, followed by 100 mL of DI water, 100 mL carbon disulfide and finally 100 mL

ethyl ether. Each liquid was allowed to drain before the next one was added. The solid was then placed in the N_2-filled glove-box and transferred to a Petri dish for drying under vacuum over P_2O_5. X-Ray diffraction analysis of the product revealed a spectrum indicative of an amorphous compound, which is what was expected since Re_2S_7 is not crystalline (Schwarz et al., 2004).

5.2.5 Total Sulfide, pH and UV-Vis Measurements

Total sulfide measurements were made by potentiometric titration with $HgCl_2$. An aliquot of the solution was added to 60 mL of deoxygenated, deionized water made basic with 0.2 g of NaOH (final pH~13). These mixtures were prepared inside a N_2 filled glove box. The vials were then sealed with screw-on lids, and removed from the glovebox just before titration. The samples were titrated against 1.25 mM or 0.2883 mM $HgCl_2$, using a Brinkmann Metrohm716 DMS Titrino Automatic titrator equipped with an Ag_2S indicating electrode and a double junction reference Ag/AgCl electrode. The end point of the titration was the steepest point on the plot of potential vs. mL of titrant delivered. Rhenium thio-anions may have been measured as sulfide ions; however the concentration of rhenium thio-anions is at least 2 orders of magnitude less than the concentration of sulfide ions (these data are presented in the results section). Thus the inaccuracy resulting from rhenium thio-anions is 1% or less of the measured ΣS^{2-} value.

All pH measurements were made with an Orion model 420A meter equipped with an Orion model 8103 combination microelectrode. At the beginning of each day, the meter was calibrated between pH 7 and 10 with VWR commercial buffers. The error associated with all pH measurements was ± 0.05.

Ultraviolet-Visible spectra were recorded on a Hewlett Packard Model 8452 Diode Array Spectrophotometer, using deionized water as the blank solution. The wavelength range of this instrument is 190 nm to 820 nm. Quartz cuvettes were used with 0.1 cm, 1 cm and 10 cm path-lengths.

5.2.3 Isotope Dilution ICP-MS

Isotope Dilution was used to analyze the ampoule contents for total rhenium concentration. The following procedure has been modified from Colodner et al. (1993b) and Geboy (2006). The ^{185}Re spike used was a dilution of the enriched isotope spike obtained from Oak Ridge National Laboratory. Natural rhenium has two isotopes, ^{185}Re has an abundance of 37.4% and ^{187}Re has an abundance of 62.6%. In the enriched spike ^{185}Re has an abundance of 99.53% and ^{187}Re has an abundance of 0.47%.

The procedural blank was checked by adding 40 µL of the 430.22pg ^{185}Re spike directly to the anion exchange column. The Re concentration of the eluant was used to determine if there were any issues from the anion exchange process. The detection limit for analyses was also determined from these blank measurements. The detection limit is defined as three times the standard deviation of ten blank measurements. The detection limit for this method was 7.3 pg.

The samples extracted from ampoules had to be diluted 1000 fold, via one 1:10 dilution followed by a 1:100 dilution, due to the high Re concentration. The diluted samples were then spiked with ^{185}Re at least 24 hours before any other processing. The ^{185}Re species was $^{185}ReO_4^-$ since this is the predominant Re species present in aqueous solution. The amount of spike added to each sample mixture was 4

times the expected Re concentration in the sample (R. J. Walker personal communication). After equilibration the samples were uncovered and placed under heat lamps in a laminar flow hood for 5-6 hours or until they had dried down to a white film. Samples were then reconstituted with 0.8 N (teflon distilled) HNO_3 and placed on a hot-plate at 100 ºC for 1-2 hours.

The anion-exchange columns were made from 5 ml disposable polyethylene pipettes and silicon wool. They were soaked in 6 N HCl for at least 24 hours. Afterwards, they were rinsed thoroughly with MilliQ water and filled with 0.25 mL of pre-cleaned resin (Biorad AG1-x8, 100-200 mesh, Cl- form). The resin was precleaned with 12 N HNO_3 at 90 ºC, followed by 8 N HNO_3, MilliQ water, 6 N HCl and 0.5 N HCl. The resin was prepared for use by eluting 5 mL MilliQ, followed by 2 mL 0.8 N HNO_3, 3 mL 6 N HNO_3 three times and finally 2 mL 0.8 N HNO_3. The sample was then loaded onto the column. Salts and loosely held metal ions were then removed by eluting 1 mL of 0.8 N HNO_3 twice. Rhenium was eluted with 4 ml of 6 N HNO_3 and collected in teflon vials. The eluant was then dried down under heat lamps in a laminar flow hood. At least 12 hours before ICP-MS analysis the samples were reconstituted with 2% v/v HNO_3. Nitric acid was used because it has the lowest instrument background for ICP-MS (Watters et al., 1997).

The samples were analyzed using a Nu Plasma Multi-Collector ICP-MS, interfaced with a CETAC Aridus Sample Introduction System. Operating conditions varied daily and the average settings are presented in Table 10 below.

Table 10 Daily Operating conditions

NuPlasma	
RF Power (W)	1100
Coolant (mL/min)	13
Auxillary Gas (mL/min)	1.4 - 2.0
Aridus	
Spray Chamber (ºC)	105
Desolvator (ºC)	160
Sweep Gas (L/min)	2.40 - 3.20
N_2 (mL/min)	0.08 - 0.14

In ICP-MS, mass spectrometry is used to quantify the ions generated by the inductively coupled plasma (Bea, 1999). This plasma is an electrodeless discharge in argon at atmospheric pressure. Energy from a radio frequency generator is coupled to the plasma and maintains it. An assembly of quartz tubes, known as the torch, houses the plasma. The torch provides physical separation between the region where electricity is added and the region containing the sample. Thus, the chemical composition of the sample solution can vary substantially without affecting the electrical processes that sustain the plasma. This is the main reason for the minimal physical and chemical interferences in ICP compared to those seen in other spectrochemical sources (Jarvis and Jarvis, 1992).

The NuPlasma is a forward geometry double-focusing mass spectrometer with double dispersion. It is fitted with a conventional ICP-MS source and water-cooled sampler and skimmer cones. Ions, at 4kV (Halliday et al., 2000) are directed into the mass spectrometer by small orifices in the sampler and skimmer cones (Jarvis and Jarvis, 1992). After passing though the cones, the ion beam is collimated and focused

by an intermediate circular aperture and two independent Einzel lenses at 2kV. The beam then enters the rectangular defining slit of the mass spectrometer. A 35 cm radius electrostatic analyzer followed by a 25 cm radius magnet, provide electrostatic beam steering (Halliday et al., 2000).

In magnetic sector instruments with ICP sources, it is necessary to move the collectors to measure the flat portion of the peak of the signal for adjacent isotopes. This is due to the mass dependent spatial separation of these ion beams (Halliday et al., 2000). In the NuPlasma the detectors have fixed positions due to the use of a variable zoom optic device (Belshaw et al., 1998). This allows the rapid determination of a suite of isotopes using very small sample quantities (Halliday et al., 2000). The collectors consists of 12 Faraday Cups and 3 Ion Counters. These detectors are directly interfaced with a computer that provides isotope ratios as well as the voltage attributed to each isotope of interest. The ratio provided, which is background corrected, can then be used in the equation below (Shabani and Masuda, 1992):

$$C = M_s K/V * (A_s - B_s R_m)/BR_m - A) \qquad 1)$$

C = rhenium concentration in sample (pg ml^{-})
M_s = mass of the stable isotope spike (pg)
V = volume of the sample to which the isotopic spike was added
A = natural abundance of the reference spike
B = natural abundance of the spike isotope
A_s = abundance of the reference isotope in the spike (from ICP-MS measurements)
B_s = abundance of the spike isotope in the spike (from ICP-MS measurements)
K = ratio of the natural and spike atomic weights
R_m = measured ratio (reference isotope/ spike isotope)

Error Analysis

There are two sources of analytical error in all ICP-MS measurements presented. The first is due to personal errors. Some sources of these errors were reading the level of liquid in a volumetric flask or pipette as well dispensing volumes from 100 μL and 1000 μL pipettes. I used my estimates of significant figures to quantify the degree of uncertainty present due to these errors. In all of my volume measurements the number of significant figures used was 3, where the first 2 figures were certain and the last digit was uncertain. So for example a 1.00 mL sample delivered to a centrifuge tube was reported as 1.00 ±0.05 mL.

The second type of error was instrumental error reported by the instrument as a relative standard deviation for each sample analyzed. This was on average ±10% (or 1/10) of the reported value. For the samples presented in Table 13, 13 and 14 the samples were first diluted 1:10 by adding 1.00±0.05 mL sample to 9.00±0.05 mL 2% v/v nitric acid. This was followed by a 1:100 dilution where 0.100±0.005 mL sample was added to 9.90±0.05 mL 2% v/v nitric acid. The total relative standard deviation in the undiluted concentration is given by:

$$\sigma_{[Re]}/[Re] = [(0.05/1)^2+(0.05/9)^2]^{1/2}+[(0.005/0.1)^2+(0.05/9)^2]^{1/2} + 1/10 = 0.20 \qquad 2)$$

Thus, for a sample with undiluted concentration of 1.103 μM the uncertainty is 0.20 of 1.103μM. The final concentration including uncertainty is 1.1 ± 0.2 μM.

I was concerned that the ^{185}Re spike was equilibrating with all of the Re in the sample. I performed a method comparison to evaluate this issue. I analyzed all of the Re_2S_7 ampoules by the solution ICP-MS method described in Chapter 4. In this method all of the Re in the solution enters the ICP, is ionized and subsequently

measured by the mass spectrometer. The Re_{TOT} values obtained by solution ICP-MS were systematically 15% lower than those obtained by ID-ICP-MS. If the ^{185}Re spike was not equilibrated with all of the Re in the sample, the solution ICP-MS values would be systematically lower. This 15% difference is within the 20% uncertainty for the ID-ICP-MS method calculated above. I thus felt confident that all the Re in the solutions was equilibrating with the spike when I used the ID-ICP-MS method.

5.2.4 Procedures for Thioperrhenate Formation Experiments

Sodium hydrogen sulfide (NaHS) was prepared from NaOH and H_2S gas as described above. Two phosphate buffers at pH 6.21 and 7.20 and two ammonia buffers at pH 9.24 and 10.28 were prepared. Two hundred and fifty milliliters of each of these buffers was deoxygenated with N_2 gas and passed into an N_2 filled glove box. Each ampoule contained 1 mM perrhenate and 95 mM buffer. The sulfide concentration ranged from 1 mM to 10 mM.

Each ampoule was filled with approximately 20 mL of liquid inside an N_2 filled glovebox. After all ampoules were filled they were capped with a piece of rubber tubing closed off on one end with a balloon. The ampoules were then passed out of the glove box and prepared for sealing. This involved wrapping pieces of aluminum foil around the rubber tubing to prevent burning of the rubber. The ampoules were then sealed with a propane/O_2 flame. The ampoules were allowed to equilibrate at 20 ºC for the periods of time indicated in the data tables.

The majority of the remaining ampoules referred to in this section were prepared by Alfred Addo-Mensah, a former student in the Helz lab. Quantitative

details about the initial contents of these ampoules were not available; however, useful information can still be gleaned from analyzing the contents. These ampoules contained perrhenate and sulfide equilibrated for over 4 years at different pH's.

A few ampoules were opened at a time inside an N_2-filled glove box. While, in the glove-box, the contents were analyzed for pH and an aliquot preserved at high pH for total sulfide (ΣS^{2-}) analysis as described above. The ampoule contents were then filtered using 0.02 μm (Whatman) syringe-filters and analyzed via UV-Vis spectroscopy immediately after being passed out of the glove box. An aliquot of the sample was filtered with Centricon YM-3 centrifugal filters (3000 NMLW, Millipore) and analyzed using the Isotope Dilution ICP-MS method for total Re described above. This procedure is illustrated in the flowchart in Figure 23.

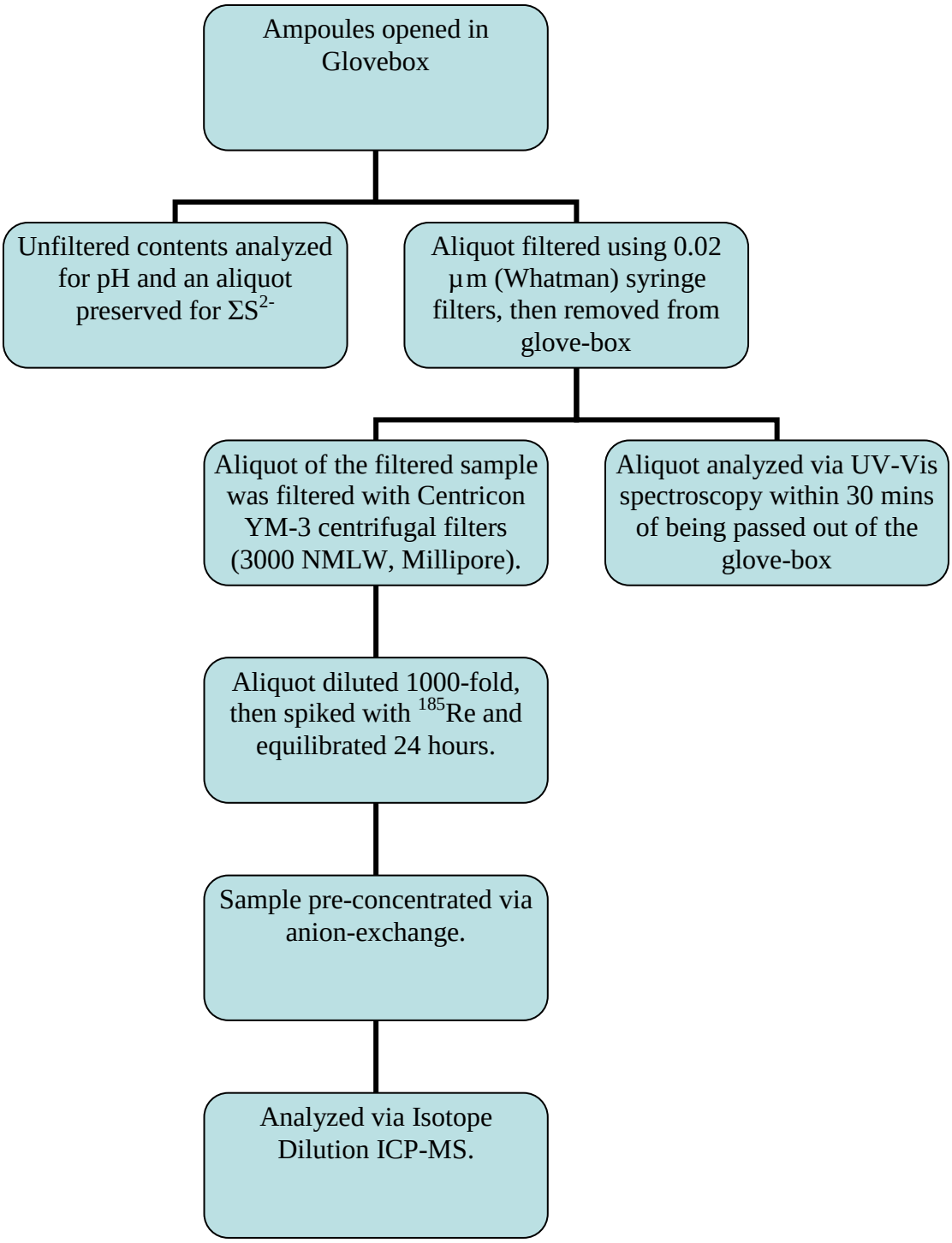

Figure 23 Flowchart illustrating procedure for opening ampoules.

5.2.5 Procedures for Solubility Experiments

Both rhenium heptasulfide and rhenium disulfide were equilibrated in 1mM and 10mM sulfide solutions ($HS^-_{(aq)}$) with 10mM phosphate or ammonia buffer and 0.1M NaCl. Note that despite similar concentrations of sulfide and buffer in some experiments pH did not change appreciably in any of these experiments. Rhenium heptasulfide was also equilibrated with polysulfide solutions. An aliquot of the polysulfide stock solution was added to the contents of the ampoule. The polysulfide stock was agitated prior to the aliquot being drawn to ensure that orthorhombic sulfur was transferred along with the dissolved polysulfides. The sealed ampoules contained orthorhombic sulfur after equilibration. Rhenium heptasulfide may contain polysulfides (Hibble et al, 1999 and Schwarz et al., 2004) so this method may be the best way to explore the solubility of this compound. The ampoules were sealed using the methods described above.

After equilibration, the resulting mixtures were filtered and analyzed for pH, sulfide, UV-Vis and total Re as described above in Section 5.2.4 and Figure 23.

5.3 Results

5.3.1 Optical Chromophores

All of the wavelengths for the thioperrhenate species were obtained from (Diemann and Muller, 1973; Muller et al., 1981) and agree well with predictions by Tossell (2005) and Zalis et al. (1999). The extinction coefficients for perrhenate (ReO_4^-) were measured in our laboratory (Dolor, 2005) and closely matched the literature values (Colton, 1965). The extinction coefficients for monothioperrhenate

(ReO_3S^-) were obtained from Muller et al. (1967). The extinction coefficients for di- and tri- thioperrhenates ($ReO_2S_2^-$ and $ReOS_3^-$) were obtained from Ranade et al. (1970). Tetrathioperrhenate (ReS_4^-) extinction coefficients were obtained from Muller et al. (1970). These values are presented below in Table 11.

Table 11 Molar extinction coefficients (ε) and corresponding wavelengths (λ_{max}) for thioperrhenate optical chromophores.

Species	Literature[1] λ_{max}(nm)	Literature[1] $\varepsilon(M^{-1}cm^{-1})$	Tossell[2] λ_{max}(nm)	Zalis[2] λ_{max}(nm)
ReO_4^-	228	$3.61x10^3$	214	
ReO_4^-	206	$6.06x10^{-3}$		
ReO_3S^-	350	$5.10x10^2$	356	
ReO_3S^-	298	$6.10x10^3$		
ReO_3S^-	215	-		
$ReO_2S_2^-$	400	-	388	
$ReO_2S_2^-$	313	-		
$ReOS_3^-$	505	-	497	
$ReOS_3^-$	392	-		
$ReOS_3^-$	310	-		
ReS_4^-	505	$9.70x10^3$	518	511
ReS_4^-	313	$1.80x10^4$		314
ReS_4^-	227	$3.00x10^4$		

[1] Literature values: perrhenate (Colton, 1965) and thioperrhenates (Diemann and Muller, 1973, Muller et al. 1967; 1973; 1981).
[2] Tossell and Zalis values are calculated.

To fit the thioperrhenate peaks Gaussian functions were used in the Scientist 3.0 program (MicroMath Scientific Software). These functions follow the form:

$$f(x) = a_1 e^{-(x-b1)\wedge 2/(c1\wedge 2)} + a_2 e^{-(x-b2)\wedge 2/(c2\wedge 2)} + \ldots \qquad 3)$$

Where,
$x = 1/(\lambda * 10^{-4})$; where λ in nm so that x is the frequency in Kk units i.e. 1000 cm^{-1}
$a = \varepsilon_b$ (extinction coefficient)
$b = 1/(\lambda_{max} * 10^{-4})$, centroid of absorption peak
c = the width of the peak at 1 standard deviation

The constants a and b were obtained from the literature and c was determined by fitting one spectrum from Dolor, 2005 that contained only ReO_4^- peaks and another that contained peaks for both ReO_3S^- and ReS_4^-. The di- and tri- thioperrhenates ($ReO_2S_2^-$ and $ReOS_3^-$) were never observed. This is consistent with Tossell's (2005) predictions that their peaks would be minor due to their relative instability.

Table 12 includes the constants used in the Gaussian functions in the Scientist model. The optical parameters for the polysulfides are from Giggenbach (1972). Figure 24 illustrates the Gaussian functions of the different components in the UV-Vis spectra obtained. Polysulfides dominate in the 340 – 460 nm wavelength range, although scattering from colloidal polymer can interfere in this range.

Table 12 Constants used for Gaussian functions: a, b and c for optical chromophores used in Scientist model.

Species	Extinction coefficient/ $M^{-1}cm^{-1}$ (a)	Peak Wavelength/nm	Peak Wavelength/Kk (b)	Width of peak/Kk (c)
ReO_4^-	$3.61x10^3$	227	44.05	4.5
	$5.72x10^3$	202	49.50	2.9
ReO_3S^-	$5.10x10^2$	350	28.57	1.2
	$6.10x10^3$	298	33.56	1.9
ReS_4^-	$9.60x10^3$	503	19.89	0.97
	$1.80x10^4$	312	32.05	1.0
	$3.00x10^4$	227	44.00	2.0
HS^-	$7.80x10^4$	230	43.50	3.1
S_4	$3.20x10^2$	368	27.20	3.3
	$1.14x10^3$	303	33.00	3.3
	$1.50x10^3$	268	37.30	2.3
S_5	$6.40x10^2$	375	26.70	3.3
	$2.00x10^3$	299	33.40	3.3
	$8.80x10^3$	268	37.30	2.3

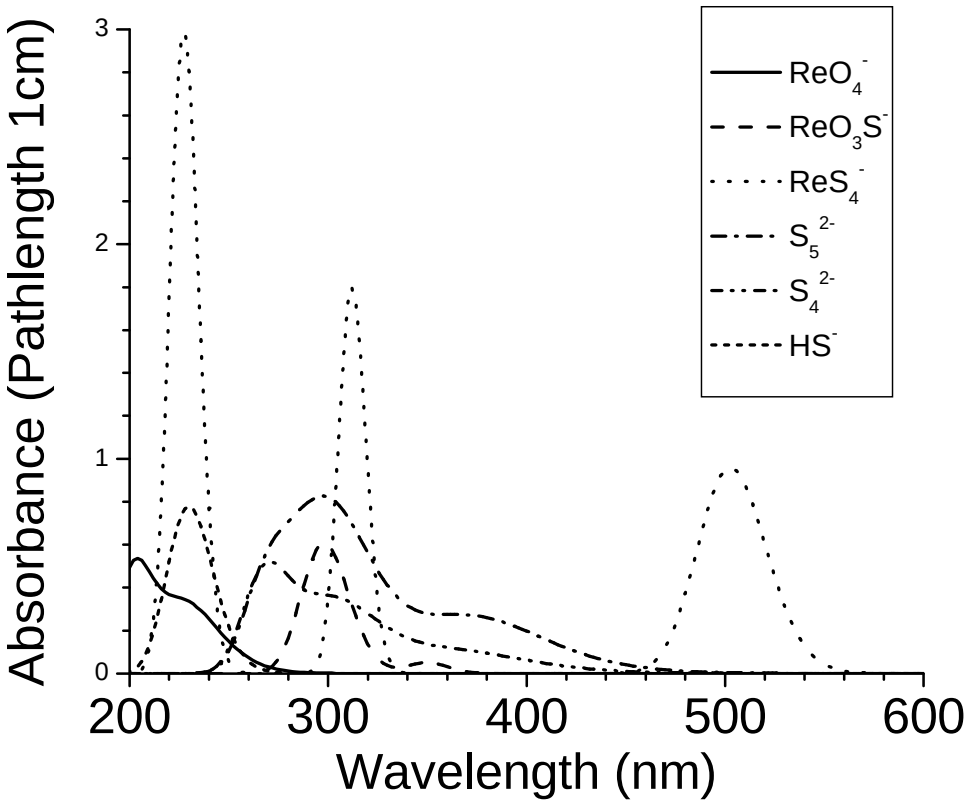

Figure 24 Optical chromophores, each shown at 10^{-4} M.

5.3.2 Data

In Table 13 results from thioperrhenate formation experiments are presented. Equilibration times range from 8 to 250 weeks, pH ranges from 6.36 to 10.26, ΣS^{2-} ranges from $1.30x10^{-4}$ M to $2.80x10^{-2}$ M and measured Re_{TOT} ranges from $1.2x10^{-5}$ M to $1.4x10^{-2}$ M. Ampoule contents from Dolor (2005) were not analyzed for total dissolved Re, thus the values presented are the initial ReO_4^- concentrations in the ampoules calculated from the dilutions made. The color reported for each ampoule persisted after filtration with 3000 NMLW filters. This indicated that the polymer goes through the filter. There was no visible precipitate in any of the ampoules prior to filtration.

UV-Vis spectra are presented in Figures 24 and 25. The peaks at approximately 300nm are due to a combination of ReO_3S^-, ReS_4^- and polysulfides: S_5^{2-} and S_4^{2-}, that absorb at 298nm, 313nm, 300nm and 303nm respectively. The peaks at 505nm could be due to $ReOS_3^-$ and/or ReS_4^-. However, it can be deduced that these peaks are only due to ReS_4^- since $ReOS_3^-$ has a peak at 392nm which is not visible in any of the spectra. Another important component of a number of the spectra is a baseline that curves upwards at shorter wavelengths, which is possibly due to a colloidal species. Tyndall beam experiments support this hypothesis since a Tyndall beam was present in all the ampoules which exhibited a color other than pink. I hypothesize that the colloidal particles are a Re-S polymer. Notably, this polymer is stable in solutions that have been equilibrated for over 5 years. Also, at similar ΣS^{2-}, more polymer is formed in ampoules at lower pHs.

Thioperrhenates in aqueous solution are known to polymerize and form an insoluble rhenium sulfide species before equilibrium is achieved (Peacock, 1966, Ranade et al., 1970, Dolor 2005). Some of the thioperrhenate formation experiments (Section 5.2.4) I undertook for my M.S. work were equilibrated at 75 ºC. A black precipitate, which could be isolated by filtration, formed in these ampoules. I analyzed this precipitate using an energy dispersive X-Ray spectrometer (a component of an Electron Probe Microanalyzer). A semi-quantitative Re:S ratio of 3:7 was obtained, indicating that the material might be structurally related to Re_2S_7. These results are for experiments performed at 75ºC so the results may not extrapolate down to 25ºC, the temperature at which the experiments presented in this chapter were performed.

Spectra A1 – A6 display a prominent peak near 300nm. These runs were all near neutral pH. Spectra B1 – B3 are near pH 9, the peak at 300nm is less prominent and declines with decreasing sulfide. Spectra A7 – A9 are near pH 10 and the peak at 300 nm is even less prominent and only clearly visible in the run with the highest sulfide. The peaks at 505 nm, although small at this scale, show the same trends with pH and sulfide as the peaks at 300 nm. Spectra D7, C3, D10, D11 and D12 are the only runs in Figure 26 that exhibit a peak at 505 nm. The sloping baseline due to the presence of a polymer is most prominent at low pH and high sulfide and is negligible at pH 10.

Table 13 Ampoules equilibrated at 25 C. Total Re was measured by ICP-MS of the filtered sample. **Samples in *italicized-bold* were not analyzed so the presented values represent the initial concentration of ReO_4^- placed in the ampoule.**

a Figure Label	Cell Size/cm	Equilibration time/weeks	Final pH	Measured [Total S2-]/mM	b Final [H2S]/mM	Total [Re]/mM	Color
A1	0.1	8	6.49	4.70	3.52	***1***	brown
A2	0.1	8	6.43	0.92	0.71	***1***	orangish brown
A3	0.1	8	6.36	0.13	0.10	***1***	pale orangish brown
A4	0.1	8	7.47	6.3	1.5	***1***	orangish brown
A5	0.1	8	7.33	1.8	0.54	***1***	orangish brown
A6	0.1	8	7.31	0.63	0.20	***1***	pale orangish brown
B1	1.0	12	9.11	9.1	0.064	***1***	colorless
B2	1.0	12	9.10	2.86	0.021	***1***	colorless
B3	1.0	12	9.10	0.58	0.0042	***1***	colorless
A7	1.0	8	10.19	9.60	0.0057	***1***	colorless
A8	1.0	8	10.20	2.70	0.0016	***1***	colorless
A9	1.0	8	10.19	0.96	0.0006	***1***	colorless
E1	1.0	250	7.01	21.5	10.2	0.04	very pale brown
D1	1.0	200	6.89	22.4	12.2	0.02	colorless
C1	1.0	40	6.89	17.3	9.40	0.04	orangish brown
E2	1.0	250	7.49	7.00	1.61	1.40	pale yellow
D2	1.0	200	7.30	2.10	0.665	0.01	pale yellow
D3	1.0	200	7.02	2.00	0.937	3.50	colorless
D4	1.0	200	7.81	26.0	3.25	0.07	pale brown
C2	1.0	40	7.64	21.2	3.70	0.04	orangish brown
D5	1.0	200	7.64	16.0	2.79	0.05	very pale brown
D6	1.0	200	7.74	7.30	1.05	1.50	pale yellow
D7	1.0	200	7.74	7.00	1.01	0.10	pink
E3	1.0	250	8.18	3.70	0.213	0.04	pale brown
D8	1.0	200	9.80	28.0	0.041	0.01	colorless
C3	1.0	40	10.26	27.8	0.014	0.10	pale pink
D9	1.0	200	8.89	27.4	0.322	0.01	colorless
D10	1.0	200	8.21	8.30	0.447	1.40	faint brown hue
D11	1.0	200	9.64	1.80	0.00380	0.02	colorless
D12	1.0	200	9.00	1.27	0.0116	0.09	pale pink

a Samples with Figure labels A and B were prepared as part of the author's M.S. Thesis (Dolor, 2005)and these data are being re-analyzed for this work.

b HS^- was calculated from total S^{2-} using the following relationships:

$\Sigma S^{2-} = HS^- + H_2S$ and $H_2S_{(aq)} \leftrightarrow HS^-_{(aq)} + H^+_{(aq)}$, K_a of $10^{-7.01}$

The activity coefficient of HS^- was calculated to be 0.90 at the 0.01M ionic strength of these solutions and the activity coefficient of H_2S was assumed to be 1.

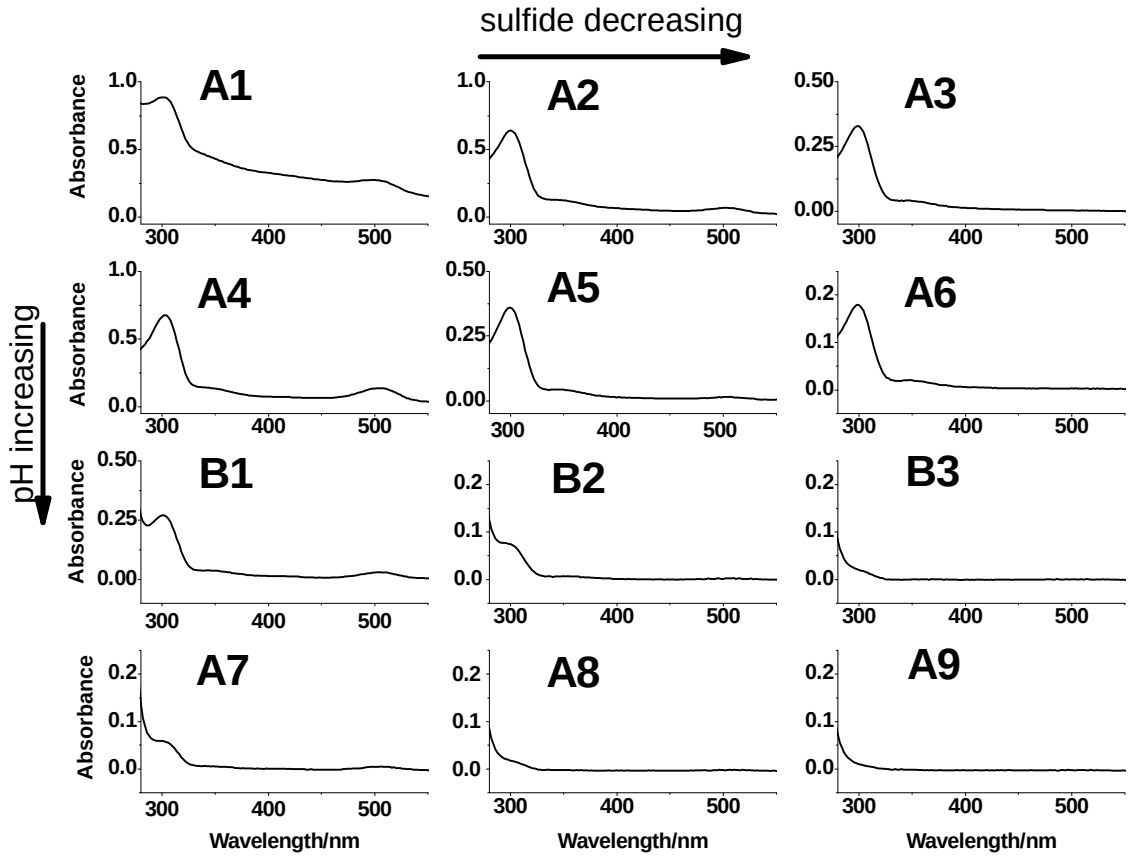

Figure 25 UV-Vis Spectra for ampoules from M.S. Thesis (Dolor 2005). Details of ampoule contents are outlined in Table 13. All samples contained 1 mM total Re and were equilibrated for 8-12 weeks at room temperature. Spectra A1-A6 were taken in 0.1 cm cuvette; other spectra were taken in a 1.0 cm cuvette.

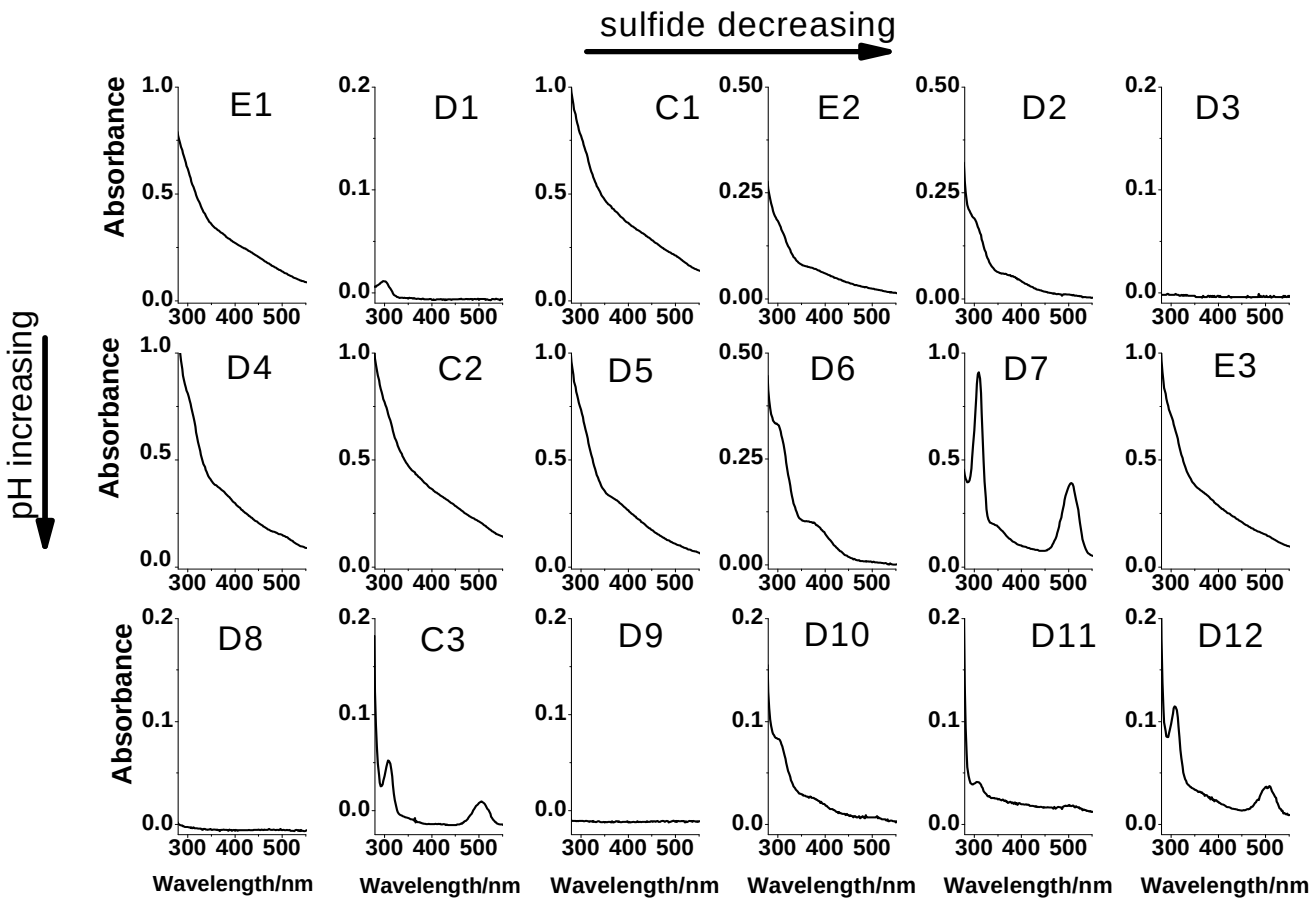

Figure 26 UV-Vis Spectra of ampoules equilibrated for longer time periods (C: 40 weeks, D: 200 weeks; E: 250 weeks). Details of ampoule contents are outlined in Table 13. All Spectra were taken in a 1.0 cm cuvette.

In Table 14 data for Re_2S_7 solubility experiments are presented. Equilibration times are either 7 or 18 weeks, pH ranges from 7.35 to 11.43, ΣS^{2-} ranges from 0.07 mM to 6.20 mM and Re_{TOT} ranges from 2.00 µM to 37.4 µM. UV-Vis spectra are presented in Figure 27. The peaks at 300 nm are the tail-end of the very large (i.e. absorbance > 2) peaks due to HS^- centered at 230nm. Spectrum G1 is the only run that exhibits peaks at 310 nm and 505 nm. As described above, these peaks are due to ReS_4^-. The peak at 330 nm in spectrum F2 is due to an unknown absorbing species which is not visible in any of the other spectra.

Table 14 Re_2S_7 solubility

Figure Label	Cell Size/ cm	Equilibration Time/weeks	Final pH	Measured [Total S2-]/ mM	Final [H2S]/mM	S(rhom)	Total [Re]/uM
F1	10	7	7.35	0.41	0.12	no	10.6
F2	10	7	7.41	0.17	0.04	yes	9.76
F3	10	7	8.72	0.67	0.01	no	10.1
F4	1	7	8.68	0.074	0.0014	yes	16.1
F5	1	7	11.38	0.47	0.000018	no	37.4
F6	1	7	11.43	0.21	0.0000072	yes	16.7
G1	10	18	7.46	6.20	1.50	no	2.00
G2	0.1	18	7.67	2.20	0.363	yes	3.04

In Table 15 data for ReS_2 solubility experiments are presented. Equilibration times range from 13 weeks to 76 weeks, pH ranges from 7.55 to 11.95, ΣS^{2-} ranges from 0.48 mM to 8.24 mM and Re_{TOT} ranges from 0.21 µM to 2.15 µM. UV-Vis spectra are presented in Figure 28. The peaks at 300 nm are the tail-end of the very large (i.e. absorbance > 2) peaks due to HS^- centered at 230 nm. The peaks at 300 nm and 360 nm in spectra H3 and I2 are due to an unknown absorbing species which is not visible in any of the other spectra.

Table 15 ReS_2 Solubility

Figure Label	Cell Size/ cm	Equilibration Time/weeks	Final pH	Measured [Total S2-]/ mM	Final [H2S]/mM	S(rhom)	Total [Re]/uM
H1	10	13	7.55	0.61	0.13	no	1.12
No Spectrum		18	7.58	1.90	0.371	no	2.15
No Spectrum		76	7.58	0.61	0.12	yes	0.32
H2	10	13	8.75	0.78	0.013	yes	0.92
I1		18	8.85	2.00	0.0258	yes	0.68
No Spectrum		76	10.35	0.80	0.00033	no	0.94
H3	10	13	11.43	0.84	0.000029	no	1.69
I2	10	18	7.5	6.80	1.54	no	0.21
No Spectrum		52	7.41	7.15	1.89	no	0.29
I3	10	18	9.14	7.00	0.0465	no	0.73
No Spectrum		52	11.94	8.24	0.0000874	no	1.21
I4	10	18	11.95	7.80	0.0000808	no	0.64

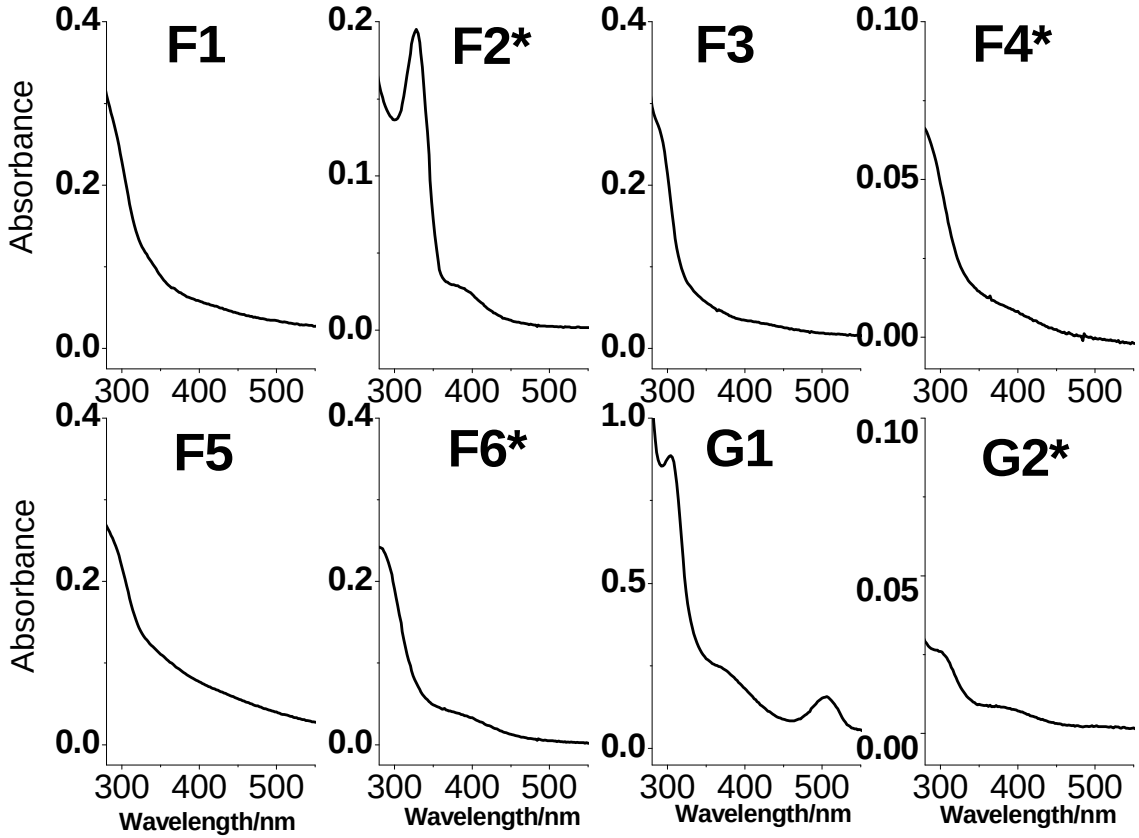

Figure 27 Re_2S_7 Solubility UV-Vis spectra. Details of ampoule contents are outlined in Table 14. F1-F3 and G1 were taken in a 10 cm cuvette, F4-F6 were taken in a 1.0 cm cuvette, and G2 was taken in a 0.1 cm cuvette. The spectra designated with an asterisk were equilibrated with orthorhombic sulfur.

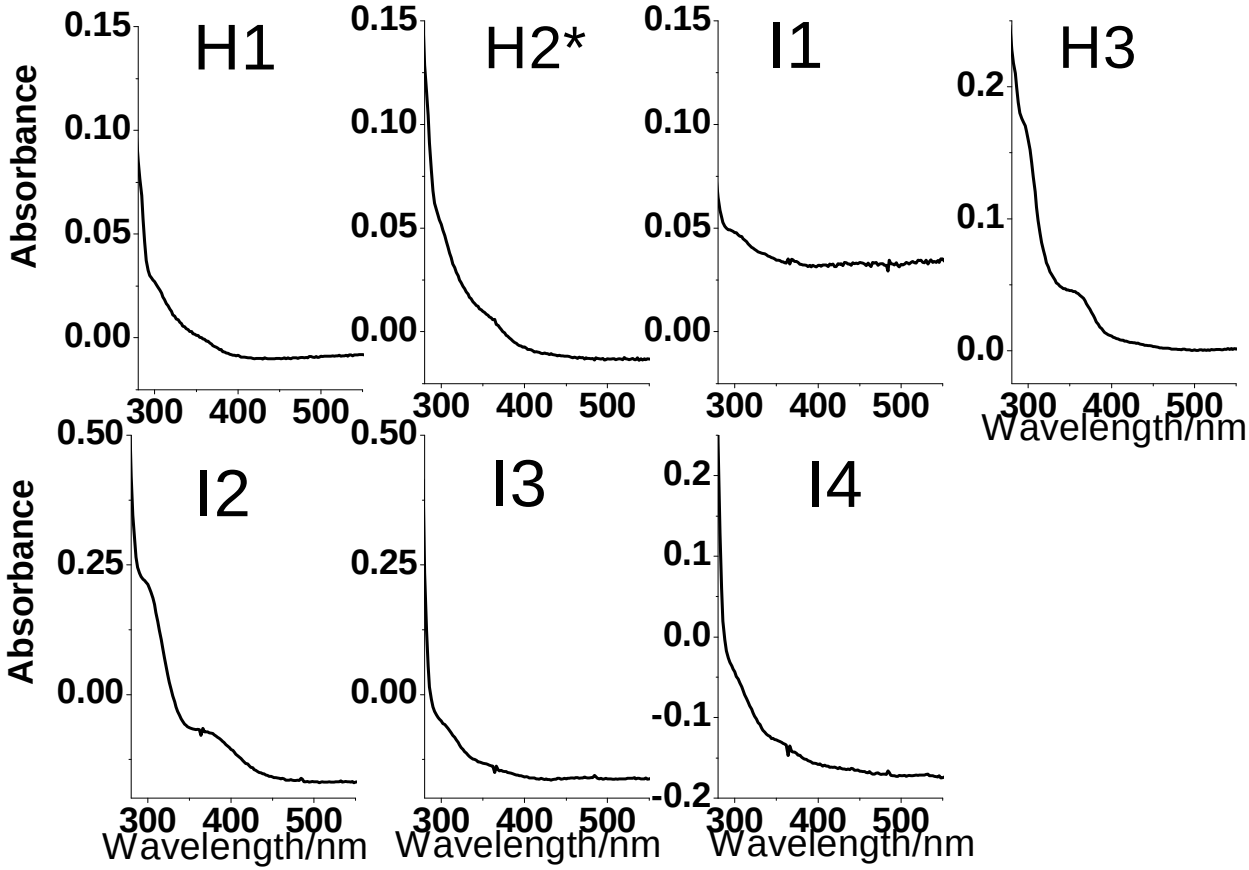

Figure 28 ReS_2 solubility UV-Vis spectra. Details of ampoule contents are outlined in Table 15. All spectra were taken in a 10 cm cuvette. The spectrum designated with an asterisk was equilibrated with orthorhombic sulfur.

5.3.3 Curve Fitting

Scientist 3.0 was used to fit the spectra. The Gaussian function detailed above in Table 12 and Figure 24 was used. I used a simple exponential decay to describe the sloping baseline which was due to the presence of a colloidal species. This function contains two parameters, the absorbance at zero wavelength (nm) and the e-fold length (the wavelength range over which the absorbance decreases by 1/e. In Figure 29 I present the results of the curve-fitting exercise for spectrum A7. This sample contained 1 mM total Re, determined from dilution and was equilibrated for 8 weeks.

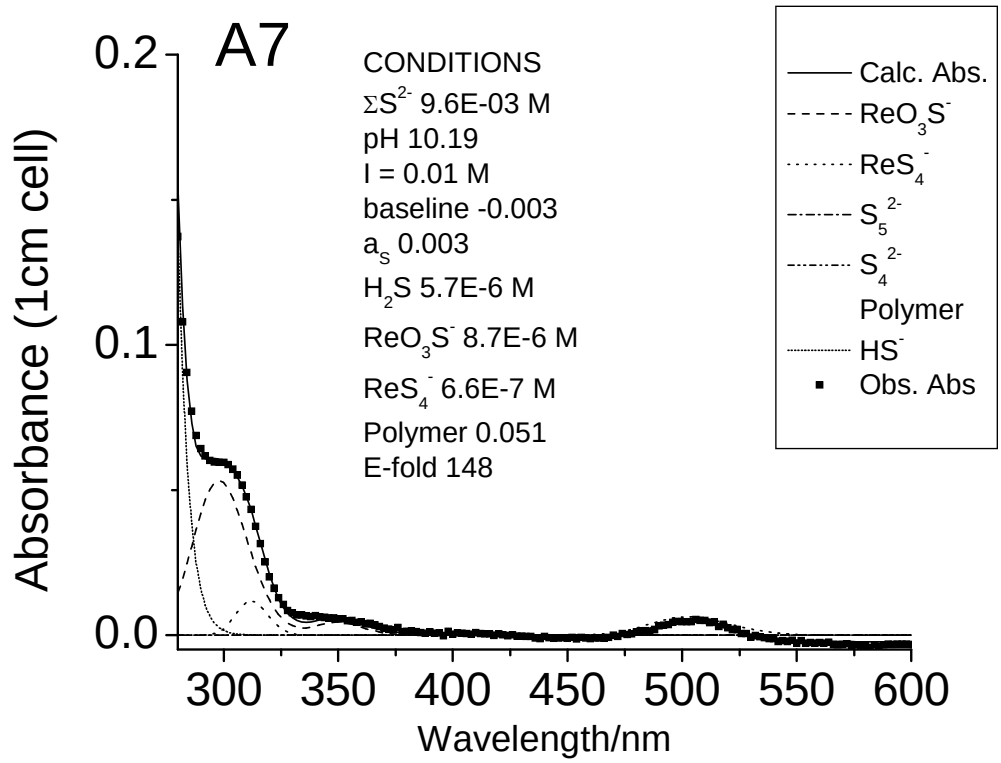

Figure 29 Scientist curve-fitting for spectrum A7 illustrating component spectra and total calculated spectrum.

5.4 Discussion

5.4.1 Thioperrhenate Formation

As described above, Scientist was used to fit the UV-VIS spectra and extract concentration information for the thioperrhenates formed. I used the spectra with the smallest sloping baselines, implying minimal polymer formation, so that I could assume that most of the Re in the system was in the form of dissolved $ReS_xO_{4-x}^-$ species ($0 \leq x \leq 4$). I assumed that the polymer (and therefore any Re in the polymer) was zero. Therefore, the ReO_4^- concentrations calculated by difference are upper limits, and the stability constants, K_{01} and K_{04} are lower limits. The concentration data and reaction quotients are presented below in Table 16.

Reactions and reaction quotient expressions:

$$ReO_4^- + H_2S \leftrightarrow ReO_3S^- + H_2O \quad (4)$$

$$K_{01} = [ReO_3S^-]/[ReO_4^-]\,[H_2S] \quad (5)$$

$$ReO_3S^- + 3H_2S \leftrightarrow ReS_4^- + 3H_2O \quad (6)$$

$$K_{14} = [ReS_4^-]/[\,ReO_3S^-]\,[H_2S]^3 \quad (7)$$

$$ReO_4^- + 4H_2S \leftrightarrow ReS_4^- + 4H_2O \quad (8)$$

$$K_{04} = [ReS_4^-]/[ReO_4^-]\,[H_2S]^4 \quad (9)$$

Table 16 Thioperrhenate formation constant calculations

Figure Label	Equilibration Time/ weeks	Final pH	Final [H2S]/M	Total [Re]/M	a [ReO3S-]/ M	a [ReS4-]/M	b [ReO4]/M	c logQ01	d LogQ14	e LogQ04	Color
A7	8	10.19	5.72E-06	***1E-03***	6.6E-06	8.7E-07	9.93E-04	3.1	14.8	17.9	colorless
A8	8	10.20	1.57E-06	***1E-03***	2.5E-06	2.4E-07	9.97E-04	3.2	16.4	19.6	colorless
C3	40	10.26	1.41E-05	9.7E-05	4.5E-06	2.3E-06	9.02E-05	3.5	14.3	17.8	pale pink
D11	200	9.64	3.80E-06	2.1E-05	1.3E-06	4.2E-07	1.93E-05	4.2	15.8	20.0	colorless
D12	200	9.00	1.16E-05	8.6E-05	5.5E-06	2.6E-06	7.79E-05	3.8	14.5	18.3	pale pink

[a] $[ReO_3S^-]$and $[ReS_4^-]$ were obtained from Scientist modeling of the UV-vis spectra.
[b] ReO_4^- was calculated as: $[ReO_4^-]$ = Total Re – $[ReO_3S^-]$ – $[ReS_4^-]$
[c] Log K_{01} : $ReO_4^- + H_2S \leftrightarrow ReO_3S^- + H_2O$ $K_{01} = [ReO_3S^-]/[ReO_4^-]\,[H_2S]$
[d] Log K_{14}: $ReO_3S^- + 3H_2S \leftrightarrow ReS_4^- + 3H_2O$ $K_{14} = [ReS_4^-]/[ReO_3S^-]\,[H_2S]^3$
[e] Log K_{04}: $ReO_4^- + 4H_2S \leftrightarrow ReS_4^- + 4H_2O$ $K_{04} = [ReS_4^-]/[ReO_4^-]\,[H_2S]^4$

The reaction quotients agree within one order of magnitude. The average values are: $K_{01} = 10^4$, $K_{14} = 10^{15}$ and $K_{04} = 10^{19}$. Tossell (2005) calculated these stability constants and reported these values: $K_{01calc} = 10^{1.5}$, $K_{14calc} = 10^{12.6}$ and $K_{04calc} = 10^{14.1}$. The differences between the experimental and calculated values are between 3 and 4 orders of magnitude. As mentioned above, the experimental values are lower limits of the formation constants, however they are higher than the calculated values.

5.4.2 Thioperrhenates as precursors of ReS_n nanophases

For the remaining samples that exhibited sloping baselines and quantifiable ReS_4^-, I attempted to quantify the stability of the polymer that I hypothesized was responsible for the sloping baseline. One example of the curve-fitting result is presented in Figure 30 and the results for all the samples are compiled in Table 17.

Tables 15 and 16 combined exclude a few of the samples presented in Table 13. This is because these data do not meet the criterion of reliably quantified ReS_4^-. Most of them display spectra that may be indicative of polysulfides or have very little absorbance leading to small signal to noise ratios.

Table 17 Table of thioperrhenate data calculated using Scientist.

Figure Label	Equilibration Time/ weeks	Final pH	Final HS-/M	Total [Re]/M	a [ReO3S-]/ M	a [ReS4-]/ M	b [ReO4]/ M	H+/HS-	color
A1	8	6.49	1.18E-03	1E-03	4.10E-05	7.70E-06	9.51E-04	2.75E-04	brown
A2	8	6.43	2.08E-04	1E-03	7.10E-05	3.80E-06	9.25E-04	1.79E-03	orangish brown
A3	8	6.36	2.58E-05	1E-03	4.20E-05	5.40E-07	9.57E-04	1.69E-02	pale orangish brown
A4	8	7.47	4.80E-03	1E-03	6.90E-05	9.80E-06	9.21E-04	7.06E-06	orangish brown
A5	8	7.33	1.26E-03	1E-03	4.80E-05	5.60E-07	9.51E-04	3.72E-05	orangish brown
A6	8	7.31	4.34E-04	1E-03	2.40E-05	3.70E-07	9.76E-04	1.13E-04	pale orangish brown
C1	40	6.89	7.90E-03	3.8E-05	1.10E-05	1.10E-06	2.59E-05	1.63E-05	orangish brown
C2	40	7.64	1.75E-02	4.2E-05	1.10E-05	1.40E-06	2.96E-05	1.31E-06	orangish brown
D4	200	7.81	2.27E-02	7.1E-05	1.10E-05	2.90E-06	5.71E-05	6.81E-07	pale brown
D5	200	7.64	1.32E-02	5.0E-05	1.60E-05	1.20E-06	3.28E-05	1.73E-06	very pale brown
E3	250	8.18	3.49E-03	3.9E-05	1.90E-05	1.80E-06	1.82E-05	1.89E-06	pale brown
D7	200	7.74	5.99E-03	9.8E-05	4.80E-05	3.30E-05	1.70E-05	3.04E-06	pink
B1	12	9.11	8.99E-03	1E-03	3.20E-05	2.90E-06	9.65E-04	8.64E-08	colorless
B2	12	9.10	2.84E-03	1.0E-03	1.10E-05	4.20E-07	9.89E-04	2.80E-07	colorless
D2	200	7.30	1.44E-03	7.9E-06	2.50E-06	1.00E-06	4.40E-06	3.49E-05	pale yellow

[a] $[ReO_3S^-]$and $[ReS_4^-]$ were obtained from Scientist modeling of the UV-vis spectra.
[b] ReO_4^- was calculated as: $[ReO_4^-]$ = Total Re – $[ReO_3S^-]$ – $[ReS_4^-]$.

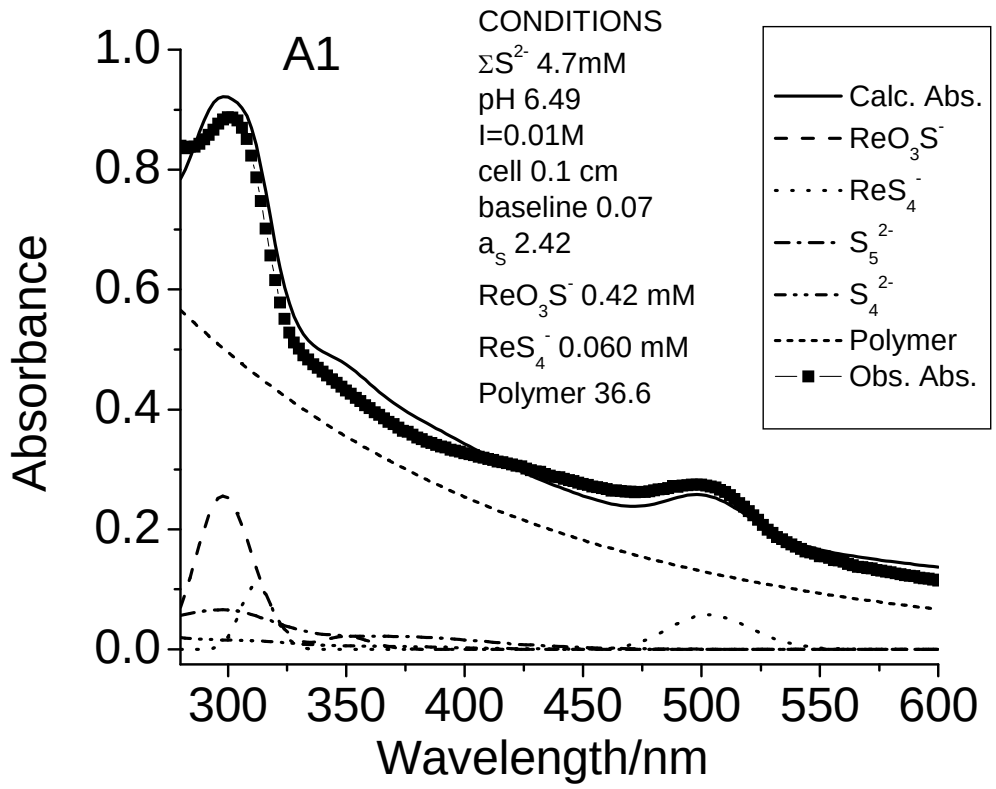

Figure 30 Scientist curve-fitting for spectrum A1 illustrating component spectra and total calculated spectrum.

In Figure 31, I have plotted the final log ReS_4^- vs. log (H^+/HS^-) for all of the runs with reliably quantified ReS_4^- (Table 17). Figure 31 is based on the assumption that the reaction shown will control the relationship between Re_2S_7 and ReS_4^-. Samples for which this assumption is valid will be expected to fall on a saturation line with a slope of -0.5. Solid squares represent samples that were visually determined to have an orange or brown color, which I associate with a polymer.

The region between the two lines in the figure has been labeled the polymer formation zone based on the fact that most samples that fall in this region are observed to have a brownish color. Samples below this region (circles) are clear and often pink, owing to ReS_4^-.

If the polymer were a pure solid, all samples containing this material would fall on a single saturation line and samples that were undersaturated would scatter below it. This behavior clearly does not occur in the figure probably because the rhenium sulfide polymer consists of materials within a range of physical and chemical properties (e.g. molecular weight). Note that some samples within the polymer formation zone did not form polymer, as scored visually. However, the spectral fits presented above suggest that some polymer is present nonetheless.

A likely reason that the points in Figure 31 do not fall on a line is that there is an uncontrolled variable affecting the solubility. A plausible candidate is the activity of zero-valent sulfur, which in combination with sulfide controls polysulfide concentrations through

$$H_2S + nS^0 \leftrightarrow S_{n+1}^{2-} + H^+ \qquad 10)$$

The reason for suspecting this is that Schwarz et al. (2004) has shown that Re_2S_7 contains polysulfide sulfur. Results of EXAFS experiments were used to propose that two idealized compositions for Re_2S_7 are $Re^{IV}(S)_{0.5}(S_2)_{1.5}$ and $Re^{V}(S)_{1.5}(S_2)_1$ (Schwarz et al., 2004).

In terms of our experimental aim, evaluating potential sinks of rhenium under reducing conditions, the most important characteristic of this polymer, is that it is very soluble. These experiments were performed at H^+/HS^- ratios that cover the range found in nature and dissolved Re concentrations never fell below 10^{-7} M. This indicates that this polymer on its own is not a likely candidate as the sink of Re in nature. However, the fact that this polymer forms under such a wide range of H^+/HS^- ratios means that it could play a role in controlling the fate of Re under reducing conditions. For example, this polymer could adhere to organic matter and be the ultimate sink of Re. These results thus provide the foundation for future experiments exploring Re/S behavior.

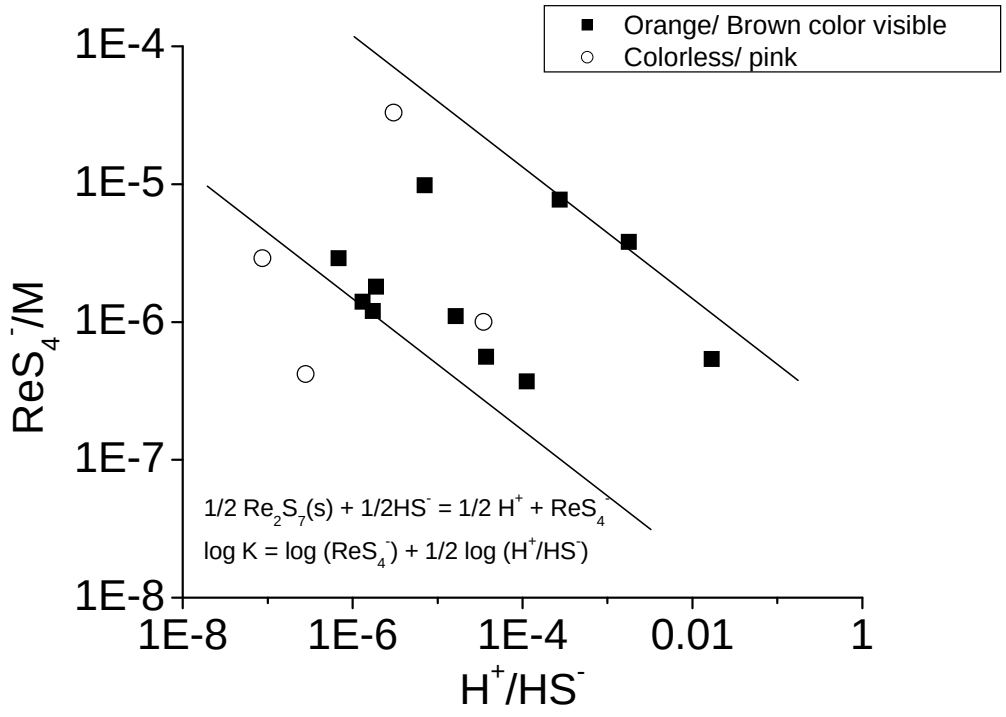

Figure 31 Plot of ReS_4^- vs. H^+/HS^-. This figure is based on the assumption that the reaction shown will control the relationship between Re_2S_7 and ReS_4^-.

5.4.2 Solubility of ReS_2

I present ReS_2 solubility data, separated into groups according to sulfide concentration in Figure 32. If either a stable or meta-stable solubility equilibrium controls the concentrations of Re in solution, then the solubility reaction does not produce or consume protons. This is clear from the fact that there is no trend in data covering five orders of magnitude in H^+. The samples containing orthorhombic sulfur are not distinguishable in their Re concentration from samples containing no orthorhombic sulfur. This shows that the dissolved Re species do not contain polysulfides. It probably also rules out a redox sensitive equilibrium, since the samples containing orthorhombic sulfur should be more oxidized. Thus, if any equilibrium is controlling, then the dissolved species probably have the same oxidation state as the solid, i.e. Re(IV).

In Figure 32, I have also included a shaded area that illustrates ReO_2 solubility as reported by Kim and Boulegue (2003) of $4 \times 10^{-7} - 10^{-6}$ M. Kim and Boulegue (2003) hypothesize that the reaction controlling ReO_2 solubility is:

$$ReO_{2(cr)} + H_2O_{(l)} \leftrightarrow ReO(OH)_2^{0}{}_{(aq)} \qquad 11)$$

Based on experiments with solid Re metal in hydrothermal solutions Xiong et al. (2006) proposed that the temperature dependence of the equilibrium reaction above is:

$$\text{Log } K = (-4700 \pm 760/\ T) + 6.2 \pm 2.0\ (2\sigma) \qquad 12)$$

Thus, the range of log K values at 25 ºC is -14 to -5. This range encompasses the solubility of ReO_2 reported by Kim and Boulegue (2003) of $4 \times 10^{-7} - 10^{-6}$ M.

My data fall in the same concentration range and this could be accidental. However, if not, it could be indicating that ReS_2 dissolves irreversibly and the products hydrolyze to $ReO(OH)_2^0$. If such a process continues, eventually the $ReO(OH)_2^0$ concentration will grow to exceed the solubility of ReO_2, after which it will cease to rise as ReO_2 starts to precipitate. In this interpretation, ReS_2 behaves like MoS_2, which seems to not precipitate from aqueous solution at room temperature. The net, irreversible reaction would be:

$$ReS_2 + 2H_2O \rightarrow ReO_2 + 2H_2S \qquad 13)$$

Very likely this process would stop after the outer layers of the ReS_2 particles become coated with ReO_2.

A concern is that this irreversible hydrolysis reaction proposed is thermodynamically unfavorable. The log K of this reaction is -37.39. Thus any $H_2S_{(aq)}$ concentration above $10^{-18.7}$ would drive the reaction to the left. This means that hydrolysis would not happen spontaneously. Probably the ReO_2 with which the system seems to equilibrate has been formed by oxidation of the ReS_2 starting material before the experiment.

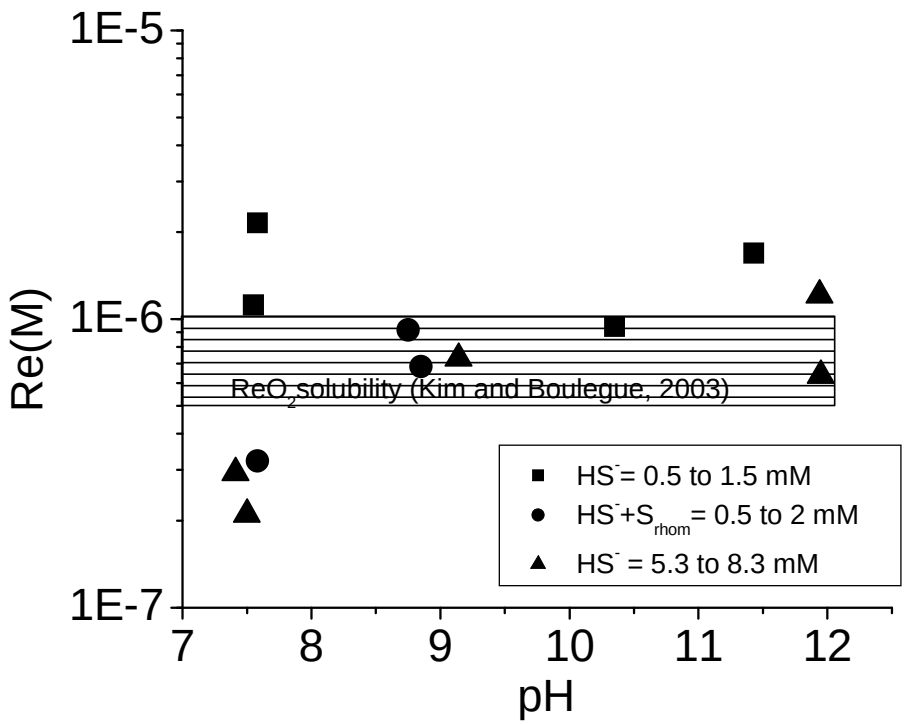

Figure 32 ReS_2 solubility data separated into groups according to sulfide concentration. Shaded area is the concentration range of ReO2 solubility measured by Kim and Boulegue (2003).

5.4.3 Solubility of Re_2S_7

I present Re_2S_7 solubility data, separated into groups according to presence of orthorhombic sulfur in Figure 33. The proposed reactions are:

At low sulfide: $4H_2O_{(l)} + {}^1/_2Re_2S_{7\,(s)} = ReO_4^-{}_{(aq)} + {}^7/_2HS^-_{(aq)} + {}^9/_2H^+{}_{(aq)}$ 14)

$3H_2O_{(l)} + {}^1/_2Re_2S_{7(s)} = ReO_3S^-_{(aq)} + {}^5/_2HS^-_{(aq)} + {}^7/_2H^+_{(aq)}$ 15)

At high pH: ${}^1/_2HS^-_{(aq)} + {}^1/_2Re_2S_{7\,(aq)} = ReS_4^-{}_{(aq)} + {}^1/_2H^+_{(aq)}$ 16)

There is a slight trend in solubility, where five orders of magnitude increase in pH results in just over one order of magnitude increase in solubility. This suggests that the solubility reaction releases protons. Below pH 9 the samples that contain orthorhombic sulfur exhibit slightly higher or nearly equal solubility as those that do not. Above pH 11 this trend is reversed and the samples that do not contain orthorhombic sulfur exhibit higher solubility. This result is unexpected. Schwarz et al. (2004) have proposed that the structure of Re_2S_7 contains polysulfides. This would result in decreased solubility in the presence of polysulfides. I only observe this at pH above 11.

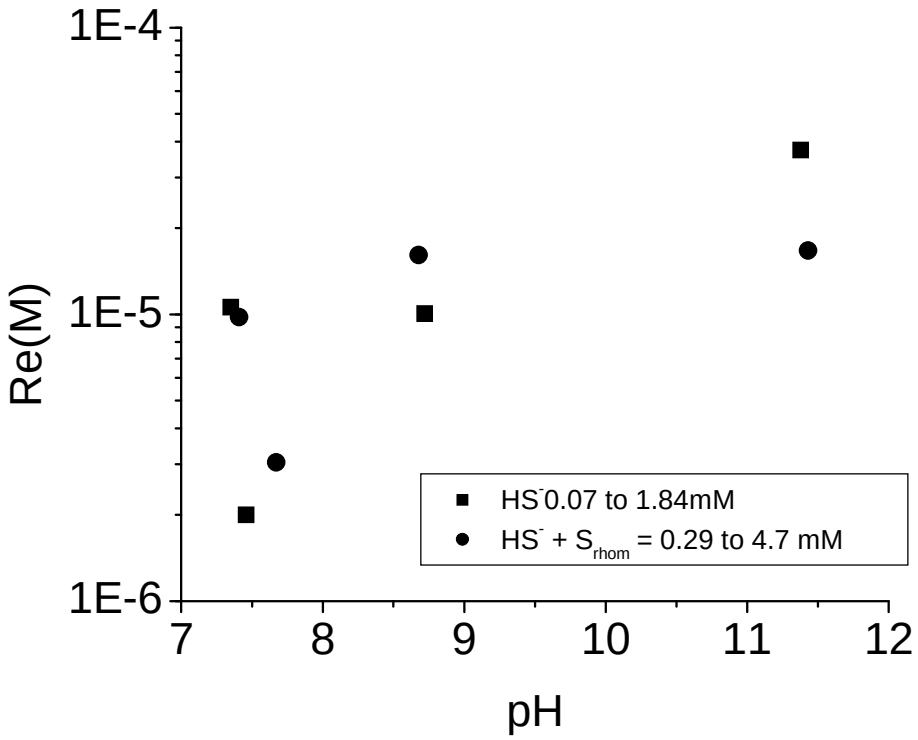

Figure 33 Re_2S_7 solubility data separated into groups according to presence of orthorhombic sulfur.

In Figure 34 I present a modified version of Figure 31 that includes the data point for the one Re_2S_7 solubility experiment that contained quantifiable ReS_4^- (spectrum G1). This experiment contained the highest concentration of total sulfide by almost an order of magnitude and this is probably why it is the only one to exhibit a ReS_4^- peak.

The data point for this experiment (denoted by a star), falls within the polymer formation zone but well below the upper line which denotes agreement with the proposed reaction. My starting material was Re_2S_7 so I expected this point to be much closer to the upper line. This is most likely because the starting material Re_2S_7 is more stable and thus less soluble that the Re_2S_7-related polymer. More experiments with a range of pH and total sulfide are needed to adequately evaluate this hypothesis.

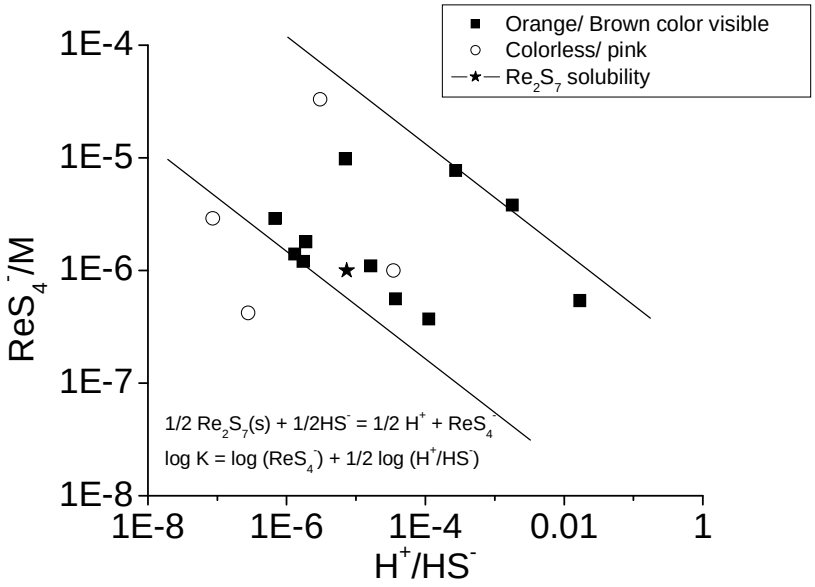

Figure 34 Plot of ReS_4^- vs. H^+/HS^- including data point for dissolution of Re_2S_7.

Chapter 6: Conclusion

In this work I approached the problem of determining rhenium's fixation mechanisms from three angles. The first was using Laser Ablation ICP-MS to investigate correlation coefficients between rhenium and other elements such as sulfur, molybdenum and iron. The second approach was to investigate microbial fixation of rhenium via two species of iron-reducers and two-species of sulfate reducers. The third approach was to explore thioperrhenate formation thermodynamics and rhenium sulfide solubilities.

In Chapter 2, I demonstrated that fine grain sediment samples can be pelletized without a binder for analysis by Laser Ablation Inductively Coupled Plasma Mass Spectrometry. I also evaluated the accuracy and precision of this method. Using a laser spot size of 100 microns, relative standard deviations (RSDs) obtained from the pellets of powdered sediment and shale Standard Reference Materials (SRMs) were comparable to RSDs obtained from a homogenous glass SRM, NST 610. Although the glass SRM was probably more accurately calibrated, when it was used to analyze the sediment and shale SRMs, substantially less accurate results were obtained for a large group of elements. More accurate results were obtained when the shale and sediment are analyzed against each other. This emphasized the importance of matrix matching.

I then applied this method, LA-ICP-MS, to Chesapeake Bay samples since it provided a new approach that minimized sample preparation and contamination while

yielding data on a much larger list of elements simultaneously. Anthropogenic influences on trace element profiles in dated sediments from estuaries have been often documented, with the vast majority of studies focusing on a short list of high-abundance trace elements. I presented concentrations and enrichment factor profiles for 22 elements at a locality that was 50 km southeast of Baltimore, the principal industrial city on Chesapeake Bay. Samples representing deposition over almost the entire 20th century were obtained from two archived cores collected 20 years apart.

The following elements exhibited profiles consistent with a strong anthropogenic influence, i.e. enrichment after 1920 followed by decline after ca.1980, possibly reflecting increased regulatory efforts: Mn, Co, Cu, Zn, Ag, Cd, In, Sn, Sb, Te, Tl, Pb and Bi. As expected, the redox-sensitive elements: Mo, Re and U had similar profiles to one another. The remaining elements exhibited featureless profiles: Ti, Fe, Ga, Ge and Nb. Previously, the potentially hazardous elements, Ag, In, Sb, Te, Tl and Bi, had been measured only rarely in estuarine sediments and never in Chesapeake Bay.

In Chapter 3, I presented my final use of LA-ICP-MS: to explore correlations between chalcophile elements. In particular, I wanted to investigate what elements were spatially correlated with rhenium in sediments. I analyzed the raw counts per second data from the instrument using statistical tools and obtained correlation coefficients. I determined that it was only possible to use LA-ICP-MS in this way for elements with a large enough abundance such as Mo or As. The method was not as useful for Re because of its low abundance and the large beam-sizes needed to get an adequate signal.

Rhenium is fixed at sediment depths where iron reduction and sulfate reduction are the dominant microbial terminal electron-accepting processes. In Chapter 4, I investigated Re behavior in pure, batch cultures of two dissimilatory sulfate-reducing strains (*Desulfovibrio desulfuricans* subsp. *desulfuricans* and *Desulfovibrio desulfuricans* ND132) and two iron-reducing strains (*Geobacter metallireducens* GS-15 *and Shewanella oneidensis* MR-1). Perrhenate concentrations ranged from 0.05 to 12 μM. These concentrations ranged from 4 to 7 orders of magnitude larger than seawater Re concentrations. None of the organisms tested significantly removed Re from solution during one week's growth to stationary phase at 30°C; nor was Re significantly precipitated or sorbed to inactive cells incubated at 4°C. Despite these results, the sulfate reducing cultures appeared to have reached supersaturation relative to $ReS_{2(s)}$, and the iron reducing cultures may have reached supersaturation relative to $ReO_{2(s)}$.

I concluded that neither direct nor short-term indirect microbial processes are likely to explain Re fixation in sediments. My results could not exclude the possibility that microbial metabolites, such as Fe(II) or sulfide, drive abiotic Re fixation over longer periods of time. The lack of Re reduction by dissimilatory sulfate reducing bacteria and iron-reducing bacteria contrasted with published reports of Tc behavior. Despite many qualitative similarities between Re and Tc, it was clear that these two elements were quantitatively dissimilar, with Re fixation requiring more intensely reducing conditions.

In Chapter 5, I explored methods for determining the stability constants of rhenium sulfide species in order to test the hypothesis that Re is accumulated as a

sulfide under reducing conditions. In the first set of experiments, I established lower limits for the stability constants of ReO_3S^- and ReS_4: $K_{01} = 10^4$, $K_{14} = 10^{15}$ and $K_{04} = 10^{19}$. In the second set of experiments I evaluated the hypothesis that Re_2S_7 or ReS_2 have low enough solubilities to be the sink of Re under reducing conditions. My results did not support this hypothesis. However in the case of ReS_2 it is possible that ReO_2 (which is very soluble) formed on the surface of the ReS_2 before the experiment began. Further work must be done to eliminate this possibility. In the case of Re_2S_7, my results indicate that this is not the likely sink of Re under reducing conditions.

The values presented in this work are the first experimentally determined stability constants for thioperrhenates and future work will be aimed at verifying these values. Future work should also involve characterizing and exploring the sorption characteristics of the Re-S polymer formed when ReO_4^- is exposed to sulfide at environmentally relevant H^+/HS^- ratios. This species is likely to play a crucial role in Re fixation mechanisms in reducing environments.

Appendices

Table A I Correlation coefficients for Core 7430 54, 55 laser track one.

	S33	Ca43	Ti49	V51	Mn55	Fe57	Co59	Ni60	Cu63	Zn66	As75	Se77	Mo95	Mo97	Sb121	Sb123	Re185	Re187	Tl205	Pb208
S33	1.00																			
Ca43	-0.25	1.00																		
Ti49	-0.27	0.41	1.00																	
V51	-0.43	0.31	0.62	1.00																
Mn55	0.31	-0.09	-0.10	-0.11	1.00															
Fe57	0.76	-0.27	-0.27	-0.51	0.34	1.00														
Co59	0.16	0.03	0.21	0.12	0.22	0.11	1.00													
Ni60	0.24	-0.04	0.03	-0.01	0.21	0.13	0.50	1.00												
Cu63	0.27	0.03	0.19	0.06	0.32	0.13	0.52	0.33	1.00											
Zn66	0.04	-0.13	0.24	0.39	0.16	0.14	0.38	0.15	0.22	1.00										
As75	0.68	-0.03	-0.13	-0.19	0.36	0.61	0.02	0.13	0.12	-0.04	1.00									
Se77	0.05	-0.09	-0.02	-0.14	0.01	0.08	0.14	-0.03	0.08	0.41	0.01	1.00								
Mo95	0.77	-0.21	-0.29	-0.44	0.38	0.80	0.12	0.23	0.01	0.12	0.79	0.08	1.00							
Mo97	0.78	-0.25	-0.28	-0.44	0.44	0.80	0.07	0.17	0.00	0.09	0.75	0.07	0.93	1.00						
Sb121	0.14	0.05	0.04	0.20	0.12	-0.08	0.38	0.44	0.39	0.08	0.12	0.04	0.07	0.04	1.00					
Sb123	0.23	0.00	0.08	0.12	0.19	0.05	0.43	0.52	0.36	0.12	0.20	0.11	0.15	0.16	0.75	1.00				
Re185	0.07	0.35	0.36	0.40	0.24	-0.04	0.55	0.46	0.44	0.12	0.15	0.01	0.05	0.01	0.59	0.63	1.00			
Re187	0.14	0.33	0.39	0.47	0.20	-0.01	0.53	0.48	0.51	0.12	0.17	-0.02	0.04	-0.01	0.65	0.65	0.89	1.00		
Tl205	0.22	0.07	-0.06	0.06	0.25	0.05	0.32	0.46	0.44	0.10	0.18	0.05	0.09	0.08	0.57	0.51	0.45	0.46	1.00	
Pb208	-0.12	0.49	0.22	0.26	-0.06	-0.19	0.26	0.19	0.28	-0.10	-0.01	-0.03	-0.11	-0.18	0.33	0.37	0.52	0.55	0.30	1.00

Table A II Correlation coefficients for Core 7430 54, 55 laser track two.

	S33	Ca43	Ti49	Mn55	Fe57	Co59	Ni60	Cu63	Zn66	As75	Se77	Mo95	Mo97	Sb121	Sb123	Re185	Re187	Tl205	Pb208
S33	1.00																		
Ca43	0.23	1.00																	
Ti49	-0.27	-0.18	1.00																
Mn55	0.28	0.11	0.14	1.00															
Fe57	0.69	0.23	-0.21	0.13	1.00														
Co59	0.51	0.16	-0.27	0.23	0.41	1.00													
Ni60	0.47	0.19	-0.20	0.40	0.52	0.50	1.00												
Cu63	0.07	0.11	0.00	0.10	0.10	0.15	0.12	1.00											
Zn66	0.17	0.03	0.18	0.31	0.18	0.22	0.41	-0.01	1.00										
As75	0.69	0.12	-0.21	0.25	0.70	0.60	0.62	-0.02	0.33	1.00									
Se77	0.42	0.14	-0.24	0.13	0.36	0.42	0.35	0.11	0.02	0.45	1.00								
Mo95	0.61	0.24	-0.03	0.24	0.73	0.43	0.56	-0.04	0.23	0.79	0.35	1.00							
Mo97	0.60	0.21	-0.01	0.20	0.70	0.42	0.53	-0.05	0.33	0.74	0.29	0.91	1.00						
Sb121	0.60	0.12	-0.27	0.16	0.52	0.47	0.43	0.00	0.40	0.65	0.46	0.58	0.59	1.00					
Sb123	0.60	0.20	-0.17	0.21	0.59	0.48	0.38	0.02	0.25	0.66	0.41	0.56	0.54	0.61	1.00				
Re185	0.20	0.14	0.38	0.33	0.20	0.17	0.34	0.10	0.45	0.25	0.13	0.48	0.51	0.28	0.15	1.00			
Re187	0.22	0.15	0.36	0.34	0.22	0.21	0.37	0.13	0.39	0.29	0.21	0.47	0.54	0.31	0.26	0.78	1.00		
Tl205	0.66	0.19	-0.26	0.12	0.58	0.52	0.50	0.07	0.16	0.69	0.32	0.59	0.55	0.45	0.56	0.16	0.21	1.00	
Pb208	0.51	0.19	-0.11	0.21	0.42	0.53	0.32	0.16	0.03	0.52	0.55	0.47	0.43	0.41	0.48	0.05	0.17	0.44	1.00

Table A III Correlation coefficients for Core 7430 54, 55 laser track three.

	S33	Ca43	Ti49	Mn55	Fe57	Co59	Ni60	Cu63	Zn66	As75	Se77	Mo95	Mo97	Sb121	Sb123	Re185	Re187	Tl205	Pb208
S33	1.00																		
Ca43	-0.13	1.00																	
Ti49	-0.40	0.09	1.00																
Mn55	0.42	-0.06	0.09	1.00															
Fe57	0.69	-0.08	-0.29	0.51	1.00														
Co59	0.19	-0.15	0.04	0.43	0.30	1.00													
Ni60	0.11	-0.14	-0.03	0.36	0.34	0.52	1.00												
Cu63	0.06	-0.06	0.13	0.26	0.19	0.32	0.18	1.00											
Zn66	-0.02	0.59	0.09	0.23	0.10	-0.08	-0.03	0.16	1.00										
As75	0.66	-0.07	-0.25	0.45	0.59	0.32	0.34	0.16	0.08	1.00									
Se77	0.18	-0.22	0.00	0.39	0.25	0.67	0.50	0.31	-0.09	0.43	1.00								
Mo95	0.63	0.01	-0.35	0.46	0.60	0.26	0.24	0.02	0.07	0.88	0.31	1.00							
Mo97	0.69	-0.03	-0.35	0.42	0.62	0.23	0.19	0.01	0.05	0.89	0.29	0.94	1.00						
Sb121	0.26	-0.04	-0.11	0.22	0.26	0.17	0.45	0.16	0.06	0.58	0.45	0.45	0.42	1.00					
Sb123	0.15	-0.06	-0.07	0.13	0.18	0.19	0.41	0.33	-0.03	0.39	0.37	0.28	0.25	0.56	1.00				
Re185	-0.39	-0.08	0.23	-0.14	-0.32	0.16	-0.08	0.00	0.00	-0.12	0.06	-0.08	-0.15	-0.06	-0.04	1.00			
Re187	-0.34	-0.07	0.21	-0.02	-0.24	0.26	0.05	0.09	0.02	-0.04	0.20	-0.04	-0.11	-0.03	0.00	0.80	1.00		
Tl205	0.17	-0.15	0.05	0.26	0.21	0.27	0.41	0.29	0.01	0.39	0.36	0.29	0.30	0.55	0.34	-0.13	0.07	1.00	
Pb208	-0.03	-0.16	0.12	0.23	0.05	0.50	0.45	0.21	-0.10	0.00	0.39	-0.12	-0.12	0.02	0.06	0.07	0.16	0.18	1.00

Table A IV Correlation coefficients for Core 7430 54, 55 laser track four.

	S33	Ca43	Ti49	Mn55	Fe57	Co59	Ni60	Cu63	Zn66	As75	Se77	Mo95	Mo97	Sb121	Sb123	Re185	Re187	Tl205	Pb208
S33	1.00																		
Ca43	0.06	1.00																	
Ti49	-0.11	0.05	1.00																
Mn55	0.24	0.09	-0.05	1.00															
Fe57	0.56	-0.07	-0.15	0.32	1.00														
Co59	0.17	-0.04	0.12	0.24	0.38	1.00													
Ni60	0.05	0.07	0.09	0.00	0.22	0.42	1.00												
Cu63	-0.15	-0.14	0.14	0.09	0.05	0.21	0.35	1.00											
Zn66	0.06	0.00	0.25	0.15	0.14	0.34	0.14	0.14	1.00										
As75	0.61	0.05	-0.04	0.20	0.57	0.23	0.25	0.09	0.14	1.00									
Se77	-0.07	-0.08	-0.01	0.00	-0.04	0.15	0.25	0.20	0.12	-0.01	1.00								
Mo95	0.64	0.06	-0.08	0.06	0.51	0.11	0.28	0.02	0.09	0.72	-0.10	1.00							
Mo97	0.62	0.04	0.01	0.05	0.51	0.09	0.28	0.05	0.06	0.69	-0.11	0.90	1.00						
Sb121	-0.09	0.17	0.15	0.04	0.01	0.20	0.31	0.19	0.08	0.14	0.14	0.13	0.10	1.00					
Sb123	0.06	-0.01	0.02	0.09	0.12	0.34	0.25	0.30	0.20	0.15	0.16	0.06	0.00	0.42	1.00				
Re185	0.12	-0.12	0.16	0.13	0.26	0.34	0.40	0.22	0.21	0.34	0.09	0.29	0.20	0.38	0.21	1.00			
Re187	0.12	-0.16	0.12	0.00	0.18	0.26	0.40	0.30	0.12	0.35	0.11	0.30	0.19	0.47	0.19	0.81	1.00		
Tl205	0.00	-0.13	0.06	0.00	0.11	0.29	0.28	0.40	0.08	-0.05	0.12	-0.08	-0.13	0.14	0.20	0.19	0.33	1.00	
Pb208	-0.20	-0.08	0.15	-0.01	-0.15	0.18	0.31	0.20	0.03	-0.06	0.11	-0.11	-0.14	0.34	0.24	0.25	0.34	0.34	1.00

Table A V Correlation coefficients for Core 7430 54, 55 laser track five.

	S33	Ca43	Ti49	Mn55	Fe57	Co59	Ni60	Cu63	Zn66	As75	Se77	Mo95	Mo97	Sb121	Sb123	Re185	Re187	Tl205	Pb208
S33	1.00																		
Ca43	-0.56	1.00																	
Ti49	0.33	-0.40	1.00																
Mn55	0.35	0.02	0.13	1.00															
Fe57	0.77	-0.52	0.36	0.43	1.00														
Co59	0.48	-0.42	0.26	0.26	0.48	1.00													
Ni60	0.61	-0.44	0.14	0.28	0.59	0.49	1.00												
Cu63	0.16	-0.05	0.16	0.04	0.05	0.18	0.12	1.00											
Zn66	0.03	-0.09	-0.06	0.18	-0.04	0.20	0.09	0.06	1.00										
As75	0.69	-0.47	0.34	0.37	0.69	0.42	0.57	-0.01	-0.08	1.00									
Se77	0.36	-0.13	0.14	0.31	0.44	0.23	0.25	0.11	0.18	0.48	1.00								
Mo95	0.72	-0.51	0.38	0.40	0.77	0.49	0.62	0.06	-0.11	0.85	0.57	1.00							
Mo97	0.65	-0.51	0.41	0.39	0.73	0.40	0.61	0.04	-0.12	0.85	0.60	0.94	1.00						
Sb121	0.22	-0.36	0.32	-0.01	0.20	0.29	0.17	0.25	0.15	0.36	0.27	0.39	0.40	1.00					
Sb123	0.20	-0.35	0.43	0.15	0.32	0.48	0.27	0.23	0.07	0.37	0.35	0.46	0.50	0.61	1.00				
Re185	-0.08	-0.19	0.06	0.12	-0.11	0.02	-0.04	0.06	0.29	0.03	0.02	-0.08	-0.04	0.18	0.16	1.00			
Re187	-0.10	-0.15	0.00	0.15	-0.11	0.06	-0.03	0.11	0.26	-0.03	-0.08	-0.10	-0.05	0.10	0.06	0.87	1.00		
Tl205	0.47	-0.42	0.32	0.31	0.58	0.42	0.48	-0.01	0.02	0.72	0.39	0.65	0.70	0.44	0.47	0.07	0.00	1.00	
Pb208	0.18	-0.20	0.15	0.17	0.26	0.20	0.24	0.06	0.09	0.15	0.09	0.14	0.16	0.22	0.29	0.29	0.38	0.22	1.00

Table A VI Correlation coefficients for Core 7430 54, 17 laser track one.

	S33	Ca43	Ti49	Mn55	Fe57	Co59	Ni60	Cu63	Zn66	As75	Se77	Mo95	Mo97	Sb121	Sb123	Re185	Re187	Tl205	Pb208
S33	1.00																		
Ca43	0.39	1.00																	
Ti49	0.18	0.36	1.00																
Mn55	0.17	0.37	0.42	1.00															
Fe57	0.25	0.35	0.24	0.37	1.00														
Co59	0.38	0.38	0.27	0.43	0.48	1.00													
Ni60	0.24	0.21	0.40	0.39	0.26	0.44	1.00												
Cu63	0.58	0.39	0.21	0.35	0.36	0.31	0.44	1.00											
Zn66	0.34	0.28	0.37	0.27	0.36	0.65	0.35	0.46	1.00										
As75	0.05	0.07	0.10	-0.06	0.00	0.03	0.13	0.07	0.03	1.00									
Se77	0.39	0.49	0.23	0.36	0.28	0.41	0.34	0.52	0.42	0.07	1.00								
Mo95	0.27	0.33	0.25	0.08	0.35	0.34	0.37	0.62	0.44	0.18	0.70	1.00							
Mo97	0.32	0.26	0.17	0.04	0.37	0.33	0.31	0.59	0.48	0.11	0.67	0.94	1.00						
Sb121	0.23	0.28	0.16	0.26	0.20	0.32	0.12	0.35	0.39	-0.03	0.41	0.56	0.58	1.00					
Sb123	0.31	0.27	0.20	0.19	0.37	0.37	0.22	0.50	0.37	0.10	0.44	0.56	0.58	0.45	1.00				
Re185	0.35	0.24	0.30	0.13	0.16	0.24	0.14	0.43	0.28	0.40	0.37	0.53	0.52	0.47	0.41	1.00			
Re187	0.33	0.26	0.35	0.17	0.34	0.27	0.27	0.55	0.40	0.48	0.38	0.60	0.60	0.36	0.44	0.81	1.00		
Tl205	0.38	0.25	0.11	0.20	0.27	0.38	0.25	0.48	0.52	0.20	0.43	0.48	0.49	0.45	0.48	0.50	0.49	1.00	
Pb208	0.40	0.30	0.23	0.30	0.27	0.32	0.15	0.44	0.42	0.03	0.42	0.38	0.44	0.51	0.58	0.47	0.50	0.53	1.00

Table A VII Correlation coefficients for Core 7430 54, 17 laser track two.

	S33	Ca43	Ti49	Mn55	Fe57	Co59	Ni60	Cu63	Zn66	As75	Se77	Mo95	Mo97	Sb121	Sb123	Re185	Re187	Tl205	Pb208
S33	1.00																		
Ca43	0.38	1.00																	
Ti49	0.28	0.19	1.00																
Mn55	0.37	0.43	0.32	1.00															
Fe57	0.22	0.12	0.36	0.17	1.00														
Co59	0.40	0.20	0.26	0.28	0.50	1.00													
Ni60	0.20	0.15	0.22	0.12	0.42	0.55	1.00												
Cu63	0.38	0.00	0.42	0.18	0.12	0.21	-0.03	1.00											
Zn66	0.12	0.12	0.24	0.21	0.30	0.16	0.04	0.70	1.00										
As75	0.31	0.14	0.21	0.28	0.46	0.52	0.32	0.26	0.17	1.00									
Se77	0.51	0.26	0.50	0.29	0.16	0.29	0.16	0.57	0.43	0.30	1.00								
Mo95	0.05	0.06	-0.08	-0.16	0.30	0.48	0.71	-0.07	-0.05	0.32	0.04	1.00							
Mo97	0.04	0.06	-0.02	-0.17	0.34	0.49	0.70	-0.03	-0.01	0.37	0.09	0.97	1.00						
Sb121	0.36	0.12	0.22	0.16	0.35	0.53	0.48	0.28	0.05	0.44	0.40	0.61	0.60	1.00					
Sb123	0.41	0.23	0.13	0.10	0.34	0.45	0.53	-0.02	0.07	0.29	0.19	0.50	0.51	0.45	1.00				
Re185	0.12	0.19	0.01	0.08	0.24	0.28	0.52	-0.09	-0.11	0.35	0.17	0.62	0.63	0.41	0.26	1.00			
Re187	0.07	0.08	0.03	0.02	0.24	0.25	0.57	-0.09	-0.17	0.25	0.09	0.62	0.60	0.40	0.27	0.86	1.00		
Tl205	0.25	0.27	-0.03	0.19	0.30	0.45	0.38	0.04	0.13	0.43	0.10	0.51	0.50	0.56	0.31	0.54	0.50	1.00	
Pb208	0.35	0.16	0.14	0.33	0.27	0.34	0.19	0.25	0.03	0.36	0.28	0.28	0.30	0.41	0.23	0.30	0.29	0.44	1.00

Table A VIII Correlation coefficients for Core 7430 54, 17 laser track three.

	S33	Ca43	Ti49	V51	Mn55	Fe57	Co59	Ni60	Cu63	Zn66	As75	Se77	Mo95	Mo97	Sb121	Sb123	Re185	Re187	Tl205	Pb208
S33	1.00																			
Ca43	0.06	1.00																		
Ti49	-0.16	0.07	1.00																	
V51	0.08	0.18	0.10	1.00																
Mn55	0.17	-0.02	-0.07	-0.05	1.00															
Fe57	0.38	0.03	-0.17	0.00	0.18	1.00														
Co59	0.02	-0.04	-0.06	0.38	0.00	0.06	1.00													
Ni60	0.05	-0.03	-0.01	0.05	0.00	0.10	0.26	1.00												
Cu63	-0.03	0.01	0.04	0.24	-0.06	0.12	0.14	0.20	1.00											
Zn66	-0.30	0.21	0.16	-0.13	-0.12	-0.30	0.00	-0.03	0.12	1.00										
As75	0.54	0.22	-0.09	0.12	0.25	0.63	0.10	0.12	0.11	-0.15	1.00									
Se77	0.26	0.20	0.09	0.28	0.15	0.34	0.26	0.32	0.17	0.05	0.46	1.00								
Mo95	0.33	0.12	-0.05	0.18	0.07	0.37	0.12	0.18	0.26	-0.17	0.61	0.19	1.00							
Mo97	0.33	0.04	-0.10	0.14	0.11	0.40	0.07	0.36	0.27	-0.08	0.73	0.27	0.76	1.00						
Sb121	0.15	0.10	0.18	0.39	-0.03	0.17	0.16	0.30	0.12	-0.10	0.15	0.35	0.15	0.10	1.00					
Sb123	0.14	0.18	0.09	0.21	0.01	0.21	0.12	0.21	0.21	0.32	0.27	0.45	0.20	0.18	0.36	1.00				
Re185	0.09	0.15	0.13	0.51	0.02	0.02	0.27	0.22	0.09	-0.07	0.07	0.33	0.16	0.20	0.17	0.09	1.00			
Re187	0.13	0.08	0.18	0.45	-0.03	0.05	0.24	0.20	0.10	-0.07	0.09	0.30	0.22	0.26	0.17	0.12	0.82	1.00		
Tl205	0.09	0.01	-0.21	0.20	-0.11	0.19	0.22	0.10	0.27	-0.16	0.31	0.20	0.16	0.20	0.09	0.15	0.15	0.18	1.00	
Pb208	0.04	0.06	0.06	0.20	-0.05	-0.02	0.13	0.22	-0.06	0.11	0.01	0.33	0.10	0.08	0.11	0.20	0.18	0.15	-0.05	1.00

Table A IX Correlation coefficients for Core 7430 54, 17 laser track four.

	S33	Ca43	Ti49	V51	Mn55	Fe57	Co59	Ni60	Cu63	Zn66	As75	Se77	Mo95	Mo97	Sb121	Sb123	Re185	Re187	Tl205	Pb208
S33	1.00																			
Ca43	0.07	1.00																		
Ti49	-0.06	0.07	1.00																	
V51	0.04	0.06	0.60	1.00																
Mn55	0.61	0.01	0.05	0.19	1.00															
Fe57	0.71	0.13	-0.15	0.02	0.44	1.00														
Co59	0.03	0.16	-0.08	0.06	0.09	0.27	1.00													
Ni60	0.23	0.23	0.11	0.22	0.26	0.29	0.46	1.00												
Cu63	0.06	0.22	0.48	0.33	0.16	0.01	0.09	0.15	1.00											
Zn66	0.06	0.13	0.08	0.30	0.06	0.29	0.32	0.42	0.23	1.00										
As75	0.60	0.07	0.07	0.25	0.47	0.69	0.24	0.39	0.24	0.39	1.00									
Se77	0.24	0.14	0.07	0.19	0.10	0.30	0.09	0.14	0.09	0.20	0.35	1.00								
Mo95	0.55	-0.13	0.02	0.24	0.37	0.57	0.20	0.45	-0.05	0.29	0.85	0.31	1.00							
Mo97	0.51	-0.12	0.03	0.33	0.35	0.53	0.21	0.46	-0.05	0.32	0.85	0.34	0.91	1.00						
Sb121	0.30	0.31	0.17	0.13	0.33	0.38	0.10	0.27	0.07	0.17	0.36	0.26	0.34	0.34	1.00					
Sb123	0.24	0.05	0.24	0.15	0.24	0.26	-0.02	0.18	0.02	0.04	0.42	0.19	0.47	0.41	0.54	1.00				
Re185	0.07	0.14	0.22	0.37	0.06	0.14	0.14	0.16	0.17	0.23	0.38	0.25	0.32	0.30	0.38	0.45	1.00			
Re187	0.13	0.05	0.19	0.31	0.13	0.17	0.17	0.12	0.10	0.21	0.40	0.17	0.35	0.34	0.40	0.48	0.88	1.00		
Tl205	0.38	0.12	-0.13	-0.16	0.33	0.45	0.29	0.24	0.03	0.15	0.39	0.07	0.38	0.33	0.38	0.28	0.40	0.43	1.00	
Pb208	0.22	0.17	0.12	0.14	0.18	0.25	0.10	0.19	0.16	0.15	0.26	0.14	0.05	0.02	0.32	0.25	0.47	0.50	0.34	1.00

Table A X Correlation coefficients for Core 7430 54, 17 laser track five.

	S33	Ca43	Ti49	Mn55	Fe57	Co59	Ni60	Cu63	Zn66	As75	Se77	Mo95	Mo97	Sb121	Sb123	Re185	Re187	Tl205	Pb208
S33	1.00																		
Ca43	0.05	1.00																	
Ti49	0.02	0.11	1.00																
Mn55	0.67	0.06	0.10	1.00															
Fe57	0.73	-0.06	-0.02	0.65	1.00														
Co59	0.51	0.00	-0.07	0.73	0.60	1.00													
Ni60	0.42	-0.05	-0.16	0.69	0.54	0.70	1.00												
Cu63	0.47	-0.06	0.02	0.69	0.55	0.69	0.55	1.00											
Zn66	0.21	0.06	0.19	0.18	0.19	0.19	0.13	0.22	1.00										
As75	0.65	-0.05	0.11	0.65	0.71	0.59	0.43	0.52	0.24	1.00									
Se77	0.26	-0.10	0.05	0.30	0.31	0.33	0.09	0.37	0.04	0.34	1.00								
Mo95	0.67	0.25	0.06	0.83	0.71	0.69	0.68	0.70	0.28	0.79	0.43	1.00							
Mo97	0.69	0.24	-0.02	0.81	0.71	0.67	0.69	0.65	0.24	0.79	0.39	0.93	1.00						
Sb121	0.44	0.04	0.16	0.53	0.47	0.50	0.30	0.57	0.22	0.47	0.40	0.51	0.49	1.00					
Sb123	0.33	-0.04	0.11	0.40	0.48	0.45	0.33	0.53	0.26	0.39	0.35	0.32	0.32	0.59	1.00				
Re185	0.23	0.06	0.29	0.44	0.31	0.38	0.07	0.50	0.35	0.36	0.28	0.41	0.33	0.58	0.51	1.00			
Re187	0.22	0.04	0.23	0.37	0.28	0.41	0.08	0.49	0.31	0.34	0.37	0.41	0.36	0.54	0.50	0.89	1.00		
Tl205	0.31	-0.04	0.09	0.41	0.39	0.51	0.21	0.50	0.17	0.43	0.42	0.55	0.54	0.55	0.53	0.53	0.58	1.00	
Pb208	0.07	-0.05	0.00	0.16	0.35	0.23	0.14	0.30	0.15	0.21	0.14	0.21	0.18	0.25	0.27	0.37	0.39	0.24	1.00

Table A XI Correlation coefficients for ODP Leg 160 laser track one.

	S33	Ca43	Ti49	V51	Mn55	Fe57	Co59	Ni60	Cu63	Zn66	As75	Se77	Mo95	Mo97	Sb121	Sb123	Re185	Re187	Tl205	Pb208
S33	1.00																			
Ca43	0.00	1.00																		
Ti49	0.37	0.22	1.00																	
V51	0.42	0.24	0.51	1.00																
Mn55	0.46	0.29	0.50	0.58	1.00															
Fe57	0.58	0.11	0.50	0.62	0.58	1.00														
Co59	0.51	0.23	0.53	0.72	0.49	0.59	1.00													
Ni60	0.28	0.32	0.17	0.44	0.37	0.24	0.44	1.00												
Cu63	0.36	0.15	0.42	0.29	0.50	0.38	0.38	0.07	1.00											
Zn66	0.24	0.36	0.37	0.57	0.52	0.31	0.37	0.33	0.25	1.00										
As75	0.48	0.18	0.32	0.47	0.55	0.51	0.44	0.45	0.19	0.32	1.00									
Se77	0.55	0.08	0.37	0.41	0.34	0.42	0.59	0.23	0.24	0.20	0.49	1.00								
Mo95	0.37	0.11	0.43	0.60	0.36	0.42	0.56	0.44	0.16	0.38	0.28	0.40	1.00							
Mo97	0.34	0.08	0.24	0.59	0.41	0.35	0.51	0.48	0.03	0.30	0.32	0.33	0.71	1.00						
Sb121	0.35	0.30	0.43	0.56	0.54	0.45	0.47	0.38	0.33	0.66	0.40	0.25	0.40	0.44	1.00					
Sb123	0.31	0.17	0.33	0.47	0.44	0.40	0.37	0.41	0.16	0.54	0.37	0.29	0.39	0.43	0.66	1.00				
Re185	0.55	0.12	0.53	0.64	0.38	0.53	0.68	0.32	0.19	0.31	0.37	0.55	0.59	0.56	0.43	0.46	1.00			
Re187	0.55	0.04	0.52	0.58	0.36	0.49	0.60	0.39	0.17	0.32	0.33	0.52	0.51	0.53	0.37	0.46	0.85	1.00		
Tl205	0.47	0.05	0.40	0.53	0.33	0.51	0.71	0.22	0.24	0.21	0.48	0.56	0.43	0.36	0.20	0.27	0.52	0.46	1.00	
Pb208	0.48	0.17	0.55	0.55	0.37	0.52	0.69	0.24	0.36	0.36	0.42	0.54	0.40	0.29	0.33	0.35	0.61	0.60	0.61	1.00

Table A XII Correlation coefficients for ODP Leg 160 laser track two.

	S33	Ca43	Ti49	V51	Mn55	Fe57	Co59	Ni60	Cu63	Zn66	As75	Se77	Mo95	Mo97	Sb121	Sb123	Re185	Re187	Tl205	Pb208
S33	1.00																			
Ca43	0.12	1.00																		
Ti49	-0.14	-0.05	1.00																	
V51	0.30	0.00	0.10	1.00																
Mn55	0.45	0.08	-0.08	0.40	1.00															
Fe57	0.48	0.06	-0.03	0.35	0.35	1.00														
Co59	0.41	-0.03	-0.04	0.48	0.45	0.44	1.00													
Ni60	0.38	0.01	-0.02	0.09	0.29	0.36	0.21	1.00												
Cu63	0.13	0.02	-0.08	0.33	0.31	0.20	0.34	0.08	1.00											
Zn66	0.26	0.15	-0.05	-0.04	0.19	0.24	0.15	0.12	0.12	1.00										
As75	0.58	0.17	-0.13	0.24	0.35	0.45	0.30	0.28	0.08	0.27	1.00									
Se77	0.32	0.20	-0.08	0.22	0.28	0.24	0.27	0.09	0.11	0.16	0.28	1.00								
Mo95	0.29	0.04	-0.07	0.13	0.37	0.20	0.21	0.40	0.08	0.11	0.46	0.32	1.00							
Mo97	0.31	0.11	-0.05	0.11	0.25	0.25	0.14	0.41	0.11	0.08	0.58	0.34	0.86	1.00						
Sb121	0.26	0.04	0.10	0.19	0.32	0.21	0.22	0.04	0.10	0.45	0.01	0.09	0.01	-0.05	1.00					
Sb123	0.21	0.29	0.12	0.25	0.31	0.28	0.32	0.10	0.30	0.36	0.23	0.18	0.16	0.16	0.38	1.00				
Re185	0.24	0.12	0.07	0.27	0.23	0.22	0.35	0.15	0.08	0.17	0.11	0.25	0.15	0.11	0.38	0.30	1.00			
Re187	0.22	0.12	0.07	0.04	0.17	0.06	0.27	0.15	0.12	0.06	0.04	0.17	0.21	0.16	0.24	0.07	0.46	1.00		
Tl205	0.35	-0.03	-0.28	-0.09	0.23	0.24	0.02	0.18	-0.11	0.13	0.21	0.03	0.25	0.18	0.31	0.02	0.06	-0.04	1.00	
Pb208	0.33	-0.05	-0.02	0.18	0.36	0.26	0.39	0.14	0.19	0.36	0.22	0.27	0.13	0.07	0.26	0.10	0.24	-0.01	0.22	1.00

Table A XIII Correlation coefficients for ODP Leg 160 laser track three.

	S33	Ca43	Ti49	V51	Mn55	Fe57	Co59	Ni60	Cu63	Zn66	As75	Se77	Mo95	Mo97	Sb121	Sb123	Re185	Re187	Tl205	Pb208
S33	1.00																			
Ca43	0.47	1.00																		
Ti49	0.38	0.27	1.00																	
V51	0.57	0.38	0.64	1.00																
Mn55	0.56	0.41	0.51	0.66	1.00															
Fe57	0.52	0.24	0.44	0.57	0.40	1.00														
Co59	0.50	0.35	0.47	0.70	0.65	0.60	1.00													
Ni60	0.26	0.19	0.23	0.33	0.42	0.22	0.37	1.00												
Cu63	0.09	0.05	0.22	0.36	0.23	0.26	0.41	0.25	1.00											
Zn66	0.20	0.08	0.21	0.29	0.34	0.38	0.33	0.27	0.14	1.00										
As75	0.48	0.18	0.27	0.47	0.30	0.46	0.39	0.32	0.02	0.55	1.00									
Se77	0.38	0.29	0.30	0.28	0.36	0.36	0.41	0.12	0.19	0.23	0.34	1.00								
Mo95	0.21	0.05	0.24	0.40	0.32	0.45	0.37	0.58	0.21	0.11	0.31	0.22	1.00							
Mo97	0.19	-0.02	0.19	0.34	0.26	0.37	0.29	0.53	0.19	0.08	0.27	0.15	0.93	1.00						
Sb121	0.11	0.12	0.14	0.38	0.15	0.18	0.34	0.15	0.32	0.19	0.22	0.26	0.00	-0.06	1.00					
Sb123	0.23	0.22	0.26	0.36	0.32	0.28	0.46	0.33	0.54	0.29	0.25	0.36	0.07	0.00	0.53	1.00				
Re185	0.30	0.16	0.27	0.35	0.28	0.35	0.43	0.18	0.20	0.22	0.24	0.33	0.25	0.19	0.14	0.27	1.00			
Re187	0.25	0.18	0.27	0.42	0.38	0.26	0.43	0.29	0.28	0.17	0.21	0.32	0.14	0.12	0.22	0.36	0.48	1.00		
Tl205	0.40	0.23	0.22	0.35	0.18	0.40	0.34	0.26	0.22	0.10	0.29	0.16	0.19	0.12	0.20	0.35	0.36	0.29	1.00	
Pb208	0.21	0.15	0.30	0.25	0.25	0.25	0.41	0.20	0.37	0.23	0.22	0.28	0.14	0.05	0.27	0.49	0.35	0.48	0.20	1.00

Table A XIV Correlation coefficients for ODP Leg 160 laser track four.

	S33	Ca43	Ti49	V51	Mn55	Fe57	Co59	Ni60	Cu63	Zn66	As75	Se77	Mo95	Mo97	Sb121	Sb123	Re185	Re187	Tl205	Pb208
S33	1.00																			
Ca43	0.29	1.00																		
Ti49	0.25	0.20	1.00																	
V51	0.59	0.34	0.37	1.00																
Mn55	0.58	0.29	0.65	0.71	1.00															
Fe57	0.58	0.37	0.42	0.68	0.71	1.00														
Co59	0.58	0.35	0.33	0.79	0.74	0.81	1.00													
Ni60	0.47	0.20	0.20	0.47	0.43	0.39	0.47	1.00												
Cu63	0.44	0.14	0.25	0.66	0.63	0.66	0.72	0.38	1.00											
Zn66	0.22	0.04	0.08	0.29	0.23	0.38	0.33	0.32	0.27	1.00										
As75	0.37	0.28	0.29	0.43	0.60	0.46	0.54	0.31	0.47	0.23	1.00									
Se77	0.37	0.17	0.19	0.46	0.43	0.44	0.51	0.41	0.44	0.35	0.39	1.00								
Mo95	0.45	0.18	0.39	0.50	0.52	0.44	0.43	0.64	0.40	0.26	0.44	0.40	1.00							
Mo97	0.44	0.18	0.46	0.50	0.56	0.44	0.45	0.57	0.39	0.23	0.43	0.39	0.87	1.00						
Sb121	0.16	0.03	-0.01	0.39	0.22	0.23	0.33	0.23	0.34	0.26	0.07	0.33	0.39	0.34	1.00					
Sb123	0.21	0.07	-0.01	0.43	0.22	0.30	0.40	0.36	0.40	0.32	0.12	0.37	0.43	0.39	0.87	1.00				
Re185	0.14	0.12	-0.04	0.36	0.11	0.21	0.35	0.22	0.39	0.16	0.19	0.20	0.36	0.29	0.58	0.64	1.00			
Re187	0.14	0.11	-0.04	0.38	0.12	0.22	0.33	0.25	0.36	0.15	0.18	0.18	0.39	0.32	0.65	0.70	0.83	1.00		
Tl205	0.34	0.12	0.24	0.44	0.46	0.36	0.40	0.36	0.55	0.13	0.39	0.27	0.32	0.44	0.15	0.18	0.30	0.25	1.00	
Pb208	0.41	0.29	0.18	0.47	0.49	0.49	0.55	0.42	0.57	0.11	0.48	0.34	0.35	0.27	0.22	0.30	0.33	0.29	0.59	1.00

Table A XV Correlation coefficients for ODP Leg 160 laser track five.

	S33	Ca43	Ti49	Mn55	Fe57	Co59	Ni60	Cu63	Zn66	As75	Se77	Mo95	Mo97	Sb121	Sb123	Re185	Re187	Tl205	Pb208
S33	1.00																		
Ca43	0.41	1.00																	
Ti49	0.36	0.39	1.00																
Mn55	0.46	0.37	0.59	1.00															
Fe57	0.51	0.33	0.36	0.62	1.00														
Co59	0.45	0.31	0.36	0.45	0.74	1.00													
Ni60	0.51	0.35	0.36	0.63	0.64	0.89	1.00												
Cu63	0.44	0.26	0.28	0.24	0.47	0.48	0.56	1.00											
Zn66	0.26	0.29	0.17	0.23	0.41	0.40	0.44	0.48	1.00										
As75	0.37	0.15	0.28	0.71	0.49	0.40	0.43	0.20	0.28	1.00									
Se77	0.32	0.09	0.17	0.54	0.38	0.37	0.37	0.44	0.19	0.67	1.00								
Mo95	0.26	0.05	0.19	0.31	0.36	0.25	0.47	0.14	0.04	0.55	0.51	1.00							
Mo97	0.27	0.00	0.03	0.25	0.29	0.27	0.49	0.07	0.02	0.61	0.46	0.85	1.00						
Sb121	0.06	0.00	0.08	0.45	0.08	0.19	0.21	0.11	0.27	0.40	0.26	0.11	0.09	1.00					
Sb123	0.08	-0.09	0.08	0.35	0.09	0.25	0.19	0.15	0.25	0.37	0.29	0.12	0.08	0.91	1.00				
Re185	0.19	0.31	0.22	0.19	0.30	0.33	0.33	0.25	0.44	0.13	0.08	0.10	0.08	0.45	0.43	1.00			
Re187	0.12	0.24	0.25	0.38	0.30	0.32	0.33	0.21	0.37	0.33	0.25	0.27	0.27	0.50	0.51	0.77	1.00		
Tl205	0.30	0.16	0.24	0.48	0.43	0.41	0.39	0.32	0.19	0.46	0.47	0.38	0.38	0.30	0.37	0.41	0.57	1.00	
Pb208	0.37	0.11	0.15	0.43	0.45	0.45	0.41	0.49	0.18	0.45	0.55	0.46	0.49	0.34	0.38	0.28	0.50	0.80	1.00

Microbial Fixation

Table A XVI Culture results for sulfate reducers.

Innoculated **ND 132**	Incubation Temp/C	TiNTA 100 µL	Filtered 0.2 µm	Initial ReO_4^- / µM	Initial ReO_4^- uncertainty/ µM	Final Re/ µM	Final Re uncertainty/ µM	Optical Density	Sulfide/mM
n	4	n	y	0.04	0.004	0.04	0.01		
n	4	n	y	0.73	0.07	0.7	0.1		
n	4	n	y	1.7	0.2	1.6	0.2		
n	4	n	y	4.8	0.5	4.7	0.7		
n	4	n	y	6.6	0.7	6.6	0.9		
n	4	n	n	0.04	0.004	0.04	0.01		0.0007
n	4	n	n	0.73	0.07	0.73	0.1		
n	4	n	n	1.7	0.2	1.7	0.3		
n	4	n	n	4.8	0.5	4.8	0.7		
n	4	n	n	6.6	0.7	6.6	0.9		
n	4	y	y	0.04	0.004	0.05	0.01		
n	4	y	y	0.73	0.07	0.82	0.1		
n	4	y	y	1.7	0.2	2	0.3		
n	4	y	y	4.8	0.5	4.3	0.6		
n	4	y	y	6.5	0.7	4.7	0.7		
n	4	y	n	0.04	0.004	0.04	0.01		0.0002
n	4	y	n	0.73	0.07	0.8	0.1		
n	4	y	n	1.7	0.2	2	0.3		
n	4	y	n	4.8	0.5	4.3	0.6		
n	4	y	n	6.5	0.7	4.7	0.7		
y	4	n	y	0.04	0.004	0.05	0.01		
y	4	n	y	0.67	0.09	0.68	0.1		
y	4	n	y	1.6	0.2	1.7	0.3		
y	4	n	y	4.4	0.6	3.8	0.7		
y	4	n	y	6	0.8	4.3	0.8		
y	4	n	n	0.04	0.004	0.05	0.01	0.03	0.14
y	4	n	n	0.67	0.09	0.69	0.1	0.037	0.28
y	4	n	n	1.6	0.2	1.7	0.3	0.043	0.32
y	4	n	n	4.4	0.6	3.8	0.7	0.036	0.27
y	4	n	n	6	0.8	4.4	0.8	0.039	0.32
y	4	y	y	0.04	0.01	0.05	0.01		
y	4	y	y	0.66	0.09	0.68	0.1		
y	4	y	y	1.6	0.2	1.4	0.3		
y	4	y	y	4.4	0.6	3.2	0.6		
y	4	y	y	5.9	0.8	4.5	0.8		
y	4	y	n	0.04	0.01	0.05	0.01	0.045	0.34
y	4	y	n	0.66	0.09	0.69	0.1	0.035	0.26
y	4	y	n	1.6	0.2	1.6	0.3	0.041	0.33
y	4	y	n	4.4	0.6	3.7	0.6	0.042	0.27
y	4	y	n	5.9	0.8	5	0.9	0.024	0.21
y	30	y	y	0.04	0.01	0.07	0.01		
y	30	y	y	0.66	0.09	0.75	0.1		
y	30	y	y	1.6	0.2	1.2	0.2		
y	30	y	y	4.4	0.6	3.6	0.6		
y	30	y	y	5.9	0.8	4.5	0.8		
y	30	y	n	0.04	0.01	0.06	0.01	0.275	2.49
y	30	y	n	0.66	0.09	0.81	0.1	0.091	2.32
y	30	y	n	1.6	0.2	1.3	0.2	0.278	2.46
y	30	y	n	4.4	0.6	3.9	0.7	0.279	2.38
y	30	y	n	5.9	0.8	4.8	0.8	0.268	2.51

Table A XVI cont.

Innoculated **ATCC29577**	Incubation Temp/C	TiNTA 100 µL	Filtered 0.2 µm	Initial ReO_4^- / µM	Initial ReO_4^- uncertainty/ µM	Final Re/ µM	Final Re uncertainty/ µM	Optical Density	Sulfide/mM
n	4	n	y	0.06	0.01	0.05	0.01		
n	4	n	y	0.83	0.08	0.84	0.1		
n	4	n	y	2	0.2	2	0.3		
n	4	n	y	3.9	0.4	3.5	0.5		
n	4	n	y	7.2	0.7	7	1		
n	4	n	n	0.06	0.01	0.06	0.01		0.0003
n	4	n	n	0.83	0.08	0.83	0.1		
n	4	n	n	2	0.2	2	0.3		
n	4	n	n	3.9	0.4	3.9	0.6		
n	4	n	n	7.2	0.7	7.2	1		
n	4	y	y	0.06	0.01	0.05	0.01		
n	4	y	y	0.83	0.08	0.73	0.1		
n	4	y	y	2	0.2	1.9	0.3		
n	4	y	y	3.9	0.4	3.8	0.5		
n	4	y	y	7.2	0.7	5.3	0.8		
n	4	y	n	0.06	0.01	0.07	0.01		0.0005
n	4	y	n	0.83	0.08	0.85	0.1		
n	4	y	n	2	0.2	1.9	0.3		
n	4	y	n	3.9	0.4	3.7	0.5		
n	4	y	n	7.2	0.7	5.3	0.8		
y	4	n	y	0.06	0.01	0.05	0.01		
y	4	n	y	0.76	0.11	0.81	0.1		
y	4	n	y	1.8	0.3	1.7	0.3		
y	4	n	y	3.5	0.5	3.4	0.6		
y	4	n	y	6.5	0.9	4.7	0.8		
y	4	n	n	0.06	0.01	0.05	0.01	0.052	0.1
y	4	n	n	0.76	0.11	0.76	0.1	0.035	0.1
y	4	n	n	1.8	0.3	1.7	0.3	0.021	0.07
y	4	n	n	3.5	0.5	3.4	0.6	0.016	0.06
y	4	n	n	6.5	0.9	4.8	0.8	0.017	0.06
y	4	y	y	0.06	0.01	0.06	0.01		
y	4	y	y	0.75	0.11	0.82	0.1		
y	4	y	y	1.8	0.3	1.7	0.3		
y	4	y	y	3.5	0.5	3	0.5		
y	4	y	y	6.5	0.9	4.7	0.8		
y	4	y	n	0.06	0.01	0.06	0.01	0.03	0.1
y	4	y	n	0.75	0.11	0.82	0.1	0.025	0.24
y	4	y	n	1.8	0.3	1.7	0.3	0.032	0.28
y	4	y	n	3.5	0.5	3.2	0.6	0.028	0.28
y	4	y	n	6.5	0.9	4.8	0.8	0.032	0.31
y	30	y	y	0.06	0.01	0.07	0.01		
y	30	y	y	0.75	0.11	0.74	0.1		
y	30	y	y	1.8	0.3	1.6	0.3		
y	30	y	y	3.5	0.5	3.5	0.6		
y	30	y	y	6.5	0.9	5.2	0.9		
y	30	y	n	0.06	0.01	0.05	0.01	0.36	2.35
y	30	y	n	0.75	0.11	0.74	0.1	0.318	2.46
y	30	y	n	1.8	0.3	1.8	0.3	0.288	2.32
y	30	y	n	3.5	0.5	3.7	0.7	0.249	2.2
y	30	y	n	6.5	0.9	5.5	1	0.253	2.14

Table A XVII Culture results for iron reducers.

GS15	Incubation Temp/C	0.2 µm Filt	Initial Re/O_4^- µM	Initial ReO_4^- uncertainty/ µM	Final Re Conc/µM	Final Re uncertainty/ uM	Color of final tube contents
n	4	y	0.05	0.01	0.05	0.01	Clear brown
n	4	y	2.0	0.2	2.0	0.2	Clear brown
n	4	y	11.5	1.2	12.0	1.2	Clear brown
n	4	n	0.05	0.01	0.05	0.01	Clear brown
n	4	n	2.0	0.2	2.0	0.2	Clear brown
n	4	n	11.5	1.2	11.5	1.2	Clear brown
y	4	y	0.05	0.01	0.09	0.01	Clear brown
y	4	y	1.9	0.3	3.3	0.5	Clear brown
y	4	y	10.5	1.5	11.6	1.6	Clear brown
y	4	n	0.05	0.01	0.09	0.01	Clear brown
y	4	n	1.9	0.3	2.9	0.4	Clear brown
y	4	n	10.5	1.5	11.8	1.7	Clear brown
y	30	y	0.05	0.01	0.10	0.01	Pale yellow
y	30	y	1.9	0.3	3.7	0.5	Pale yellow
y	30	y	10.5	1.5	12.4	1.8	Pale yellow
y	30	n	0.05	0.01	0.10	0.01	Pale yellow
y	30	n	1.9	0.3	3.3	0.5	Pale yellow
y	30	n	10.5	1.5	12.1	1.7	Pale yellow

MR-1	Incubation Temp/C	0.2 µm Filt	Initial ReO_4^- µM	Initial ReO_4^- uncertainty/ µM	Final Re Conc/µM	Final Re uncertainty/ µM	Color of final tube contents
n	4	y	0.11	0.01	0.11	0.01	Clear brown
n	4	y	4.2	0.4	3.8	0.4	Clear brown
n	4	y	12.4	1.2	12.3	1.2	Clear brown
n	4	n	0.11	0.01	0.11	0.01	Clear brown
n	4	n	4.2	0.4	4.2	0.4	Clear brown
n	4	n	12.4	1.2	12.4	1.2	Clear brown
y	4	y	0.11	0.02	0.13	0.02	Clear brown
y	4	y	3.8	0.5	3.1	0.4	Clear brown
y	4	y	11.3	1.6	11.0	1.6	Clear brown
y	4	n	0.11	0.02	0.13	0.02	Clear brown
y	4	n	3.8	0.5	3.2	0.5	Clear brown
y	4	n	11	1.6	11.7	1.7	Clear brown
y	30	y	0.11	0.02	0.10	0.01	Pale yellow
y	30	y	3.8	0.5	3.7	0.5	Pale yellow
y	30	y	11.3	1.6	9.5	1.3	Pale yellow
y	30	n	0.11	0.02	0.10	0.01	Pale yellow
y	30	n	3.8	0.5	3.8	0.5	Pale yellow
y	30	n	11.3	1.6	10.9	1.5	Pale yellow

Bibliography

Adelson, J.M., 1997. The Evaluation of Geochemical Indicators of Anoxia in the Chesapeake Bay. Ph.D. Dissertation, University of Maryland, College Park, MD, 214 pp.

Adelson, J.M., Helz, G.R. and Miller, C.V., 2001. Reconstructing the rise of recent coastal anoxia; molybdenum in Chesapeake Bay sediments. Geochimica et Cosmochimica Acta, 65(2): 237-252.

Alexander, R.B. and Smith, R.A., 1988. Trends in Lead Concentrations in Major United-States Rivers and Their Relation to Historical Changes in Gasoline Lead Consumption. Water Resources Bulletin, 24(3): 557-569.

Anbar, A.D., Creaser, R.A., Papanastassiou, D.A. and Wasserburg, G.J., 1992. Rhenium in Seawater - Confirmation of Generally Conservative Behavior. Geochimica et Cosmochimica Acta, 56(11): 4099-4103.

Anbar, A.D. et al., 2007. A whiff of oxygen before the Great Oxidation Event? Science, 317(5846): 1903-1906.

Antizar-Ladislao, B., 2008. Environmental levels, toxicity and human exposure to tributyltin (TBT)-contaminated marine environment. A review. Environment International, 34(2): 292-308.

Arata, T. et al., 2002. Cytotoxic effects of triphenylbismuth on rat thymocytes: Comparisons with bismuth chloride and triphenyltin chloride. Environmental Toxicology, 17(5): 472-477.

Arrowsmith, P., 1987. Laser Ablation of Solids for Elemental Analysis by Inductively Coupled Plasma Mass-Spectrometry. Analytical Chemistry, 59(10): 1437-1444.

Baker, S.A., Bi, M., Aucelio, R.Q., Smith, B.W. and Winefordner, J.D., 1999. Analysis of soil and sediment samples by laser ablation inductively coupled plasma mass spectrometry. Journal of Analytical Atomic Spectrometry, 14(1): 19-26.

Bea, F., 1999. Inductively Coupled Plasma Mass Spectrometry. In: C.P. Marshall and R.W. Fairbridge (Editors), Encyclopedia of Geochemistry. Kluwer Academic Publishers, Boston, MA, pp. 340-341.

Beaumont, A.R. and Budd, M.D., 1984. High Mortality of the Larvae of the Common Mussel at Low Concentrations of Tributyltin. Marine Pollution Bulletin, 15(11): 402-405.

Bednar, A.J., Jones, W.T., Boyd, R.E., Ringelberg, D.B. and Larson, S.L., 2008. Geochemical parameters influencing tungsten mobility in soils. Journal of Environmental Quality, 37(1): 229-233.

Beyer, W.N., Day, D., Morton, A. and Pachepsky, Y., 1998. Relation of lead exposure to sediment ingestion in mute swans on the Chesapeake Bay, USA. Environmental Toxicology and Chemistry, 17(11): 2298-2301.

Biggs, R.B., 1970. Sources and Distribution of Suspended Sediment in Northern Chesapeake-Bay. Marine Geology, 9(3): 187-201.

Bleiner, D. and Gunther, D., 2001. Theoretical description and experimental observation of aerosol transport processes in laser ablation inductively coupled plasma mass spectrometry. Journal of Analytical Atomic Spectrometry, 16(5): 449-456.

Boning, P. et al., 2004. Geochemistry of Peruvian near-surface sediments. Geochimica et Cosmochimica Acta, 68(21): 4429-4451.

Bostick, B.C., Fendorf, S. and Helz, G.R., 2003. Differential adsorption of molybdate and tetrathiomolybdate on pyrite (FeS2). Environmental Science & Technology, 37(2): 285-291.

Brenan, J.M., McDonough, W.F. and Ash, R., 2005. An experimental study of the solubility and partitioning of iridium, osmium and gold between olivine and silicate melt. Earth and Planetary Science Letters, 237(3-4): 855-872.

Brenan, J.M., McDonough, W.F. and Dalpe, C., 2003. Experimental constraints on the partitioning of rhenium and some platinum-group elements between olivine and silicate melt. Earth and Planetary Science Letters, 212(1-2): 135-150.

Brookins, D.G., 1986. Rhenium as analog for fissiogenic technetium: Eh-pH diagram (25 C, 1bar) constraints. Applied Geochemistry, 1: 513-517.

Brown, E.T., Le Callonnec, L. and German, C.R., 2000. Geochemical cycling of redox-sensitive metals in sediments from Lake Malawi: A diagnostic paleotracer for episodic changes in mixing depth. Geochimica et Cosmochimica Acta, 64(20): 3515-3523.

Brumsack, H.J., 2006. The trace metal content of recent organic carbon-rich sediments: Implications for Cretaceous black shale formation. Palaeogeography Palaeoclimatology Palaeoecology, 232(2-4): 344-361.

Buchauer, M.J., 1973. Contamination of Soil and Vegetation near a Zinc Smelter by Zinc, Cadmium, Copper, and Lead. Environmental Science & Technology, 7(2): 131-135.

Burke, I.T. et al., 2005. Effects of progressive anoxia on the solubility of technetium in sediments. Environmental Science & Technology, 39(11): 4109-4116.

Burton, E.D., Bush, R.T., Sullivan, L.A. and Mitchell, D.R.G., 2007. Reductive transformation of iron and sulfur in schwertmannite-rich accumulations associated with acidified coastal lowlands. Geochimica et Cosmochimica Acta, 71(18): 4456-4473.

Calvert, S.E. and Pedersen, T.F., 1993. Geochemistry of Recent Oxic and Anoxic Marine-Sediments - Implications for the Geological Record. Marine Geology, 113(1-2): 67-88.

Cantillo, A.Y., 1982. Trace element deposition histories in the Chesapeake Bay. Ph.D. Dissertation, University of Maryland, College Park, MD, 298 pp.

Cantillo, A.Y., Sinex, S.A. and Helz, G.R., 1984. Elemental Analysis of Estuarine Sediments by Lithium Metaborate Fusion and Direct-Current Plasma Emission-Spectrometry. Analytical Chemistry, 56(1): 33-37.

Chaillou, G., Anschutz, P., Lavaux, G., Schafer, J. and Blanc, G., 2002. The distribution of Mo, U, and Cd in relation to major redox species in muddy sediments of the Bay of Biscay. Marine Chemistry, 80(1): 41-59.

Chappaz, A., Gobeil, C. and Tessier, A., 2008. Sequestration mechanisms and anthropogenic inputs of rhenium in sediments from Eastern Canada lakes. Geochimica et Cosmochimica Acta, 72(24): 6027-6036.
Chen, Y.W., Deng, T.L., Filella, M. and Belzile, N., 2003. Distribution and early diagenesis of antimony species in sediments and porewaters of freshwater lakes. Environmental Science & Technology, 37(6): 1163-1168.
Coedo, A.G., Padilla, I. and Dorado, M.T., 2004. Comparison of laser ablation and dried solution aerosol as sampling systems in inductively coupled plasma mass spectrometry. Applied Spectroscopy, 58(12): 1481-1487.
Colodner, D., Edmond, J. and Boyle, E., 1995. Rhenium in the Black-Sea - Comparison with Molybdenum and Uranium. Earth and Planetary Science Letters, 131(1-2): 1-15.
Colodner, D. et al., 1993a. The Geochemical Cycle of Rhenium - a Reconnaissance. Earth and Planetary Science Letters, 117(1-2): 205-221.
Colodner, D. et al., 1993a. The Geochemical Cycle of Rhenium - a Reconnaissance. Earth and Planetary Science Letters, 117(1-2): 205-221.
Colodner, D.C., Boyle, E.A. and Edmond, J.M., 1993b. Determination of Rhenium and Platinum in Natural-Waters and Sediments, and Iridium in Sediments by Flow-Injection Isotope-Dilution Inductively Coupled Plasma-Mass Spectrometry. Analytical Chemistry, 65(10): 1419-1425.
Colton, R., 1965. The Chemistry of Rhenium and Technetium. Interscience Publishers, New York, New York, 185 pp.
Crain, J., J Hansel, J. and Troxel, J.E., 1992. Determining regulated metals in soil. Spectroscopy 7(5): 40-46.
Cromwell, E.F. and Arrowsmith, P., 1995. Semiquantitative Analysis with Laser-Ablation Inductively-Coupled Plasma-Mass Spectrometry. Analytical Chemistry, 67(1): 131-138.
Crusius, J., Calvert, S., Pedersen, T. and Sage, D., 1996. Rhenium and molybdenum enrichments in sediments as indicators of oxic, suboxic and sulfidic conditions of deposition. Earth and Planetary Science Letters, 145(1-4): 65-78.
Crusius, J. and Thomson, J., 2000. Comparative behavior of authigenic Re, U, and Mo during reoxidation and subsequent long-term burial in marine sediments. Geochimica et Cosmochimica Acta, 64(13): 2233-2242.
D'Ulivo, A., 1997. Determination of selenium and tellurium in environmental samples. Analyst, 122(12): 117R-144R.
Dalai, T.K., Singh, S.K., Trivedi, J.R. and Krishnaswami, S., 2002. Dissolved rhenium in the Yamuna River System and the Ganga in the Himalaya: Role of black shale weathering on the budgets of Re, Os, and U in rivers and CO2 in the atmosphere. Geochimica et Cosmochimica Acta, 66(1): 29-43.
Daskalakis, K.D. and O'Connor, T.P., 1995. Normalization and Elemental Sediment Contamination in the Coastal United-States. Environmental Science & Technology, 29(2): 470-477.
Dellwig, O., Bottcher, M.E., Lipinski, M. and Brumsack, H.J., 2002. Trace metals in Holocene coastal peats and their relation to pyrite formation (NW Germany). Chemical Geology, 182(2-4): 423-442.

Denoyer, E.R., 1992. Semiquantitative Analysis of Environmental Materials by Laser Sampling Inductively Coupled Plasma Mass-Spectrometry. Journal of Analytical Atomic Spectrometry, 7(8): 1187-1193.
Diemann, E. and Muller, A., 1973. Thio and Seleno Compounds of Transition-Metals with Do Configuration. Coordination Chemistry Reviews, 10(1-2): 79-122.
Dipalma, J.R., 1988. Bismuth Toxicity. American Family Physician, 38(5): 244-246.
Dolor, M.K., 2005. The Mechanism of Rhenium Fixation in Reducing Sediments. M.S. Thesis, University of Maryland, College Park, MD, 119 pp.
Dopp, E., Hartmann, L.M., Florea, A.M., Rettenmeier, A.W. and Hirner, A.V., 2004. Environmental distribution, analysis, and toxicity of organometal(loid) compounds. Critical Reviews in Toxicology, 34(3): 301-333.
Du, P., Xue, N.D., Liu, L. and Li, F.S., 2008. Distribution of Cd, Pb, Zn and Cu and their chemical speciations in soils from a peri-smelter area in northeast China. Environmental Geology, 55(1): 205-213.
Durrant, S.F., 1999. Laser ablation inductively coupled plasma mass spectrometry: achievements, problems, prospects. Journal of Analytical Atomic Spectrometry, 14(9): 1385-1403.
Durrant, S.F. and Ward, N.I., 1993. Rapid Multielemental Analysis of Chinese Reference Soils by Laser Ablation Inductively Coupled Plasma-Source Mass-Spectrometry. Fresenius Journal of Analytical Chemistry, 345(7): 512-517.
Durrant, S.F. and Ward, N.I., 2005. Recent biological and environmental applications of laser ablation inductively coupled plasma mass spectrometry (LA-ICP-MS). Journal of Analytical Atomic Spectrometry, 20(9): 821-829.
Edgington, D.N. and Robbins, J.A., 1976. Records of Lead Deposition in Lake-Michigan Sediments since 1800. Environmental Science & Technology, 10(3): 266-274.
Eggins, S.M., 2003. Laser ablation ICP-MS analysis of geological materials prepared as lithium bordte glasses. Geostandards Newsletter-the Journal of Geostandards and Geoanalysis, 27(2): 147-162.
Eggins, S.M., Kinsley, L.P.J. and Shelley, J.M.G., 1998. Deposition and element fractionation processes during atmospheric pressure laser sampling for analysis by ICP-MS. Applied Surface Science, 129: 278-286.
Eisenreich, S.J., Metzer, N.A., Urban, N.R. and Robbins, J.A., 1986. Response of Atmospheric Lead to Decreased Use of Lead in Gasoline. Environmental Science & Technology, 20(2): 171-174.
Elbaz-Poulichet, F. et al., 2005. Sedimentary record of redox-sensitive elements (U, Mn, Mo) in a transitory anoxic basin (the Thau lagoon, France). Marine Chemistry, 95(3-4): 271-281.
Ferri, K.L., 1977. Input of trace metals to mid-Chesapekae Bay from shore erosions. M.S. Thesis, University of Maryland, College Park, MD, 80 pp.
Flanagan, F.J., 1967. Us Geological Survey Silicate Rock Standards. Geochimica et Cosmochimica Acta, 31(3): 289-308.
Geboy, N.J., 2006 Rhenium-Osmium Age Determinations of Glaciogenic Shales from the Mesoproterozoic Vazante Formation, Brazil. M.S. Thesis, University of Maryland, College Park, MD, 99 pp.

Giggenbach, W., 1972. Optical-Spectra and Equilibrium Distribution of Polysulfide Ions in Aqueous-Solution at 20 Degrees. Inorganic Chemistry, 11(6): 1201-1206.
Gilmour, C., Tuttle, J. and J., M., 1985. Tin metyhlation in sulfide bearing sediments. In: A. Sigleo and A. Hattori (Editors), Marine and estuarine geochemistry. Lewis Publishers inc., Chelsea, MI, pp. 239-258.
Goldschmidt, V.M., 1958. Geochemistry. Okford Claredon Press, 730 pp.
Graney, J.R. et al., 1995. Isotopic Record of Lead Pollution in Lake-Sediments from the Northeastern United-States. Geochimica et Cosmochimica Acta, 59(9): 1715-1728.
Gray, A.L., 1985. Solid Sample Introduction by Laser Ablation for Inductively Coupled Plasma Source-Mass Spectrometry. Analyst, 110(5): 551-556.
Gunther, D. and Heinrich, C.A., 1999. Enhanced sensitivity in laser ablation-ICP mass spectrometry using helium-argon mixtures as aerosol carrier - Plenary lecture. Journal of Analytical Atomic Spectrometry, 14(9): 1363-1368.
Gunther, D., Jackson, S.E. and Longerich, H.P., 1999. Laser ablation and arc/spark solid sample introduction into inductively coupled plasma mass spectrometers. Spectrochimica Acta Part B-Atomic Spectroscopy, 54(3-4): 381-409.
Halliday, A.N. et al., 2000. Multiple-Collector Inductively Coupled Plasma Mass Spectrometry. In: C.M. Basrhick, Duckwork D.C., and Smith D.H. (Editor), Inorganic Mass Spectrometry. Marcel Dekker, New York, pp. 291-328.
Heit, M., Tan, Y., Klusek, C. and Burke, J.C., 1981. Anthropogenic Trace-Elements and Polycyclic Aromatic Hydrocarbon Levels in Sediment Cores from 2 Lakes in the Adirondack Acid Lake Region. Water Air and Soil Pollution, 15(4): 441-464.
Helz, G.R., 1976. Trace-Element Inventory for Northern Chesapeake Bay with Emphasis on Influence of Man. Geochimica et Cosmochimica Acta, 40(6): 573-580.
Helz, G.R. et al., 2000. Osmium isotopes demonstrate distal transport of contaminated sediments in Chesapeake Bay. Environmental Science & Technology, 34(12): 2528-2534.
Helz, G.R., Huggett, R.J. and Hill, J.M., 1975. Behavior of Mn, Fe, Cu, Zn, Cd and Pb Discharged from a Wastewater Treatment Plant into an Estuarine Environment. Water Research, 9(7): 631-636.
Helz, G.R. et al., 1996. Mechanism of molybdenum removal from the sea and its concentration in black shales: EXAFS evidence. Geochimica et Cosmochimica Acta, 60(19): 3631-3642.
Helz, G.R., Setlock, G.H., Cantillo, A.Y. and Moore, W.S., 1985b. Processes Controlling the Regional Distribution of Pb-210, Ra-226 and Anthropogenic Zinc in Estuarine Sediments. Earth and Planetary Science Letters, 76(1-2): 23-34.
Helz, G.R., Sinex, S.A., Ferri, K.L. and Nichols, M., 1985a. Processes Controlling Fe, Mn and Zn in Sediments of Northern Chesapeake Bay. Estuarine Coastal and Shelf Science, 21(1): 1-16.

Henrot, J., 1989. Bioaccumulation and Chemical Modification of Tc by Soil Bacteria. Health Physics, 57(2): 239-245.
Hoffmann, E. et al., 2002. New methodical and instrumental developments in laser ablation inductively coupled plasma mass spectrometry. Spectrochimica Acta Part B-Atomic Spectroscopy, 57(10): 1535-1545.
Hong, S.M., Candelone, J.P., Patterson, C.C. and Boutron, C.F., 1996. History of ancient copper smelting pollution during Roman and medieval times recorded in Greenland ice. Science, 272(5259): 246-249.
Horzempa, L.M. and Helz, G.R., 1979. Controls on the Stability of Sulfide Sols - Colloidal Covellite as an Example. Geochimica et Cosmochimica Acta, 43(10): 1645-1650.
Hou, A., Takamatsu, T., Koshikawa, M.K. and Hosomi, M., 2005. Migration of silver, indium, tin, antimony, and bismuth and variations in their chemical fractions on addition to uncontaminated soils. Soil Science, 170(8): 624-639.
Hu, Z. and Gao, S., 2008. Upper Crustal Abundances of Trace Elements, Chemical Geology.
Huertadiaz, M.A. and Morse, J.W., 1990. A Quantitative Method for Determination of Trace-Metal Concentrations in Sedimentary Pyrite. Marine Chemistry, 29(2-3): 119-144.
Itoh, N., Tani, Y., Nagatani, T. and Soma, M., 2003. Phototrophic activity and redox condition in Lake Hamana, Japan, indicated by sedimentary photosynthetic pigments and molybdenum over the last similar to 250 years. Journal of Paleolimnology, 29(4): 403-422.
Jaffe, L.A., Peucker-Ehrenbrink, B. and Petsch, S.T., 2002. Mobility of rhenium, platinum group elements and organic carbon during black shale weathering. Earth and Planetary Science Letters, 198(3-4): 339-353.
Jarvis, I. and Jarvis, K.E., 1992. Plasma Spectrometry in the Earth-Sciences - Techniques, Applications and Future-Trends. Chemical Geology, 95(1-2): 1-33.
Jochum, K.P., 2008. GeoReM: Geological and Environmental Reference Materials, http://georem.mpch-mainz.gwdg.de/. GWDG.
Jochum, K.P. et al., 2005. GeoReM: A new geochemical database for reference materials and isotopic standards. Geostandards and Geoanalytical Research, 29(3): 333-338.
Jochum, K.P. and Willbold, M., 2006. Reference materials in geoanalytical research - Review for 2004 and 2005. Geostandards and Geoanalytical Research, 30(3): 143-156.
Karlsson, S., Duker, A. and Grahn, E., 2007. Sediment chronologies of As, Bi, and Ga in Sweden - impact of industrialisation. Journal of Environmental Science and Health Part a-Toxic/Hazardous Substances & Environmental Engineering, 42(2): 155-164.
Kim, E. and Boulegue, J., 2003. Chemistry of rhenium as an analogue of technetium: Experimental studies of the dissolution of rhenium oxides in aqueous solutions. Radiochimica Acta, 91(4): 211-216.
Klein, D.H. et al., 1975. Pathways of 37 Trace-Elements through Coal-Fired Power-Plant. Environmental Science & Technology, 9(10): 973-979.

Koide, M., Hodge, V., Yang, J.S. and Goldberg, E.D., 1987. Determination of Rhenium in Marine Waters and Sediments by Graphite-Furnace Atomic-Absorption Spectrometry. Analytical Chemistry, 59(14): 1802-1805.
Koide, M. et al., 1986. Some comparative marine chemistries of rhenium, gold, silver and molydbenum. Applied Geochemistry, 1(6): 705-714.
Laanbroek, H.J. and Pfennig, N., 1981. Oxidation of Short-Chain Fatty-Acids by Sulfate-Reducing Bacteria in Fresh-Water and in Marine-Sediments. Archives of Microbiology, 128(3): 330-335.
Langmyhr, F.J., 1967. Removal of Hydrofluoric Acid by Evaporation in Presence of Sulfuric or Perchloric Acids. Analytica Chimica Acta, 39(4): 516-518.
Lantzy, R.J. and Mackenzie, F.T., 1979. Atmospheric Trace-Metals - Global Cycles and Assessment of Mans Impact. Geochimica et Cosmochimica Acta, 43(4): 511-525.
Lawson, N.M. and Mason, R.P., 2001. Concentration of mercury, methylmercury, cadmium, lead, arsenic,and selenium in the rain and stream water of two contrasting watersheds in Western Maryland. Water Research, 35(17): 4039-4052.
Lawson, N.M., Mason, R.P. and Laporte, J.M., 2001. The fate and transport of mercury, methylmercury, and other trace metals in Chesapeake Bay tributaries. Water Research, 35(2): 501-515.
Lee, Y.L., Chang, C.C. and Jiang, S.J., 2003. Laser ablation inductively coupled plasma mass spectrometry for the determination of trace elements in soil. Spectrochimica Acta Part B-Atomic Spectroscopy, 58(3): 523-530.
Li, Y.-H., 2000. A compendium of geochemistry: from solar processes to the human brain. Princeton University Press, Princeton, New Jersey, 475 pp.
Lima, A.L. et al., 2005. High-resolution historical records from Pettaquamscutt River basin sediments: 1. Pb-210 and varve chronologies validate record of Cs-137 released by the Chernobyl accident. Geochimica et Cosmochimica Acta, 69(7): 1803-1812.
Liu, Y., Terry, J. and Jurisson, S., 2007. Pertechnetate immobilization in aqueous media with hydrogen sulfide under anaerobic and aerobic environments. Radiochimica Acta, 95(12): 717-725.
Livens, F.R. et al., 2004. X-ray absorption spectroscopy studies of reactions of technetium, uranium and neptunium with mackinawite. Journal of Environmental Radioactivity, 74(1-3): 211-219.
Lloyd, J.R., Harding, C.L. and Macaskie, L.E., 1997. Tc(VII) reduction and accumulation by immobilized cells of Escherichia coli. Biotechnology and Bioengineering, 55(3): 505-510.
Lloyd, J.R. and Macaskie, L.E., 1997. Microbially-mediated reduction and removal of technetium from solution. Research in Microbiology, 148(6): 530-532.
Lloyd, J.R., Nolting, H.F., Sole, V.A. and Bosecker, K., 1998. Technetium reduction and precipitation by sulfate-reducing bacteria. Geomicrobiology Journal, 15(1): 45-58.

Lloyd, J.R., Ridley, J., Khizniak, T., Lyalikova, N.N. and Macaskie, L.E., 1999. Reduction of technetium by Desulfovibrio desulfuricans: Biocatalyst characterization and use in a flowthrough bioreactor. Applied and Environmental Microbiology, 65(6): 2691-2696.

Lloyd, J.R., Sole, V.A., Van Praagh, C.V.G. and Lovley, D.R., 2000. Direct and Fe(II)-mediated reduction of technetium by Fe(III)-reducing bacteria. Applied and Environmental Microbiology, 66(9): 3743-3749.

Longerich, H.P., Jackson, S.E. and Gunther, D., 1996. Laser ablation inductively coupled plasma mass spectrometric transient signal data acquisition and analyte concentration calculation. Journal of Analytical Atomic Spectrometry, 11(9): 899-904.

Lovley, D.R. et al., 1993. Geobacter-Metallireducens Gen-Nov Sp-Nov, a Microorganism Capable of Coupling the Complete Oxidation of Organic-Compounds to the Reduction of Iron and Other Metals. Archives of Microbiology, 159(4): 336-344.

Lovley, D.R. and Phillips, E.J.P., 1992. Reduction of Uranium by Desulfovibrio-Desulfuricans. Applied and Environmental Microbiology, 58(3): 850-856.

Lundstrom, C.C., Sutton, A.L., Chaussidon, M., McDonough, W.F. and Ash, R., 2006. Trace element partitioning between type BCAI melts and melilite and spinel: Implications for trace element distribution during CAI formation. Geochimica et Cosmochimica Acta, 70(13): 3421-3435.

Madigan, M.T. and Martinko, J.M., 2005. Brock Biology of Microorganisms, 11th Ed. Pearson Prentice Hall, Upper Saddle River, NJ.

Marcantonio, F., Zimmerman, A., Xu, Y.F. and Canuel, E., 2002. A Pb isotope record of mid-Atlantic US atmospheric Pb emissions in Chesapeake Bay sediments. Marine Chemistry, 77(2-3): 123-132.

Maset, E.R. et al., 2006. Effect of organic co-contaminants on technetium and rhenium speciation and solubility under reducing conditions. Environmental Science & Technology, 40(17): 5472-5477.

Mason, R.P., Kim, E.H. and Cornwell, J., 2004. Metal accumulation in Baltimore Harbor: current and past inputs. Applied Geochemistry, 19(11): 1801-1825.

Miller, C.V., 1992. Sedimentary Molybdenum: A Geochemical Indicator of Anoxia in Chesapeake Bay. Ph.D. Dissertation, University of Maryland, College Park, MD, 245 pp.

Mokgalaka, N.S. and Gardea-Torresdey, J.L., 2006. Laser ablation inductively coupled plasma mass spectrometry: Principles and applications. Applied Spectroscopy Reviews, 41(2): 131-150.

Morford, J., Kalnejais, L., Martin, W., Francois, R. and Karle, I.M., 2003. Sampling marine pore waters for Mn, Fe, U, Re and Mo: modifications on diffusional equilibration thin film gel probes. Journal of Experimental Marine Biology and Ecology, 285: 85-103.

Morford, J.L. and Emerson, S., 1999. The geochemistry of redox sensitive trace metals in sediments. Geochimica et Cosmochimica Acta, 63(11-12): 1735-1750.

Morford, J.L., Emerson, S.R., Breckel, E.J. and Kim, S.H., 2005. Diagenesis of oxyanions (V, U, Re, and Mo) in pore waters and sediments from a continental margin. Geochimica et Cosmochimica Acta, 69(21): 5021-5032.
Morford, J.L. et al., 2007. Insights on geochemical cycling of U, Re and Mo from seasonal sampling in Boston Harbor, Massachusetts, USA. Geochimica et Cosmochimica Acta, 71(4): 895-917.
Morford, J.L., Russell, A.D. and Emerson, S., 2001. Trace metal evidence for changes in the redox environment associated with the transition from terrigenous clay to diatomaceous sediment, Saanich Inlet, BC. Marine Geology, 174(1-4): 355-369.
Morrison, C.A., Lambert, D.D., Morrison, R.J.S., Ahlers, W.W. and Nicholls, I.A., 1995. Laser-Ablation Inductively-Coupled Plasma-Mass Spectrometry - an Investigation of Elemental Responses and Matrix Effects in the Analysis of Geostandard Materials. Chemical Geology, 119(1-4): 13-29.
Muller, A., Diemann, E., Jostes, R. and Bogge, H., 1981. Transition-Metal Thiometalates - Properties and Significance in Complex and Bioinorganic Chemistry. Angewandte Chemie-International Edition in English, 20(11): 934-955.
Muller, A., Diemann, E. and Rao, V.V.K., 1970. Transition Metall Chalkogen Compounds - Preparation, Properties and X-Ray Study of Tetrathioperrhenates Vibrational and Electronic Spectra, Normal Coordinate Analysis of ReS4^-Ion. Chemische Berichte-Recueil, 103(9): 2961-2971.
Muller, A., Krebs, B. and Diemann, E., 1967. Die Reaktion von TcO4- und ReO4- mit Schwefelwasserstoff Darstellung des Tetrathioperrhenat-Ions in Losung. Zeitschrift Fur Anorganische Und Allgemeine Chemie, 353(5-6): 259-264.
Nakajima, M. et al., 2000. Comparative developmental toxicity study of indium in rats and mice. Teratogenesis Carcinogenesis and Mutagenesis, 20(4): 219-227.
Nameroff, T.J., Balistrieri, L.S. and Murray, J.W., 2002. Suboxic trace metal geochemistry in the eastern tropical North Pacific. Geochimica et Cosmochimica Acta, 66(7): 1139-1158.
Newcombe, C.L. and Horne, W.A., 1938. Oxygen poor waters of the Chesapeake Bay. Science, 88: 80-81.
Officer, C.B. et al., 1984a. Chesapeake Bay Anoxia - Origin, Development, and Significance. Science, 223(4631): 22-27.
Officer, C.B., Lynch, D.R., Setlock, G.H. and Helz, G.R., 1984b. Recent sedimentation rates in Chesapeake Bay. In: V.S. Kennedy (Editor), The Estuary As a Filter. Academic Press, Orlando, Fl, pp. 131-158.
Olesik, J.W., 2000. Inductively Coupled Plasma Mass Spectrometry. In: C.M. Basrhick, Duckwork D.C., and Smith D.H. (Editor), Inorganic Mass Spectrometry. Marcel Dekker, New York, pp. 67-158.
Pankratz, L.D., Mah, A.D. and Watson, S.W., 1987. Thermodynamic Properties of Sulfides. Bull. 689. U. S. Bureau of Mines, Washington D.C., pp. 427.
Peretyazhko, T. et al., 2008. Reduction of Tc(VII) by Fe(II) sorbed on Al (hydr)oxides. Environmental Science & Technology, 42(15): 5499-5506.

Poledniok, J., 2007. A sensitive spectrophotometric method for determination of trace quantities of indium in soil. Water Air and Soil Pollution, 186(1-4): 343-349.
Ranade, A.C., Muller, A. and Diemann, E., 1970. Transition Metal Chacogen Compounds - Evidence for Existence of a New Thioanions of Vanadium and Rhenium by Their Electronic Spectra. Zeitschrift Fur Anorganische Und Allgemeine Chemie, 373(3): 258-264.
Rauch, S., Hemond, H.F. and Brabander, D.J., 2006. High spatial resolution analysis of lake sediment cores by laser ablation-inductively coupled plasma-mass spectrometry (LA-ICP-MS). Limnology and Oceanography-Methods, 4: 268-274.
Ravizza, G., Turekian, K.K. and Hay, B.J., 1991. The Geochemistry of Rhenium and Osmium in Recent Sediments from the Black-Sea. Geochimica et Cosmochimica Acta, 55(12): 3741-3752.
Reed, W.P., 1992. "Certificate of Analysis, Standards Reference Materials, 610, 611". https://srmors.nist.gov/view_cert.cfm?srm=610 accessed Feb. 26 2007.
Reinhardt, H. et al., 2003. Application of LA-ICP-MS in polar ice core studies. Analytical and Bioanalytical Chemistry, 375(8): 1265-1275.
Reinhardt, H. et al., 2001. Laser ablation inductively coupled plasma mass spectrometry: a new tool for trace element analysis in ice cores. Fresenius Journal of Analytical Chemistry, 370(5): 629-636.
Riedel, G.F. and Sanders, J.G., 1998. Trace element speciation and behavior in the tidal Delaware River. Estuaries, 21(1): 78-90.
Riedel, G.F., Sanders, J.G. and Osman, R.W., 1997. Biogeochemical control on the flux of trace elements from estuarine sediments: Water column oxygen concentrations and benthic infauna. Estuarine Coastal and Shelf Science, 44(1): 23-38.
Riedel, G.F., Sanders, J.G. and Osman, R.W., 1999. Biogeochemical control on the flux of trace elements from estuarine sediments: effects of seasonal and short-term hypoxia. Marine Environmental Research, 47(4): 349-372.
Rinna, J., Warning, B., Meyers, P.A., Brumsack, H.J. and Rullkotter, J., 2002. Combined organic and inorganic geochemical reconstruction of paleodepositional conditions of a Pliocene sapropel from the eastern Mediterranean Sea. Geochimica et Cosmochimica Acta, 66(11): 1969-1986.
Russo, R.E., Mao, X.L., Liu, C. and Gonzalez, J., 2004. Laser assisted plasma spectrochemistry: laser ablation. Journal of Analytical Atomic Spectrometry, 19(9): 1084-1089.
Sadeh, T., 1987. Biological and biochemical aspects of tellurium derivatives. In: S. Patai (Editor), The Chemistry of Organic Selenium and Tellurium Compounds. John Wiley & Sons ltd., Chichester, pp. 367-376.
Sanudo-Wilhelmy, S.A. and Flegal, A.R., 1992. Anthropogenic Silver in the Southern California Bight - a New Tracer of Sewage in Coastal Waters. Environmental Science & Technology, 26(11): 2147-2151.
Schaller, T., Moor, H.C. and Wehrli, B., 1997. Sedimentary profiles of Fe, Mn, V, Cr, As and Mo as indicators of benthic redox conditions in Baldeggersee. Aquatic Sciences, 59(4): 345-361.

Schaller, T., Morford, J., Emerson, S.R. and Feely, R.A., 2000. Oxyanions in metalliferous sediments: Tracers for paleoseawater metal concentrations? Geochimica et Cosmochimica Acta, 64(13): 2243-2254.

Schubel, J.R., 1968. Turbidity Maximum of Northern Chesapeake Bay. Science, 161(3845): 1013-1015.

Schultz, L.G., Tourtelot, H.A. and Flanagan, F.J., 1976. Descriptions and analyses of eight new USGS rock standards: Cody Shale SCo-1 From Natrona County, Wyoming. In: G.S.p. paper (Editor). U.S. Govt. Print. Off., pp. 21-23.

Schwarz, D.E., Frenkel, A.I., Nuzzo, R.G., Rauchfuss, T.B. and Vairavamurthy, A., 2004. Electrosynthesis of ReS4 center dot XAS analysis of ReS2, Re2S7, and ReS4. Chemistry of Materials, 16(1): 151-158.

Shabani, M.B. and Masuda, A., 1992. Determination of Trace Rhenium in Sea-Water by Inductively Coupled Plasma Mass-Spectrometry with Online Preconcentration. Analytica Chimica Acta, 261(1-2): 315-321.

Shaw, T.J., Sholkovitz, E.R. and Klinkhammer, G., 1994. Redox Dynamics in the Chesapeake Bay - the Effect on Sediment-Water Uranium Exchange. Geochimica et Cosmochimica Acta, 58(14): 2985-2995.

Sinex, S.A., 1981. Trace element geochemistry of modern sediments from Chesapeake Bay Ph.D. Dissertation, University of Maryland, College Park, MD, 190 pp.

Sinex, S.A. and Helz, G.R., 1981. Regional Geochemistry of Trace-Elements in Chesapeake Bay Sediments. Environmental Geology, 3(6): 315-323.

Sinex, S.A. and Helz, G.R., 1982. Entrapment of Zinc and Other Trace-Elements in a Rapidly Flushed Industrialized Harbor. Environmental Science & Technology, 16(11): 820-825.

Skoog, D.A. and J.J., L., 1992. Principles of Instrumental Analysis. Saunders College Publishing, Philadelphia, 700 pp.

Smith, B., 2007. 25 years of lasers and analytical chemistry: A reluctant pairing with a promising future. Trac-Trends in Analytical Chemistry, 26(1): 60-64.

Tao, G.H., Fujikawa, Y., Mitsui, M. and Yamada, R., 2002. Determination of mercury in sediment samples by laser ablation inductively coupled plasma mass spectrometry. Journal of Analytical Atomic Spectrometry, 17(5): 560-562.

Tossell, J.A., 2005. Calculation of the UV-visible spectra and the stability of Mo and Re oxysulfides in aqueous solution. Geochimica et Cosmochimica Acta, 69(10): 2497-2503.

Tu, W.X. and Denizot, B., 2007. Synthesis of small-sized rhenium sulfide colloidal nanoparticles. Journal of Colloid and Interface Science, 310(1): 167-170.

Turekian, K.K. and Wedepohl, K.H., 1961. Distribution of the Elements in Some Major Units of the Earths Crust. Geological Society of America Bulletin, 72(2): 175-191.

USGS, 2005. Statistics and information on the worldwide supply, demand, and flow of minerals and materials essential to the US economy, the national security, and protection of the environment. U.S. Geological Survey. http://minerals.usgs.gov/minerals/pubs/commodity/ accessed Nov. 17 2007.

Van-Loon, J.C., 1985. Selected methods of trace metal analysis: Biological and environmental samples. . John Wiley & Sons., New York, 357 pp.
Venkateswaran, K. et al., 1999. Polyphasic taxonomy of the genus Shewanella and description of Shewanella oneidensis sp. nov. International Journal of Systematic Bacteriology, 49: 705-724.
Vorlicek, T.P., 2002. Toward a better understanding of molybdenum fixation in sediments: the roles of mineral catalysis, zero-valent sulfur and metal sulfides. Ph.D. Dissertation, University of Maryland, College Park, MD, 154 pp.
Vorlicek, T.P., Kahn, M.D., Kasuya, Y. and Helz, G.R., 2004. Capture of molybdenum in pyrite-forming sediments: Role of ligand-induced reduction by polysulfides. Geochimica et Cosmochimica Acta, 68(3): 547-556.
Wagman, D.D. et al., 1982. The NBS Tables of Chemical Thermodynamic Properties. Journal of Physical and Chemical Reference Data, 11: Suppl. 2.
Watters, R.L., Eberhardt, K.R., Beary, E.S. and Fassett, J.D., 1997. Protocol for isotope dilution using inductively coupled plasma-mass spectrometry (ICP-MS) for the determination of inorganic elements. Metrologia, 34(1): 87-96.
Wharton, M.J. et al., 2000. An X-ray absorption spectroscopy study of the coprecipitation of Tc and Re with mackinawite (FeS). Applied Geochemistry, 15(3): 347-354.
Wheeler, K.T., Walker, D., Fei, Y.W., Minarik, W.G. and McDonough, W.F., 2006. Experimental partitioning of uranium between liquid iron sulfide and liquid silicate: Implications for radioactivity in the Earth's core. Geochimica et Cosmochimica Acta, 70(6): 1537-1547.
Wildung, R.E. et al., 2004. Technetium reduction in sediments of a shallow aquifer exhibiting dissimilatory iron reduction potential. Fems Microbiology Ecology, 49(1): 151-162.
Williams, J.G. and Jarvis, K.E., 1993. Preliminary Assessment of Laser Ablation Inductively Coupled Plasma Mass-Spectrometry for Quantitative Multielement Determination in Silicates. Journal of Analytical Atomic Spectrometry, 8(1): 25-34.
Winefordner, J.D., Gornushkin, I.B., Pappas, D., Matveev, O.I. and Smith, B.W., 2000. Novel uses of lasers in atomic spectroscopy. Journal of Analytical Atomic Spectrometry, 15(9): 1161-1189.
Winship, K.A., 1983. Toxicity of Bismuth Salts. Adverse Drug Reactions and Toxicological Reviews, 2(2): 103-121.
Xu, H., Barton, L.L., Zhang, P. and Wang, Y., 2000. TEM Investigation of U^{6+} and Re^{7+} Reduction by Desulfovibrio desulfuricans, a Sulfate-Reducing Bacterium. MATERIALS RESEARCH SOCIETY SYMPOSIUM PROCEEDINGS, 608: 299-306.
Yamashita, Y., Takahashi, Y., Haba, H., Enomoto, S. and Shimizu, H., 2007. Comparison of reductive accumulation of Re and Os in seawater-sediment systems. Geochimica et Cosmochimica Acta, 71(14): 3458-3475.
Zalis, S., Stoll, H., Baerends, E.J. and Kaim, W., 1999. The d(0), d(1) and d(2) configurations in known and unknown tetrathiometal compounds MS4n- (M = Mo, Tc, Ru; W, Re, Os). A quantum chemical study. Inorganic Chemistry, 38(26): 6101-6105.

Zheng, Y., Weinman, B., Cronin, T., Fleisher, M.Q. and Anderson, R.F., 2003. A rapid procedure for the determination of thorium, uranium, cadmium and molybdenum in small sediment samples by inductively coupled plasma-mass spectrometry: application in Chesapeake Bay. Applied Geochemistry, 18(4): 539-549.

Zimmerman, A., 2000. Organic matter composition of sediments and the history of eutrophication and anoxia in the mesohaline Chesapeake Bay. Ph.D. Dissertation, College of William and Mary, 237 pp.

Zimmerman, A.R. and Canuel, E.A., 2002. Sediment geochemical records of eutrophication in the mesohaline Chesapeake Bay. Limnology and Oceanography, 47(4): 1084-1093.